

Structural assessment of composite bolted joints under bearing-bypass load interaction using analytical methods

**Vom Fachbereich Maschinenbau
der Technischen Universität Darmstadt**

zur Erlangung des akademischen Grades
eines Doktoringenieurs (Dr.-Ing.) genehmigte

D i s s e r t a t i o n

von

Minh Nguyen-Hoang, M.Sc.

aus Bremen

Referent: Prof. Dr.-Ing. habil. W. Becker

Korreferent: Prof. Dr.-Ing. habil. Dr. h. c. mult. H. Altenbach

Tag der Einreichung: 19.01.2022

Tag der mündlichen Prüfung: 13.04.2022

Darmstadt 2022

D17

Minh Nguyen-Hoang

Structural assessment of composite bolted joints under bearing-bypass load interaction using analytical methods


Darmstadt, Technische Universität Darmstadt

Published online on TUprints in 2022

Date of oral exam: 13.04.2022

URN: urn:nbn:de:tuda-tuprints-212643

URL: <https://tuprints.ulb.tu-darmstadt.de/21264>

 Creative Commons License (CC BY–NC–ND 4.0 International), 2022.

Free to copy and redistribute, attribution, noncommercial, no derivatives.

Preface

This dissertation is the result of my work as a doctoral student at the Institute of Structural Mechanics (FSM) at Technische Universität Darmstadt. On this occasion I would like to thank everyone who contributed to this work.

I would like to thank Prof. Dr.-Ing. habil. W. Becker for suggesting the research topic, his support and promotion of my scientific work as well as the freedom he has given me.

I thank Prof. Dr.-Ing. habil. Dr. h. c. mult. H. Altenbach for his interest in my work and for reviewing this thesis.

Special thanks also to Dr.-Ing. W. Hansel for having shown me the interesting field of open holes and bolted joints in composite structures during my internship and Master's thesis at Airbus within the A350 BOS STRESS department.

Thanks to the LTH Composite Design Criteria (FL) and IASB working groups, currently led by Dipl.-Ing. R. Herrmann and Dr.-Ing. T. Kremer, respectively, for the fruitful discussions and their interest in my research. I would also like to thank Dr. J. Broede for providing the fitting functions in a HSB method sheet.

Many thanks to all colleagues, family and friends in and outside the Institute for their support, exciting projects and good times.

Abstract

Bolted joints are a common means to connect thin parts due to benefits such as inexpensive manufacturing and their ability to be disassembled. These parts can be plates made of composite laminates, which is common practice for many lightweight structures such as air- and spacecraft. However, holes need to be introduced and stress concentrations arise. In structural analysis, special focus should lie on preventing fatal tension failure. This is the most critical failure mode leading to instantaneous destruction of the connection and must not occur in safety-relevant structures. Hence, precise structural assessment means are crucial to create safe and lightweight optimal designs. These means can be based on analytical methods, which are advantageous in terms of computational effort. Hence, the purpose of the present thesis is to develop an efficient and comprehensive framework for tension failure assessment of composite bolted joints using analytical means.

Usually, rows of fasteners are placed in a plate. Then, one part of the load is introduced into a bolt while the remaining load stays in the plate. This problem setting is also referred to as bolted joint under combined bearing-bypass load and is treated analytically in this work using linear two-dimensional models. In doing so, the bolted joint under bearing-bypass load is idealised as a superposition of the open- and pin-loaded hole in a plate with finite dimensions. Regarding the latter setting, the bolt contact is idealised by sinusoidal radial tractions along half of the hole edge.

First, the stress field of the joint's mechanical model is determined. In doing so, use is made of the complex potential method in the Lekhnitskii formalism for stress state representation of orthotropic composite laminates. One objective is to render finite plate dimensions since narrow connections are prone for tension failure. This is achieved by an iterative calculation scheme. Therein, an important part is the development of a novel periodic arrangement technique that enables the efficient and robust implementation of stress-free edges of symmetric finite-domain problems. The results are validated against Finite Element analyses showing excellent agreement for common geometries and layups. Further, the impact of finite dimensions, material orthotropy and ratio between bearing and bypass loads on the characteristic stresses and the corresponding stress concentration factors is extensively investigated.

Abstract

Based on the stress results, a failure analysis is conducted, which aims to precisely predict the critical and minimal loads that lead to tension failure. This part is dedicated to quasi-isotropic laminates only. The following nonlocal concepts capable of capturing the hole size effect are employed: first, the Theory of Critical Distances (TCD), which is frequently used in industry contexts and second, the recent state-of-the-art concept of Finite Fracture Mechanics serving as reference to assess the limits of the TCD. The predictions for the special cases of open and filled holes are validated against test data and good agreement is found. Then, the failure load reduction with increasing hole and bolt diameter in the context of the hole size effect is analysed and effects by finite dimensions as well as the ratio between bearing and bypass load are investigated. Furthermore, the sustained bolt loads are discussed with focus on the nonlinear load interaction. Moreover, failure envelopes that enable the engineer to graphically obtain the critical bearing and bypass stresses are provided.

Kurzfassung

Bolzen- und Nietverbindungen werden häufig verwendet, um dünne und flächige Strukturbauteile zu verbinden. Hierbei sind sowohl die kostengünstige Fertigung als auch die Demontierbarkeit als wesentliche Vorteile zu nennen. Die zu fügenden Bauteile können Faserverbunde sein, was gängige Praxis in vielen Leichtbaustrukturen, zum Beispiel in der Luft- und Raumfahrt, ist. Jedoch sind Löcher in den zu fügenden Strukturen erforderlich, so dass Spannungskonzentrationen entstehen. Im Rahmen der Strukturanalyse ist dem kritischsten Versagensmodus Tension Failure (auch Flankenzugbruch) besondere Aufmerksamkeit zu schenken. Dieser führt zur instantanen Zerstörung der Verbindung und ist in sicherheitsrelevanten Strukturbauteilen zu verhindern. Präzise Tools zur Ermittlung der Versagenslasten sind daher essentiell. Diese können auf analytischen Methoden basieren, welche Vorteile im Berechnungsaufwand mit sich bringen. Das Ziel der vorliegenden Arbeit ist deswegen die Entwicklung einer effizienten und physikalisch basierten Berechnungsmethode zur Bewertung von Tension Failure in Bolzen- und Nietverbindungen von Faserverbundstrukturen.

Üblicherweise werden Bolzenreihen gesetzt, so dass sich die gesamte eingeleitete Last aufteilt: Ein Teil der Last verbleibt in dem Strukturbauteil (Bypass-Last), während der restliche Anteil in den Bolzen übertragen wird (Bearing- oder Lochleibungslast). Diese Struktursituation wird auch als Bolzen- oder Nietverbindung unter Bearing-Bypass-Last bezeichnet. Zur analytischen Berechnung soll die vorliegende Situation als lineares 2D-Scheibenproblem idealisiert werden. Dabei sind folgenden Teilprobleme zu superponieren: Der Bypass-Lastfall wird als Open Hole (lastfreies Loch), der Bearing-Lastfall als Pin-loaded Hole (rein Bolzen-belastetes Loch) jeweils mit finiter Scheiben-geometrie modelliert. Bei letzterem Teilproblem ist eine Bolzenkontaktidealisierung in Form von sinusförmigen Radialspannungen entlang des halben Lochrandumfangs vorgesehen.

Zunächst wird das Spannungsfeld dieses mechanischen Modells der Bolzenverbindung bestimmt. Dabei werden komplexe Potentiale im Lekhnitskii-Formalismus zur Berechnung von Spannungen in orthotropen Faserverbunden verwendet. Ein wichtiges Ziel ist es finite Fügeteilabmessungen zu berücksichtigen, zumal Verbindungen mit schmaler Breite für Tension Failure prädestiniert sind. Dieses Ziel wird durch ein iteratives Berechnungsverfahren

Kurzfassung

erreicht. Dessen wesentlicher Bestandteil ist dabei eine neuartige Methode periodischer Anordnungen, welche die effiziente und robuste Implementierung spannungsfreier Ränder von symmetrischen Randwertproblemen mit endlicher Geometrie ermöglicht. Die Spannungslösung zeigt exzellente Übereinstimmung mit Finite-Elemente-Analysen für typische Fügeiteilgeometrien und Lagenaufbauten des Faserverbunds.

Mit den ermittelten Spannungen als Input wird eine Festigkeitsanalyse durchgeführt. Deren Ziel ist es die kritischen und minimalen Lasten zu ermitteln, welche zu Flankenzugbruch führen. Gegenstand dieses Teils der Arbeit sind ausschließlich quasi-isotrope Faserverbunde. Im Zuge dessen werden folgende nichtlokale Konzepte zur Modellierung von Bruchvorgängen in spröden Materialien verwendet, welche den Lochgrößeneffekt abbilden können: Erstens die Theorie kritischer Distanzen (TCD), die im industriellen Umfeld häufig Anwendung findet und zweitens die Finite Bruchmechanik. Letztere entspricht dem derzeitigen Stand der Forschung und dient als Referenz zur Ermittlung der Modellgrenzen der TCD. Die Teilprobleme Open Hole und Pin-loaded Hole werden mittels Versuchsergebnisse validiert. Anschließend wird der Lochgrößeneffekt und in diesem Kontext der Abfall der Effektivfestigkeit mit zunehmendem Loch- und Bolzendurchmesser modelliert. Des Weiteren wird ein möglicher Einfluss von finiten Bauteilabmessungen sowie von dem Verhältnis zwischen Bearing- und Bypass-Lasten auf die Versagensspannungen analysiert. Diese werden auch im Hinblick auf eine nichtlineare Lastinteraktion untersucht. Schlussendlich werden Versagenskurven (auch Versagensenveloppen oder failure envelopes) zur Verfügung gestellt, mit denen die kritischen Bearing- und Bypass-Spannungen bei Versagen grafisch ermittelt werden können.

Table of contents

Abstract	v
Kurzfassung	vii
Nomenclature	xi
1 Introduction	1
1.1 Motivation and background	1
1.2 State of the art	4
1.3 Objectives and outline	12
2 Theoretical background	15
2.1 Fundamentals of linear elasticity	15
2.2 Complex potential method	20
2.3 Finite Fracture Mechanics	24
3 Stress analysis - Development of complex calculus	27
3.1 Mechanical idealisation	28
3.2 Overview of the calculus	33
3.3 Infinite-domain problem	33
3.4 Cancellation of tractions parallel to the load direction	41
3.5 Cancellation of tractions perpendicular to the load direction	44
3.6 Cancellation of violated hole boundary conditions	50
3.7 Overall iterative calculation procedure	53
4 Stress analysis - Discussion of the results	59
4.1 Finite Element model for validation	60
4.2 Investigation of force flux	60
4.3 Influence of finite dimensions on number of required auxiliary plates	61
4.4 Analysis of characteristic stresses: Open hole	65
4.5 Analysis of characteristic stresses: Filled hole	70
4.6 Analysis of characteristic stresses: Bearing-bypass interaction	76
4.7 Interpolation formulae for quasi-isotropic laminates	82

Table of contents

5	Failure analysis	87
5.1	Failure load determination	88
5.2	Discussion of the results: Open hole	92
5.3	Discussion of the results: Filled hole	100
5.4	Discussion of the results: Bearing-bypass interaction	104
6	Conclusion and outlook	115
	References	119

Nomenclature

Abbreviations

BC	boundary condition
Exp	experiment
FE	Finite Element
FFM	Finite Fracture Mechanics
HSB	Handbuch Strukturberechnung
IASB	Industrierausschuss Strukturberechnung
LTH	Luftfahrttechnisches Handbuch
SCF	stress concentration factor
Tan-HW	Tan-Heywood
TCD	Theory of Critical Distances

Indices and notations

$\min \{\square\}$	find minimum
PA (\square)	operator for periodic arrangement
$\hat{\square}$	amplitude
\square'	derivative with respect to complex variable
$\tilde{\square}$	field quantity produced by unit remote load
\square_0	remote or far field
\square_B	bolt
\square_{Bea}	bearing
\square_{By}	bypass
\square_{clb}	calibrated
\square_d	diameter
\square_F	failure
\square_{min}	minimum
\square_{red}	reduced
\square_s	symmetric
\square_{tot}	total
\square_T	Taylor
\square^\perp	perpendicular

Nomenclature

\square^{dev}	deviation
\square^{FH}	filled hole
\square^{Fo}	Fourier series
\square^{HA}	heuristic approach
\square^{HBC}	hole boundary conditions
\square^{HE}	horizontal edges
\square^{inf}	infinite
\square^{mv}	multivalued
\square^{OH}	open hole
\square^{sv}	single-valued
\square^{VE}	vertical edges

Latin symbols

$a, \Delta a$	overall defect size, finite crack length
a, b	coefficient of Airy stress function
$A, \Delta A$	area, infinitely small area
A, B, C, D	coefficients of complex potentials or Airy stress functions
\mathbf{A}, A_{ij}	matrix of extensional stiffnesses and its components
b	experimental fitting parameter involved in R-curve
\mathbf{c}, c_{ijkl}	elasticity tensor and its components
C_{ij}	components of elasticity tensor stored in matrix form
$C_i^{\phi k}$	constant
d	hole and bolt diameter
e	end distance
E, \hat{E}	Young's modulus, effective Young's modulus
f	body force
f_n, F_h, F_w	functions of fit for stress intensity factor of open hole
f, g	coefficient of Fourier series
F	Airy stress function
G, \hat{G}	shear modulus, effective shear modulus
G, H	complex coefficients of Fourier series expansions of loading functions
h_s	coefficient characterising angle-ply laminates
K_I	stress intensity factor of mode I crack opening
K_{Ic}	fracture toughness of mode I crack opening
K_{Ic}^I	initiation value of R-curve of fracture toughness
K_{Ic}^P	propagation value of R-curve of fracture toughness
K_{t0}	stress concentration factor with remote stress as reference value

K_{td}	stress concentration factor with bearing stress as reference value
l_{Fo}	wave length of Fourier series expansion
l	iteration step
L	number of iterations
n_x, n_y	number of horizontal and vertical auxiliary plates
\mathbf{n}, n_i	normal vector and its components
N	number of terms
N_x, N_y, N_{xy}	normal stress resultants
p_x, p_y	loading functions
P	force, load
Q_{ij}	reduced stiffnesses with respect to coordinate system of uni-directional single layer
\bar{Q}_{ij}	reduced stiffnesses with respect to global coordinate system of laminate
r	radial coordinate
r_c	characteristic hole distance
\tilde{r}_c	arbitrary hole distance
r_p	effective crack length of mode I through crack
R	hole and bolt radius
s	coefficient in governing equations for an orthotropic plate
s, \tilde{s}	arc length parameter
\mathbf{s}, s_{ijkl}	compliance tensor and its components
\tilde{S}_{ij}	components of compliance tensor stored in matrix form
t	thickness
t_s	coefficient characterising angle-ply laminates
\mathbf{t}, t_i	stress vector and its components
\mathbf{u}, u_i	displacement vector and its components
w	width
x_i or x, y, z	spatial coordinates
X_n, Y_n	components of external force
X_T^L	longitudinal plain strength in tension
y_k^*	location of change of sign involved in the mapping functions
z_1, z_2	complex coordinates

Greek symbols

α, β	oscillatory parameter
α	constant of real part of complex constant
β	constant of imaginary part of complex constant
β	load factor, ratio of bearing and total load

Nomenclature

γ	engineering shear strain
ε	strain
ε	linearised strain tensor
ϵ	relative error or deviation
ζ	mapping function
η	reduction factor involving remote stresses
ϑ	fibre orientation
ι	reduction factor involving bearing stresses
κ	normalised stress concentration factor
λ	ratio of radius and overall defect size
μ	complex constant
$\nu, \hat{\nu}$	Poisson's ratio, effective Poisson's ratio
ξ	relative or dimensionless coordinate
$\Delta\xi$	relative or dimensionless crack length
ϱ	hyperbolic function
$\sigma, \bar{\sigma}$	normal stress, average normal stress
$\boldsymbol{\sigma}, \sigma_{ij}$	Cauchy stress tensor and its components
τ	shear stress
φ	circumferential coordinate
ϕ	hyperbolic function involved in Airy stress function
Φ	complex potential
χ	failure load deviation by local criteria
χ	convergence criterion for load transfer
ψ	convergence criterion for free edge
ψ	fit for stress intensity factor of filled hole
Ψ, Ψ_{ij}	matrix of fitting coefficients and its components

Chapter 1

Introduction

In Section 1.1, the technical background of bolted joints and their assessment in terms of the fatal tension failure mode is outlined. Moreover, the requirements for corresponding efficient and precise structural assessment means are described. Knowledge gaps and drawbacks of existing approaches are briefly summarised, which further motivate and define the goals of the present thesis. The state of the art regarding the assessment of net-section failure of bolted joints is extensively discussed in Sect. 1.2 and existing knowledge gaps are detailed. Then, the research objectives are defined in Sect. 1.3, which also provides the structure of this work. Its overall goal is to develop an efficient and comprehensive framework for the assessment of net-section failure of composite bolted joints by analytical methods.

1.1 Motivation and background

In aerospace engineering, bolted joints are a common means to connect thin plate structures. This is motivated by the ease of manufacturing such joints and the ability to disassemble them, for example. However, circular holes need to be introduced to make the joints and stress concentrations arise at these locations. Their magnitude depend on the finite dimensions of the plate relative to the hole diameter as well as on the degree of anisotropy when use is made of composite laminates as is done in many lightweight designs.

In structural analysis, the engineer needs to be aware of the following five failure modes depicted in Fig. 1.1: tension¹, shear-out, bearing, cleavage and pull-through failure (Camanho and Matthews, 1997). The particular mode that is triggered depends on numerous parameters such as joint geometry, clamping pressure and, in the case of composite laminates, stacking sequence and fibre orientation. Corresponding tests have been conducted by Collings (1977) and Kretsis and Matthews (1985). A review regarding the parameters' influences on the failure modes can be found in Godwin and Matthews (1980). Moreover, Camanho and Lambert (2006) discuss the mechanical

¹ This mode is also referred to as net-section or tensile failure.

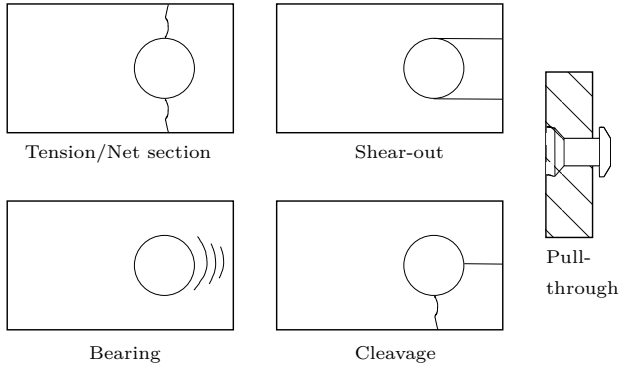


Fig. 1.1 Failure modes of bolted joints.

modelling, which includes stress and failure analysis as well as validation by the experiment. Generally, the bolted-joint connection should be designed such that bearing failure is likely triggered, which yields a gradual and fail-safe failure process whose consequences are relatively mild. This mode has been investigated experimentally by Collings (1982) and Xiao and Ishikawa (2005). By contrast, for narrow connections bounded by a width-to-hole diameter ratio $w/d \leq 4$, fatal net-section failure occurs (Hart-Smith, 1980). This mode leads to instantaneous destruction of the connection and must be avoided in safety-critical parts. Hence, accurate means for stress and failure analysis are crucial for prevention. These can be based on analytical methods, which are beneficial in terms of computational efficiency and may be documented in technical handbooks in the ideal case. Thus, analytical means shall be the focus of the present thesis. Special consideration is given to narrow connections prone for tension failure.

Generally, the structural assessment begins with a mechanical idealisation. Then, a stress and failure analysis is conducted. Usually, rows of fasteners are placed and the total load is partially transferred through a bolt (bearing load) while the remaining load stays in the plate (bypass load). This problem setting is also referred to as bolted joint under bearing-bypass load (Fig. 1.2) and is the focus of this thesis. For the purpose of the development of analytical methods, 2D modelling approaches are more feasible. In this context, the connection is not modelled as one whole problem domain that includes all fasteners, but each fastener and its surrounding plate vicinity is rendered as an individual plane stress boundary value problem with certain bearing and bypass loads as inputs. These need to be obtained through load transfer

1.1 Motivation and background

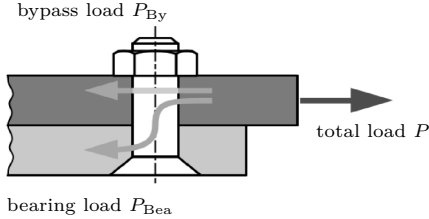


Fig. 1.2 Load transfer: The bypass load P_{By} remains in the upper plate, whereas the bearing load P_{Bea} is transferred by the bolt into the lower plate.

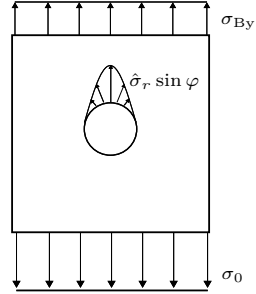


Fig. 1.3 Linear 2D idealisation of bolted joint under bearing-bypass loads with sinusoidal bolt load introduction. The stress quantities therein are introduced in Chap. 3.

calculation prior to a detailed 2D stress analysis. In particular, the present bolted-joint setting is idealised as a superposition of the open and filled (or pin-loaded) hole (Camanho and Lambert, 2006). The latter typically involves a bolt contact idealisation by radial hole traction of sinusoidal shape. Hence, the pin-loaded hole as well as the superposition model for the bolted joint under combined bearing-bypass load (Fig. 1.3) are treated as linear boundary value problems. According to the author's knowledge, there is no analytical study that investigates and identifies the main physical effects influencing the structural behaviour of the present bolted-joint setting with bearing-bypass load interaction. This refers to the steps of stress and failure analysis in structural assessment. Regarding the former, the characteristic stresses and stress concentrations are expected to be affected by parameters such as finite plate dimensions, material orthotropy as well as the load ratio between bearing and bypass load. However, there is no study yet that quantifies and extensively investigates this matter by analytical methods. This would also enable the derivation of design guidelines, which could be useful in engineering applications. Another vital aspect in stress analysis of narrow connections is having calculi that are capable of precisely and robustly rendering raised effects due to finite plate dimensions. To the author's knowledge, there is no stress calculation method for bolted joints documented in technical design guidelines such as LTH Design Criteria². A common approach to capture finite dimensions is provided by heuristic approaches. These yield good results for the

² This is a guideline established and used by many European aerospace firms. LTH $\hat{=}$ Luftfahrttechnisches Handbuch

open-hole problem (Tan, 1987, 1988; Tan and Kim, 1990; Tan, 1994). Unfortunately, the good agreement is rather coincidental than physically justified. Hence, applicability to other settings cannot be concluded. Regarding stress analysis, one main goal of the present thesis is to develop an analytical method that is robust and can be extended to other settings, e.g. different load cases and contact models. This shall be done without the necessity of optimisation routines as typically required by collocation techniques, which are common approaches in the literature. These intend to satisfy the boundary conditions (BCs) at selected discrete points or in average along a predefined section. The free coefficients are determined accordingly by using optimisation algorithms. The performance of these algorithms strongly affects the solution accuracy. Thus, the overall approach may be rather unsuitable as a foundation for technical design guidelines. Motivated by these inconveniences and drawbacks, the present stress methodology aims to continuously and robustly satisfy the stress BCs in order to provide a convenient design tool that is suitable for industry contexts while still efficiently and precisely capturing the primary physical effects.

Regarding failure, the size effect is a well known physical phenomenon and should be taken into account when aiming for safe and lightweight optimal designs. This physical effect and the corresponding failure load reduction with increasing hole and bolt diameter has not yet been quantified for the bolted joint under combined bearing-bypass load. Furthermore, it is still unknown how the failure loads and their reduction might be affected by physical and geometrical parameters such as material orthotropy, ratio between bearing and bypass load and finite dimensions. These gaps shall be also treated in this work.

1.2 State of the art

In the following, the current state of the art for structural assessment of the net-tension failure of bolted joints is provided. As this thesis emphasises the use of analytical methods, of special interest are contributions that focus on employing 2D models. This is eligible for bolted joints without secondary bending, which is true for connections containing an overall symmetry with respect to the midplane. Moreover, effects of clamping and hence stresses in the thickness direction on the tension failure fracture mechanism should be negligible. Usually, bolts are placed in rows. Using 2D approaches, their assessment is not done by modelling one whole problem domain that includes all joints. However, each joint and the surrounding vicinity of the plate is rendered as a separate boundary value problem with certain bearing and

bypass loads as input. This problem setting is also referred to as bolted joint under bearing-bypass load (Fig. 1.3). The structural analysis generally starts with a mechanical idealisation. Then, a stress and failure analysis is conducted. Corresponding means that exist in literature are summarised in the following Subsections.

Load transfer calculation

The determination of the bearing and bypass input loads for the 2D bolted joint idealisation requires a load transfer calculation prior to detailed stress analysis. This can be performed by analytical means that employ a continuous model based on a Faber series expansion and complex potentials (Wei-Xun and Chun-Tu, 1993) or on a complex variational approach for both load transfer as well as stress field determination (Xiong, 1996). Furthermore, the load transfer might be calculated using discrete spring-based models. Motivated by inaccuracies of preexisting semi-empirical formulae, e.g. Tate and Rosenfeld (1946) as well as Swift (1971), the well known expression for determination of the bolt and plate stiffnesses by Huth (1986) has been derived. This is based on an extensive experimental programme. Note that the formula has been derived based on some specific bolted-joint settings (e.g. layup, geometry) and adaption to other configurations is not physically justified. McCarthy et al. (2006) develop a spring-based model that takes the effects of bolt-hole clearance into account. This is extended by McCarthy and Gray (2011) to highly torqued bolted joints involving static friction effects. These parameters are identified to be the main contributors to load transfer. Lecomte et al. (2014) treat effects due to clearance and hole-location errors and Zhao et al. (2019) analyse hole tensile deformation in the stiffness calculation. Ekh and Schön (2006) develop a 3D Finite Element (FE) model to investigate the load transfer. An efficient FE modelling strategy, known as the global bolted-joint model, is suggested by Gray and McCarthy (2010). This strategy shows computational time savings of up to 97 % in comparison to full 3D FE models

Stress analysis

Once the bearing and bypass loads are determined, a stress analysis can be conducted. Currently, however, works that analytically treat the linear idealisation of the present bolted joint under bearing-bypass are quite rare according to the author's knowledge. The following contributions deal with anisotropic plates using the complex potential method in the formalism by Lekhnitskii (1968). Madenci et al. (1995) investigate contact stresses of a

loaded single-fastener bolted joint under combined bearing-bypass and shear loading by means of a boundary collocation method and complex variable formulation. This is extended to multiple fasteners by Madenci et al. (1998) and use is made of a modified mapping collocation technique by Bowie and Neal (1970) to implement BCs within a finite domain. In Wu and Tian (2021), the bolt contact is not idealised by sinusoidal radial hole tractions, but is instead based on displacements, as implemented by Zhang and Ueng (1984). Finite plate geometry is not taken into account and hence some errors in the net-section stresses of a unidirectional laminate with the aspect ratio $w/d = 4$ arise in comparison to FE analyses.

Regarding the special cases of open and filled (or pin-loaded) holes, there exist many works treating these problems at different levels of complexity such as material anisotropy, shape of the hole, finite dimensions and loading along the outer boundaries. Concerning the open-hole problem, an extensive review is written by Sevenois and Koussios (2014) summarising a variety of plate problems weakened by holes and notches. Furthermore, Koord et al. (2020) summarise frequently employed analytical means and validate them against both 2D and 3D FE analyses as well as against strains identified from experiments. The pioneering work of Kirsch (1898) solved the stress field of an isotropic, infinite plate with a central circular opening. The plate is under remote uniform tension. Use is made of the Airy stress function (Timoshenko and Goodier, 1951; Sadd, 2005) to represent the stress state. The elliptical hole in an infinite, isotropic plate was addressed by Savin (1961) taking into account several load cases using the complex potentials in the formulation of Muskhelishvili (1977). Problems involving anisotropic plate material were solved using the complex potential formalism by Lekhnitskii (1968). The following works treat settings with elliptical holes. The infinite anisotropic plate without bending extension coupling under uniform tension, biaxial loading and shearing was analysed by Lekhnitskii (1968) himself. Furthermore, bending extension coupling is taken into account by Becker (1993) and Ukadgaonker and Rao (2000b) regarding an arbitrary hole shape as well as arbitrarily oriented homogeneous loading and with arbitrarily oriented loading functions (Ukadgaonker and Rao, 2000a). For finite-width problems, the existing solutions can be classified into heuristic approaches and methods of calculation designed to satisfy the BCs of the finite setting. Regarding the former, Tan (1988, 1994) introduces heuristic correction factors which scale the infinite-domain solution for an ellipse under uniform tension by Lekhnitskii (1968) such that the integrated stresses along the actual width of the finite problem transfer the external load. The concept is further improved by adapting the stresses to the formula by Heywood (1952) based on photoelasticity. This leads to good correlation for the stress concentrations

and their decay in the hole vicinity (Tan and Kim, 1990). However, the Tan concept of heuristically scaling the stresses relies on the assumption that the stress decay of the finite-domain problem is of the same shape as that of the infinite-domain setting. The good agreement for open holes is therefore more or less a coincidence rather than being physically justified. Hence, it cannot be concluded that the idea is applicable to other problem settings. For instance, it has been revealed that this heuristic approach leads to erroneous results for single-fastener bolted joints (Nguyen-Hoang and Becker (2020a, 2021a) regarding isotropic and Nguyen-Hoang and Becker (2021d) concerning orthotropic plate material). Errors also arise for isotopic open holes with finite dimensions (Nguyen-Hoang and Becker, 2020b) when assessing the stresses along the entire net-section area. In this publication, a novel approach is employed to take a finite plate width into account. This is based on a periodic arrangement technique. Documented for industry contexts, the method sheet by Nguyen-Hoang and Becker (2021h) in LTH Design Criteria investigates finite orthotropic composite laminates weakened by a hole. For stress state representation, use is made of the complex potential method. Excellent agreement to FE analysis is achieved. The corresponding scientific publication can be found in Nguyen-Hoang and Becker (2022d).

Regarding the remaining special case of the filled (or pin-loaded) hole, several works treating its 2D stress analysis exist at different levels of complexity. Corresponding reviews are given by Matthews (1987) as well as Camanho and Matthews (1997). The existing solutions may be classified into approaches employing a bolt-plate contact model and concepts idealising the bolt contact to a given stress distribution along a part of the hole boundary. In this context, a sinusoidal function in the radial hole tractions is commonly assumed. This was addressed by Waszczak and Cruse (1971). For the purpose of modelling the bolt contact, the reader is referred to works treating conformal contacts. This field deals with contacting bodies that cannot be modelled as half-plane, which is due to the significant large contact area relative to the radius of the curvature (Sundaram and Farris, 2010b). Hence, Hertzian contact theory should not be applied (Johnson, 1987). The reader may also refer to Sackfield et al. (2013) concerning the field of elastic contacts. Frictionless conformal contacts were first investigated by Persson (1964). A corresponding comprehensive literature list can be taken from Gladwell (1980) and Ciavarella et al. (2006). Of special interest might be To et al. (2007), whose work covers a finite pin-loaded plate with a reinforced hole. The case of conformal contacts with friction is analysed by the following authors. Ho and Chau (1997) treat an infinite plate loaded by a rivet of different material. Interference fit and clearance fit is considered by Hou and Hills (2001). Some analytical calculi are assessed by Iyer (2001) using

Chapter 1 Introduction

FE analyses as reference. General loading conditions, particularly pin loads and remote stresses with arbitrary direction, are investigated by Sundaram and Farris (2010b) for a rigid pin. This is extended by Sundaram and Farris (2010a) for an elastic pin. The following contributions cover orthotropic plate material using complex potentials in the Lekhnitskii (1968) formalism. Zhang and Ueng (1984) analyse the effect of friction for an infinite plate, which is extended by Zhang and Ueng (1985) for arbitrary load directions. Further, Hyer and Klang (1985) and Hyer et al. (1987) analyse the effects of friction, bolt elasticity and clearance on the stresses. Song et al. (2017) take into account interference fit and finite dimensions. However, the calculus is only validated against FE results for a wide width-to-bolt diameter ratio $w/d_B = 10$ and an end-distance to bolt-diameter value of $e/d_B = 5$. Of interest might also be the finding for frictionless conforming contacts (exact and perfect fit of the bolt) that the contact area decreases but then remains constant when the load further increases. Dundurs and Stippes (1970) consider these observations as receding contact. Note that the field quantities then are proportional to the external load. Similar observations are made in Ciavarella et al. (2006) for the case including friction. Hence, it can be regarded as feasible to treat the bolted-joint problem by employing a linear model, for which the sinusoidal load introduction by Waszczak and Cruse (1971) is commonly selected. This idealisation simplifies the development of analytical methods to render other effects as finite dimensions. Further, Catalanotti and Camanho (2013) as well as Nguyen-Hoang and Becker (2020a) derive failure loads using this linear sinusoidal idealisation and obtain agreement with test data. Hence, all assumptions and idealisations including the bolt contact may be considered as acceptable for the quasi-isotropic case investigated in the cited studies. Extensive FE analyses comparing the pin-loaded hole with a contact model as well as its sinusoidal idealisation are given by Crews et al. (1981).

Calculi that take finite plate dimensions into account can mostly be found in works that involve a frictionless bolt contact idealisation of sinusoidal radial hole tractions. Concerning isotropic plates, Bickley (1928) treats infinite plate dimensions and Knight (1935) captures finite width. However, a finite end distance is not taken into account. In these two studies, use is made of Airy stress functions for stress state representation. Regarding the orthotropic case treated using complex potentials by Lekhnitskii (1968), de Jong (1976) focuses on infinite plate dimensions. The method is extended for any arbitrary load direction in de Jong and Vuil (1981). A general methodology for mixed boundary value problems with one part of the hole loaded and the remaining other unloaded is developed by Berbinau and Soutis (2001). Finite plate dimensions are rendered by de Jong (1977) using correction factors. These heuristically scale the infinite-domain solution such

that its uniform remote stresses equilibrate the external load along the actual finite width. However, the stress-free conditions are violated at the edges parallel to the loading. Therefore, the results may be acceptable for wider width-to-hole diameter ratios that yield slight finite-width effects. The method is implemented in an overall bolted joint assessment tool by Ogonowski (1981) and the circumferential stresses reveal good correlation to FE calculations for the layup $[0^\circ / \pm 45^\circ / 90^\circ]_s$ (50%/40%/10%) with $w/d = 8$, $e/d = 9$. By comparing the stress concentrations, it is further concluded that the analytical stresses are sufficiently accurate for the dimensions $e/d = 9$ and $w/d > 4$. Intending to reduce the computational cost, Echavarría et al. (2007) modify the heuristic approach by de Jong (1977) using the first terms of the series for the stress state representation only. The derived concentrations are validated against the original calculus. However, there is no comparison of either the stress concentrations or the decay to that of the actual boundary value problem. This step is essential to assess the performance of the method in failure analysis, which shall be conducted using nonlocal criteria.

Capturing finite dimensions by solving the actual boundary value problem is the aim of the following works. The rectangular plate geometry is approximated as an ellipse by Kratochvil and Becker (2010), which reveals good correlation to FE calculations in the circumferential stresses for $[\pm 45^\circ]_s$ -laminates and $w/d = 3$ as well as for $[0^\circ / 90^\circ]_s$ -laminates and $w/d = 5$. Bending extension coupling is treated by Grüber et al. (2007) showing good agreement to FE analyses for $w/d = \{15, 45\}$, an aspect ratio with slight or even vanishing finite-width effects. The calculus is extended to multilayered composite bolted joints with interference fit under thermal load (Grüber et al., 2018). An approach continuously satisfying the stress BCs relevant to the load transfer is developed by Nguyen-Hoang and Becker (2020a). In this work, tension failure of quasi-isotropic laminates is assessed by employing the Theory of Critical Distances. The predicted failure loads lead to relative deviations of $|\epsilon| \leq 10\%$ for $w/d = 2$ within $1 \text{ mm} \leq d \leq 15 \text{ mm}$ and for $w/d = 3$ within $8 \text{ mm} \leq d \leq 354 \text{ mm}$. As reference, stresses by FE analyses as well as failure loads by Finite Fracture Mechanics and by experiment are taken. This method is enhanced in Nguyen-Hoang and Becker (2021a), who additionally take into account the stress BCs that show perpendicularly to the load direction. Excellent agreement to FE analyses is achieved for the dimensions of $w/d = e/d = 3$. For fast reproduction of the net-section stresses and their concentrations, polynomial fitting functions with excellent accuracy are provided in a method sheet by Nguyen-Hoang and Becker (2022c).

This is published in the well known technical handbook HSB³ by the IASB⁴ working group. The stress calculus is extended in Nguyen-Hoang and Becker (2021d) dealing with orthotropic composite laminates. For the typically used $[0^\circ / \pm 45^\circ / 90^\circ]_s$ (50%/40%/10%) and quasi-isotropic layup with the relative dimensions $w/d = e/d = 3$, the net-section stress decay relevant for crack initiation assessment by nonlocal criteria show excellent agreement to FE data. The calculus is also documented in LTH Design Criteria (Nguyen-Hoang and Becker, 2021e), which is tailored for engineering applications.

The works by Nguyen-Hoang and Becker (2020b, 2022d, 2021h) dealing with open holes and by Nguyen-Hoang and Becker (2020a, 2021a,d) treating filled holes shall serve as a foundation for the present thesis, which includes the stress analysis of bolted joints under bearing-bypass load interaction.

Tension failure analysis

In general, assessing whether brittle crack initiation occurs can be done by means of local and nonlocal concepts. The former involves the evaluation of the stress concentrations directly at the hole boundary (Neuber, 1933, 1934; Peterson and Wahl, 1936; Neuber, 2013). By contrast, the latter requires the stress evaluation at or along a certain hole distance and stands out for being capable of capturing the size effect and the corresponding failure load reduction with increasing hole diameter. Thus, nonlocal criteria are preferred when aiming to create lightweight optimal designs. For details regarding the phenomenon size effect, see Bažant et al. (1996); Wisnom (1999); Dvorak and Suvorov (1999); Bažant (2000); Bažant et al. (2004) as well as Green et al. (2007). To mention some nonlocal concepts, the Theory of Critical Distances (TCD) and the recent state-of-the-art criterion of Finite Fracture Mechanics (FFM) are commonly employed. In the context of the TCD (Whitney and Nuismer, 1974; Taylor, 2004, 2007, 2008, 2011), failure is postulated if the net-section stresses at or averaged along the characteristic distance equal the plain strength of the material. This length is generally identified by experiments and is assumed to be invariant with respect to the absolute value of the defect size, which is the bolt or hole diameter in the present problem setting. However, the assumption contradicts findings made by Camanho and Lambert (2006). Therein, the characteristic distance is identified as a structural rather than material parameter since a dependence on geometric properties such as finite boundaries is revealed. Therefore, the characteristic distance is generally not applicable to other configurations, though it may apply under certain conditions. This matter shall be further analysed in the

³ HSB $\hat{=}$ Handbuch Strukturberechnung

⁴ IASB $\hat{=}$ Industriausschuss Strukturberechnung

present bolted-joint context. In doing so, the recent brittle failure prediction concept of Finite Fracture Mechanics (Leguillon, 2002; Cornetti et al., 2006; Weißgraeber et al., 2015c) serves as reference. This approach, suggested by Leguillon (2002), postulates failure defined as the initiation of a finite-sized crack if both the stress state as well as the energy release rate reach a corresponding critical value (Cornetti et al., 2006). Furthermore, it is advantageous that only standard material data but not structural parameters such as a critical distance as in TCD approaches are required as inputs to this model. Several studies in the literature demonstrate that the FFM concept is applicable for various problems involving brittle crack initiation (Weißgraeber et al., 2015c).

In the following, some studies relevant to the tension failure assessment of the present bolted-joint problem are mentioned. Regarding single-fastener bolted joints idealised by the pin-loaded hole, the TCD has been applied by York et al. (1982); Curtis and Grant (1984); Eriksson et al. (1995); Nguyen-Hoang and Becker (2020a) and FFM has been applied by Camanho et al. (2012); Nguyen-Hoang and Becker (2020a). Furthermore, this method is also employed for bolted joints under combined bearing-bypass load by Peng et al. (2021) using FE analyses. Another approach is given by cohesive zone models used by Kabeel et al. (2014) for the pure bearing load case. This is extended in Kabeel et al. (2015) to combined bearing-bypass loads. To name some examples related to bolted joints, the following works employ FFM. Concerning the open-hole problem under uniform tension, Li and Zhang (2006) treat infinite plate geometry and isotropic material. Hebel and Becker (2008) analyse anisotropic composite laminates using a numerical approach contrary to Camanho et al. (2012) using the enhanced Tan solution to calculate the stresses of the open-hole problem with a finite width of $w/d = \{5, 6\}$ and a quasi-isotropic laminate. Martin et al. (2012) extend the complexity to finite-width and orthotropic laminates. Weißgraeber et al. (2015a) analyse elliptical holes. Felger et al. (2017a) investigate symmetric as well as asymmetric crack patterns in a finite anisotropic plate weakened by a circular opening using an asymptotic approach that combines means of complex potentials and matched asymptotics. This is also applied to treat elliptical holes in Felger et al. (2017b). Furthermore, the load case of combined tension and in-plane bending is taken into account in Rosendahl et al. (2017) through numerical analyses. Bi-axial loading is taken into account by Sapora and Cornetti (2018). A comprehensive framework for open holes in finite orthotropic composite laminates is provided by Nguyen-Hoang and Becker (2022d). This article as well as the content in Nguyen-Hoang and Becker (2020a) dealing with single-fastener joints shall be extended to bolted joints under bearing-bypass load interaction in the present thesis.

1.3 Objectives and outline

In Chapter 2, the theoretical framework of this thesis is provided in brief. This is composed of the following topics. First, some fundamentals of the Theory of Elasticity with a focus on plane problems are introduced. Furthermore, the Classical Laminate Theory is included. Second, the complex potential method in the formalism by Lekhnitskii (1968) is covered. This is required for the modelling of the stress state of anisotropic plates and composite laminates. Third, the state of the art of the nonlocal failure concept of Finite Fracture Mechanics is outlined. The corresponding formulae shall be restricted to the case of pure mode I fracture.

Chapter 3 is dedicated to the development of the stress calculus based on the complex potential method. For quasi-isotropic laminates, however, Airy stress functions that enable the convenient modelling of their stress state are provided. For both means, special focus lies on capturing the effects of finite plate dimensions on the characteristic stresses and their concentrations. At first, the mechanical idealisation of the bolted joint as a linear 2D plane problem is presented. The underlying assumptions, capabilities and limits of this modelling approach are explained in detail. Then, the stress field of this 2D idealisation is determined. Since the present bolted joint under bearing-bypass load is modelled as a superposition of the open- and filled-hole problem these partial solutions need to be derived first. This is accomplished by taking their corresponding infinite-domain solution and then iteratively supplementing them with a set of three types of auxiliary or correction functions and potentials to take into account the stress-free edges of the actual finite-domain problem. At the core of these auxiliary functions is a novel periodic arrangement technique, which enables the efficient and robust modelling of longitudinal stress-free edges.

The stress results are extensively discussed in Chapter 4. For validation purposes, FE analyses are conducted. For a qualitative assessment of whether the stress-free BCs along the straight edges are satisfied, the force flux is investigated. For quantitative assessment, the characteristic stresses are compared against FE values. These steps are first done for the special cases of open and filled holes. This also involves the assessment of the performance of the present method against heuristic approaches. Then, the bolted joint under bearing-bypass load is treated.

Based on the results of the present stress calculus, a failure analysis is conducted in Chapter 5. The goal is to precisely predict the minimal and critical loads that lead to net-section failure. In doing so, a methodology for the derivation of the failure loads by the nonlocal concepts of Theory of Critical Distances (TCD) and of Finite Fracture Mechanics (FFM) is

1.3 Objectives and outline

briefly introduced. Then, some example predictions are validated against failure loads determined by experiments. Eventually, the hole size effect is modelled and in this context the failure load reduction with increasing hole diameter is analysed. Special focus is given to rendering the effect of finite plate dimensions upon the failure loads. The open- and filled-hole problems are discussed first. Eventually, bolted joints under bearing-bypass load are investigated. This involves quantifying the nonlinear interaction of the failure stresses with respect to the load factor. Furthermore, failure envelopes for the graphical determination of the bearing and bypass stresses at crack initiation are provided. For all settings treated, the predictions by TCD are compared against the more sophisticated FFM concept, which enables the assessment of the limits of the first criterion.

Lastly, Chapter 6 provides a summary and an outlook of the present thesis, which develops a comprehensive framework for the assessment of the tension failure mode of composite bolted joints mode based on analytical methods.

Chapter 2

Theoretical background

The theoretical background is given in brief. This shall be limited to the concepts that are employed in the present thesis, which begins with some fundamentals of linear elasticity in Sect. 2.1. Therein, the stress state of a solid body in equilibrium is explained. This is followed by small deformation theory, linear elastic material behaviour (Hooke's law) and plane stress state. Furthermore, the Classical Laminate Theory is outlined. In Section 2.2, the complex potential method in the form of the Lekhnitskii formalism is introduced. This will be employed for the stress state representation of orthotropic composite laminates under in-plane loading, which are idealised as a plane plate problem. The state-of-the-art concept of Finite Fracture Mechanics used for the prediction of crack initiation in brittle materials is outlined in Sect. 2.3. A standard nomenclature is employed. Scalar quantities are denoted by italic letters, vectors and tensors by bold italics.

2.1 Fundamentals of linear elasticity

This Section is based on the textbooks Timoshenko and Goodier (1951); Becker and Gross (2002) as well as Sadd (2005), to which one may refer for a deeper insight.

2.1.1 Equilibrium and stress state

Let us consider a solid body in equilibrium, which is exerted to any external loading. As a reaction, internal forces arise, which normalised to an infinitesimal small area ΔA yield the stress vector \mathbf{t} . This quantity is defined at any material point of the body and depends on the orientation of the area given by its normal vector \mathbf{n} . To uniquely describe the stress state of any point of the material, use is made of the second order Cauchy stress tensor

$$\boldsymbol{\sigma} = \sigma_{ij} \mathbf{e}_i \otimes \mathbf{e}_j \quad \text{with } i, j \in \{1, 2, 3\} \text{ and basis vectors } \mathbf{e}_1, \mathbf{e}_2, \mathbf{e}_3. \quad (2.1)$$

Chapter 2 Theoretical background

Therein, the components σ_{ij} with respect to a Cartesian coordinate system may be conveniently stored in the matrix form

$$[\sigma_{ij}] = \begin{bmatrix} \sigma_{11} & \sigma_{12} & \sigma_{13} \\ \sigma_{21} & \sigma_{22} & \sigma_{23} \\ \sigma_{31} & \sigma_{32} & \sigma_{33} \end{bmatrix} = \begin{bmatrix} \sigma_{11} & \tau_{12} & \tau_{13} \\ \tau_{21} & \sigma_{22} & \tau_{23} \\ \tau_{31} & \tau_{32} & \sigma_{33} \end{bmatrix}, \quad (2.2)$$

where the diagonal entries $\sigma_{11}, \sigma_{22}, \sigma_{33}$ denote the normal stresses and the nondiagonal ones such as $\tau_{12}, \tau_{23}, \tau_{13}$ are the shear stresses. Equilibrium of moments requires the Cauchy stress tensor to be symmetric, thus $\sigma_{ij} = \sigma_{ji}$. With the normal vector \mathbf{n} the relationship between stress vector and stress tensor is given by the Cauchy theorem

$$\mathbf{t} = \boldsymbol{\sigma} \cdot \mathbf{n} \quad \text{or} \quad t_i = \sigma_{ji} n_j. \quad (2.3)$$

Note that in this Chapter, Einstein's summation convention is adopted. Since the entire solid body is in equilibrium so must be any of its infinitesimally small volume element dV . This is expressed by

$$\sigma_{ji,j} + f_i = 0, \quad (2.4)$$

where f_i denote the body forces. However, these are considered to be negligible for the present bolted-joint problem.

2.1.2 Small deformation theory

When a solid body is elastic external loadings lead to deformations. In many technical structures as for the present bolted-joint problem, the deformations are small and for their quantification use is made of the second order and symmetric linearised strain tensor

$$\boldsymbol{\varepsilon} = \varepsilon_{ij} \mathbf{e}_i \otimes \mathbf{e}_j \quad \text{with components} \quad [\varepsilon_{ij}] = \begin{bmatrix} \varepsilon_{11} & \varepsilon_{12} & \varepsilon_{13} \\ \varepsilon_{12} & \varepsilon_{22} & \varepsilon_{23} \\ \varepsilon_{13} & \varepsilon_{23} & \varepsilon_{33} \end{bmatrix}. \quad (2.5)$$

With the displacement vector $\mathbf{u} = [u_1, u_2, u_3]^T$, the strains can be derived by

$$\varepsilon_{ij} = \frac{1}{2} \left(\frac{\partial u_i}{\partial x_j} + \frac{\partial u_j}{\partial x_i} \right). \quad (2.6)$$

In many technical cases, the nondiagonal components are expressed by engineering shear strains with $\varepsilon_{ij} = \gamma_{ij}/2$ for $i \neq j$. For single-valued and continuous displacements, the strains need to satisfy the compatibility equations

$$\varepsilon_{ij,kl} + \varepsilon_{kl,ij} - \varepsilon_{ik,jl} - \varepsilon_{jl,ik} = 0. \quad (2.7)$$

2.1.3 Linear elastic material behaviour (Hooke's law)

For many materials as the composite laminates investigated in this thesis, a linear elastic material behaviour can be employed. Then, the stress-strain relationship can be described by Hooke's law, which for the most general case of anisotropic materials reads as follows:

$$\boldsymbol{\sigma} = \mathbf{c} : \boldsymbol{\varepsilon} \quad \text{or} \quad \sigma_{ij} = c_{ijkl} \varepsilon_{kl}. \quad (2.8)$$

Therein, the quantity \mathbf{c} represents the fourth order elasticity tensor with 81 components that includes all elastic constants required for the characterisation of the material. Inversion leads to

$$\boldsymbol{\varepsilon} = \mathbf{s} : \boldsymbol{\sigma} \quad \text{or} \quad \varepsilon_{ij} = s_{ijkl} \sigma_{kl}, \quad (2.9)$$

where the quantity \mathbf{s} represents the fourth-order compliance tensor. Taking into account the symmetry properties of the stress and strain tensor as well as the existence of the strain energy function reveals that the 81 components of the tensors \mathbf{c} and \mathbf{s} consists of only 21 independent quantities for the general anisotropic case. This enables to conveniently express Hooke's law in the following matrix form, which is also referred to as Voigt notation.

$$\begin{bmatrix} \sigma_{11} \\ \sigma_{22} \\ \sigma_{33} \\ \tau_{23} \\ \tau_{13} \\ \tau_{12} \end{bmatrix} = \begin{bmatrix} C_{11} & C_{12} & C_{13} & C_{14} & C_{15} & C_{16} \\ C_{21} & C_{22} & C_{23} & C_{24} & C_{25} & C_{26} \\ C_{31} & C_{32} & C_{33} & C_{34} & C_{35} & C_{36} \\ C_{41} & C_{42} & C_{43} & C_{44} & C_{45} & C_{46} \\ C_{51} & C_{52} & C_{53} & C_{54} & C_{55} & C_{56} \\ C_{61} & C_{62} & C_{63} & C_{64} & C_{65} & C_{66} \end{bmatrix} \begin{bmatrix} \varepsilon_{11} \\ \varepsilon_{22} \\ \varepsilon_{33} \\ \gamma_{23} \\ \gamma_{13} \\ \gamma_{12} \end{bmatrix} \quad \text{with} \quad C_{ij} = C_{ji}. \quad (2.10)$$

Inversion allows to express Hooke's law using the compliances S_{ij} , which are in the same matrix structure as the elastic constants C_{ij} . In many technical cases, materials have symmetry planes. If three mutually perpendicular planes exist the material is called orthotropic. Then, the number of independent elastic constants further reduces to 9. This is of interest for the later investigated class of composite laminates with layups which are symmetric to their midplane. Furthermore, Hooke's law may be expressed using compliances, which are commonly written in form of using engineering constants. This reads

$$\begin{bmatrix} \varepsilon_{11} \\ \varepsilon_{22} \\ \varepsilon_{33} \\ \gamma_{23} \\ \gamma_{13} \\ \gamma_{12} \end{bmatrix} = \begin{bmatrix} \frac{1}{E_1} & -\frac{\nu_{21}}{E_2} & -\frac{\nu_{31}}{E_3} & 0 & 0 & 0 \\ -\frac{\nu_{12}}{E_1} & \frac{1}{E_2} & -\frac{\nu_{32}}{E_3} & 0 & 0 & 0 \\ -\frac{\nu_{13}}{E_1} & -\frac{\nu_{23}}{E_2} & \frac{1}{E_3} & 0 & 0 & 0 \\ 0 & 0 & 0 & \frac{1}{G_{23}} & 0 & 0 \\ 0 & 0 & 0 & 0 & \frac{1}{G_{13}} & 0 \\ 0 & 0 & 0 & 0 & 0 & \frac{1}{G_{12}} \end{bmatrix} \begin{bmatrix} \sigma_{11} \\ \sigma_{22} \\ \sigma_{33} \\ \tau_{23} \\ \tau_{13} \\ \tau_{12} \end{bmatrix}. \quad (2.11)$$

Therein, the quantities E_1, E_2 and E_3 denote Young's moduli and ν_{ij} are Poisson's ratios. The latter are defined as follows. Let i denote the longitudinal direction. Further, the material shall be exerted to a normal uniform stress in the longitudinal direction, e.g. σ_{11} . The Poisson's ratios then are the ratio of an arising transverse strain in the direction j to that in the longitudinal i -direction, e.g. $\nu_{12} = -\varepsilon_{22}/\varepsilon_{11}$. For the special case of complete symmetry, the material is isotropic. Its behaviour can then be characterised by the two independent elastic constants E and ν .

2.1.4 Plane stress state

Let us consider plate structures with a thickness that is small in comparison to the lateral dimensions. Furthermore, the external loads shall lie within the plane of the plate only. Then, a plane stress state can be assumed as a good approximation and a 2D mechanical idealisation can be employed. This is beneficial when aiming to find solutions based on analytical methods since the modelling complexity reduces. In particular, the stresses in thickness (typically x_3 -) direction are assumed to vanish: $\sigma_{33} = \tau_{13} = \tau_{23} = 0$.

2.1.5 Classical Laminate Theory for plane composite problems

This Section is based on Becker and Gross (2002) as well as Mittelstedt and Becker (2016). Also refer to the textbooks by Halpin (1992); Reddy (2004) and Tsai (2008). Let us consider a composite laminate made of a layup which is symmetric with respect to its midplane. Furthermore, the external loads shall lie within it. Then, the setting, its stresses and deformations can be described as a plane problem. Use will be made of this idealisation to treat the present bolted-joint problem. Note that bending deformations or lay-ups without symmetry to the midplane cannot be treated as a pure plane problem. Regarding the latter setting, bending-extension coupling shall be taken into account. Refer to the textbooks cited above for further details.

2.1 Fundamentals of linear elasticity

Now, Hooke's law for symmetric laminates under in-plane loads is derived. First, let us consider a unidirectional layer, for which a plane stress state is assumed. The x_1 -coordinate shows along the fibre (or longitudinal) direction, the x_2 -coordinate in the lateral direction and the x_3 -coordinates in the thickness (or out-of-plane) direction. With respect to these material principal axes, Hooke's law reads

$$\begin{bmatrix} \sigma_1 \\ \sigma_2 \\ \tau_{12} \end{bmatrix} = \begin{bmatrix} Q_{11} & Q_{12} & 0 \\ Q_{21} & Q_{22} & 0 \\ 0 & 0 & Q_{66} \end{bmatrix} \begin{bmatrix} \varepsilon_1 \\ \varepsilon_2 \\ \gamma_{12} \end{bmatrix}. \quad (2.12)$$

Therein, the quantities Q_{ij} represent the reduced stiffnesses, which are inter-related to the engineering constants as follows:

$$\begin{aligned} Q_{11} &= \frac{E_1}{1 - \nu_{12} \nu_{21}}, & Q_{12} &= \frac{\nu_{12} E_2}{1 - \nu_{12} \nu_{21}}, \\ Q_{22} &= \frac{E_2}{1 - \nu_{12} \nu_{21}}, & Q_{66} &= G_{12}. \end{aligned} \quad (2.13)$$

Hooke's law of the single ply with respect to the global x, y, z -coordinate system of the whole laminate is expressed by

$$\begin{bmatrix} \sigma_x \\ \sigma_y \\ \tau_{xy} \end{bmatrix}_k = \begin{bmatrix} \bar{Q}_{11} & \bar{Q}_{12} & \bar{Q}_{16} \\ \bar{Q}_{12} & \bar{Q}_{22} & \bar{Q}_{26} \\ \bar{Q}_{16} & \bar{Q}_{26} & \bar{Q}_{66} \end{bmatrix}_k \begin{bmatrix} \varepsilon_x \\ \varepsilon_y \\ \gamma_{xy} \end{bmatrix}. \quad (2.14)$$

Therein, the quantity k represents the index of a single ply. Commonly, its offset towards the x -axis is measured by the angle (or fibre orientation) ϑ , which is counted anti-clockwise. The reduced stiffnesses \bar{Q}_{ij} of a single ply with respect to the global x, y, z -coordinate system can be calculated by the relations

$$\begin{aligned} \bar{Q}_{11} &= Q_{11} \cos^4 \vartheta + 2(Q_{12} + 2Q_{66}) \cos^2 \vartheta \sin^2 \vartheta + Q_{22} \sin^4 \vartheta, \\ \bar{Q}_{12} &= (Q_{11} + Q_{22} - 4Q_{66}) \cos^2 \vartheta \sin^2 \vartheta + Q_{12}(\cos^4 \vartheta + \sin^4 \vartheta), \\ \bar{Q}_{22} &= Q_{11} \sin^4 \vartheta + 2(Q_{12} + 2Q_{66}) \cos^2 \vartheta \sin^2 \vartheta + Q_{22} \cos^4 \vartheta, \\ \bar{Q}_{16} &= (Q_{11} - Q_{12} - 2Q_{66}) \cos^3 \vartheta \sin \vartheta + (Q_{12} - Q_{22} + 2Q_{66}) \cos \vartheta \sin^3 \vartheta, \\ \bar{Q}_{26} &= (Q_{11} - Q_{12} - 2Q_{66}) \cos \vartheta \sin^3 \vartheta + (Q_{12} - Q_{22} + 2Q_{66}) \cos^3 \vartheta \sin \vartheta, \\ \bar{Q}_{66} &= (Q_{11} + Q_{22} - 2Q_{12} - 2Q_{66}) \cos^2 \vartheta \sin^2 \vartheta + Q_{66}(\cos^4 \vartheta + \sin^4 \vartheta). \end{aligned} \quad (2.15)$$

Chapter 2 Theoretical background

The integration of Eq. (2.14) along the thickness direction (z -direction) leads to the effective constitutive law of the composite laminate. Taking into account that layups symmetric with respect to their midplane under in-plane loads are treated in this work, the effective constitutive law can be described as follows. With the normal stress resultants N_x, N_y, N_{xy} , the integration yields

$$\begin{bmatrix} N_x \\ N_y \\ N_{xy} \end{bmatrix} = \underbrace{\begin{bmatrix} A_{11} & A_{12} & A_{16} \\ A_{12} & A_{22} & A_{26} \\ A_{16} & A_{26} & A_{66} \end{bmatrix}}_{=\mathbf{A}} \begin{bmatrix} \varepsilon_x \\ \varepsilon_y \\ \gamma_{xy} \end{bmatrix}, \quad (2.16)$$

where the quantity \mathbf{A} represents the matrix of the extensional stiffnesses. Its components can be obtained by

$$A_{ij} = \sum_{k=1}^N (\bar{Q}_{ij})_k (z_k - z_{k-1}). \quad (2.17)$$

Therein, the quantity N is the of number of single plies. Further, z_k and z_{k-1} denote the upper and lower coordinates in the thickness direction of a ply k . When orthotropic composite laminates are exerted to in-plane loadings only these are then commonly idealised as an orthotropic plate, for which the effective stiffnesses of the laminate need to be assigned. Their calculation can be done as follows. Let t be the thickness of the laminate and A_{ij}^{-1} the components of the inverse of the extensional stiffness matrix \mathbf{A} . Then, the in-plane effective stiffnesses read (Schürmann, 2007)

$$\hat{E}_x = \frac{1}{A_{11}^{-1}t}, \quad \hat{E}_y = \frac{1}{A_{22}^{-1}t}, \quad \hat{G}_{xy} = \frac{1}{A_{66}^{-1}t}, \quad \hat{\nu}_{xy} = -\frac{A_{12}^{-1}}{A_{11}^{-1}}, \quad \hat{\nu}_{yx} = -\frac{A_{12}^{-1}}{A_{22}^{-1}}. \quad (2.18)$$

The in-plane strains of the idealisation as an orthotropic plate equal those of the laminate. Once the field quantities of the orthotropic plate are determined, the stresses of each ply may be calculated by inserting the strains in Eq. (2.14).

2.2 Complex potential method

The complex potential method in the formalism by Lekhnitskii is shortly introduced based on Savin (1961); Lekhnitskii (1968) and Sadd (2005). Let us assume a two-dimensional plane strain or plane stress state with linear

elastic and anisotropic material behaviour. Hooke's law for the plate then can be expressed by

$$\begin{bmatrix} \varepsilon_x \\ \varepsilon_y \\ \gamma_{xy} \end{bmatrix} = \begin{bmatrix} S_{11} & S_{12} & S_{16} \\ S_{21} & S_{22} & S_{26} \\ S_{16} & S_{26} & S_{66} \end{bmatrix} \begin{bmatrix} \sigma_x \\ \sigma_y \\ \tau_{xy} \end{bmatrix}, \quad (2.19)$$

where the quantities $\varepsilon_x, \varepsilon_y, \gamma_{xy}$ denote the in-plane strains and S_{ij} the compliances. If the material is a composite laminate, the corresponding effective compliances need to be inserted. These may be calculated as described in Subsect. 2.1.5 or in Halpin (1992) and Tsai (2008), for example. The stresses then are related to an idealisation as a plate with smeared stiffnesses whose plane strains equal those of the laminate. The stresses of each single ply may be derived using Classical Laminate Theory. Furthermore, the compatibility condition for plane problems specialises to

$$\frac{\partial^2 \varepsilon_x}{\partial y^2} + \frac{\partial^2 \varepsilon_y}{\partial x^2} = \frac{\partial^2 \gamma_{xy}}{\partial x \partial y}. \quad (2.20)$$

With vanishing body forces, the stress components may be expressed by the Airy stress function F automatically satisfying the equilibrium (Timoshenko and Goodier, 1951; Becker and Gross, 2002; Sadd, 2005), in particular

$$\sigma_x = \frac{\partial^2 F}{\partial y^2}, \quad \sigma_y = \frac{\partial^2 F}{\partial x^2}, \quad \tau_{xy} = -\frac{\partial^2 F}{\partial x \partial y}, \quad (2.21)$$

$$\sigma_r = \frac{1}{r} \frac{\partial F}{\partial r} + \frac{1}{r^2} \frac{\partial^2 F}{\partial \varphi^2}, \quad \sigma_\varphi = \frac{\partial^2 F}{\partial r^2}, \quad \tau_{r\varphi} = -\frac{\partial}{\partial r} \left(\frac{1}{r} \frac{\partial F}{\partial \varphi} \right). \quad (2.22)$$

Expressing the strains by Eq. (2.19), inserting in Eq. (2.20) and formulating the Cartesian stress components using Eq. (2.21) leads to the governing equation

$$\begin{aligned} S_{22} \frac{\partial^4 F}{\partial x^4} - 2S_{26} \frac{\partial^4 F}{\partial x^3 \partial y} + (2S_{12} + S_{66}) \frac{\partial^4 F}{\partial x^2 \partial y^2} - \\ 2S_{16} \frac{\partial^4 F}{\partial x \partial y^3} + S_{11} \frac{\partial^4 F}{\partial y^4} = 0. \end{aligned} \quad (2.23)$$

In order to find its solutions, let us attempt to express the Airy stress function in the form $F = F(x + \mu y)$. At this stage, the quantity μ is an unknown constant to be determined. Inserting this ansatz into Eq. (2.23) eventually yields the characteristic equation

$$S_{11} \mu^4 - 2S_{16} \mu^3 + (2S_{12} + S_{66}) \mu^2 - 2S_{26} \mu + S_{22} = 0. \quad (2.24)$$

Chapter 2 Theoretical background

Based on finite nonzero elastic moduli, the roots of the Eq. (2.24) above and the constant μ turn out to be complex (Lekhnitskii, 1968). This quantity characterises the degree of the anisotropy of the plate and appears in the conjugate pairs $\mu_3 = \bar{\mu}_1, \mu_4 = \bar{\mu}_2$ with $\mu_k = \alpha_k + i\beta_k, \{\alpha_k, \beta_k\} \in \mathbb{R}$. Then, the solution is of the general form

$$\begin{aligned}
 F &= F_1(x + \mu_1 y) + F_2(x + \mu_2 y) + F_3(x + \mu_3 y) + F_4(x + \mu_4 y) \\
 &= F_1(x + \mu_1 y) + F_2(x + \mu_2 y) + F_3(x + \bar{\mu}_1 y) + F_4(x + \bar{\mu}_2 y) \\
 &= 2 \operatorname{Re} [F_1(x + \mu_1 y) + F_2(x + \mu_2 y)] \\
 &= 2 \operatorname{Re} [F_1(z_1) + F_2(z_2)] \quad \text{with complex variables} \quad z_k = x + \mu_k y.
 \end{aligned} \tag{2.25}$$

For reasons of convenience, the complex potentials

$$\Phi_1(z_1) = \frac{dF_1}{dz_1} = F'_1, \quad \Phi_2(z_2) = \frac{dF_2}{dz_2} = F'_2 \tag{2.26}$$

are introduced, by which the corresponding stress components can be represented as follows:

$$\begin{aligned}
 \sigma_x &= 2 \operatorname{Re} [\mu_1^2 \Phi'_1(z_1) + \mu_2^2 \Phi'_2(z_2)], \\
 \sigma_y &= 2 \operatorname{Re} [\Phi'_1(z_1) + \Phi'_2(z_2)], \\
 \tau_{xy} &= -2 \operatorname{Re} [\mu_1 \Phi'_1(z_1) + \mu_2 \Phi'_2(z_2)],
 \end{aligned} \tag{2.27}$$

$$\begin{aligned}
 \sigma_r &= 2 \operatorname{Re} [(\sin \varphi - \mu_1 \cos \varphi)^2 \Phi'_1(z_1) + (\sin \varphi - \mu_2 \cos \varphi)^2 \Phi'_2(z_2)], \\
 \sigma_\varphi &= 2 \operatorname{Re} [(\cos \varphi + \mu_1 \sin \varphi)^2 \Phi'_1(z_1) + (\cos \varphi + \mu_2 \sin \varphi)^2 \Phi'_2(z_2)], \\
 \tau_{r\varphi} &= 2 \operatorname{Re} [(\sin \varphi - \mu_1 \cos \varphi)(\cos \varphi + \mu_1 \sin \varphi) \Phi'_1(z_1) + \\
 &\quad (\sin \varphi - \mu_2 \cos \varphi)(\cos \varphi + \mu_2 \sin \varphi) \Phi'_2(z_2)].
 \end{aligned} \tag{2.28}$$

In the framework of complex potential method, tractions along any curved contour with the coordinate s are typically applied using the loading functions

$$\begin{aligned}
 p_x(s) &= 2 \operatorname{Re} [\mu_1 \Phi_1(z_1) + \mu_2 \Phi_2(z_2)], \\
 p_y(s) &= 2 \operatorname{Re} [\Phi_1(z_1) + \Phi_2(z_2)].
 \end{aligned} \tag{2.29}$$

For illustration of the following explanations, also see Fig. 2.1. In the general case of multiply connected regions surrounded by a single external and one or more internal boundaries, the relationship between the stress components $\sigma_x, \sigma_y, \tau_{xy}$ and the loading functions is provided by

$$\begin{aligned}
 p_x(s) &= \pm \int_0^s X_n d\tilde{s}, \quad X_n = \sigma_x \cos(\mathbf{n}, x) + \tau_{xy} \cos(\mathbf{n}, y), \\
 p_y(s) &= \mp \int_0^s Y_n d\tilde{s}, \quad Y_n = \tau_{xy} \cos(\mathbf{n}, x) + \sigma_y \cos(\mathbf{n}, y).
 \end{aligned} \tag{2.30}$$

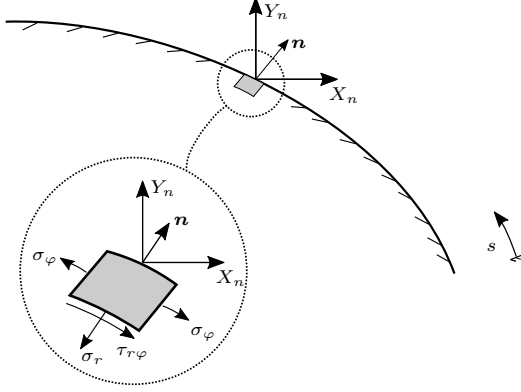


Fig. 2.1 External forces X_n, Y_n along external contour equilibrated by the stress components $\bar{\sigma}_r, \bar{\tau}_{r\varphi}$

Herein, the quantities X_n, Y_n represent the components of the external force along the arc length parameter s , which are in equilibrium with the stress components. The upper/lower sign in the formulae is selected if the contour is tangent to an external/internal boundary. To treat circular hole problems (Savin, 1961; Lekhnitskii, 1968; Sadd, 2005), use is made of conformal mapping which projects the infinite open-hole domain onto the circular unit domain and the tractions are applied on the corresponding single external boundary. With the hole radius $R = d/2$, the mapping functions

$$\zeta_k = \frac{z_k \pm \sqrt{z_k^2 - R^2(1 + \mu_k^2)}}{R(1 - i\mu_k)} \quad (2.31)$$

allow projecting back to the z_k -plane (Fig. 2.2). Therein, the sign of the conformal mapping functions $\zeta_k(z_k)$ in Eq. (2.31) is chosen such that the corresponding stresses derived using Eq. (2.27), (2.28) are continuously differentiable along any path and yield physically reasonable values. This may be ensured by checking if the prescribed stress boundary conditions (BCs) are correctly rendered. Using conformal mapping involving the circular unit domain with an external edge only, on which the tractions are applied, the upper sign in Eq. (2.30) is taken. With

$$\cos(\mathbf{n}, x) = \pm \frac{dy}{ds}, \quad \cos(\mathbf{n}, y) = \mp \frac{dx}{ds} \quad (2.32)$$

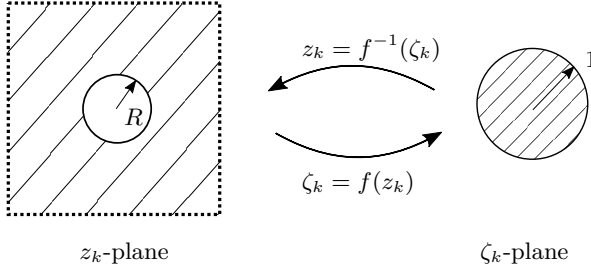


Fig. 2.2 Concept of conformal mapping. The mapping functions $f^{-1}(\zeta_k)$, $f(z_k)$ depend on the original shape of the domain.

we obtain

$$\begin{aligned} \int_0^{\bar{s}} X_n \, ds &= \int_0^{\bar{s}} \tilde{\sigma}_x \, dy - \tilde{\tau}_{xy} \, dx, \\ \int_0^{\bar{s}} Y_n \, ds &= \int_0^{\bar{s}} \tau_{xy} \, dy - \tilde{\sigma}_y \, dx. \end{aligned} \quad (2.33)$$

Along the circular hole with the radius $r = R$ and the relations

$$\begin{aligned} x &= R \cos \varphi, & y &= R \sin \varphi \\ \rightarrow dx &= -R \sin \varphi \, d\varphi, & dy &= R \cos \varphi \, d\varphi, \end{aligned} \quad (2.34)$$

Eq. (2.33) specialises to

$$\begin{aligned} \int_0^{\bar{s}} X_n \, ds &= R \int_0^{\bar{\varphi}} \tilde{\sigma}_r(R, \varphi) \cos \varphi - \tilde{\tau}_{r\varphi}(R, \varphi) \sin \varphi \, d\varphi, \\ \int_0^{\bar{s}} Y_n \, ds &= R \int_0^{\bar{\varphi}} \tilde{\tau}_{r\varphi}(R, \varphi) \cos \varphi + \tilde{\sigma}_r(R, \varphi) \sin \varphi \, d\varphi. \end{aligned} \quad (2.35)$$

Inserting in Eq. (2.30) eventually leads to the loading functions. The complex potentials are now to be selected in such a way that the corresponding stresses fulfil the prescribed stress BCs. For the present bolted-joint problem, this is extensively described in Chap. 3.

2.3 Finite Fracture Mechanics

In the context of Finite Fracture Mechanics (FFM), the instantaneous initiation of a crack with finite size is assumed (Weißgraeber et al., 2015c). This framework has been developed by Hashin (1996). To determine the critical loads and the corresponding crack length, Leguillon (2002) suggested the

so-called coupled criterion, which postulates crack initiation if both a stress and an energy criterion are satisfied at the same time. In the following, the corresponding formulae are discussed for the mode I crack occurring in a plane problem setting. This will be of interest in the failure analysis of the present bolted-joint problem (Chap. 5). For illustration, let us investigate the symmetric open-hole problem with a finite-sized crack Δa as depicted in Fig. 2.3. Therein, the quantity $\sigma_{0,F}$ denotes the far-field stress that leads to

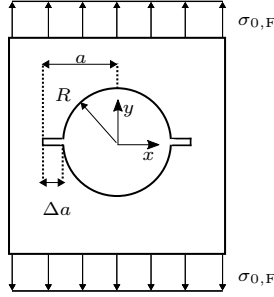


Fig. 2.3 Open-hole problem with crack of finite size Δa . Therein, the quantity $\sigma_{0,F}$ denotes the remote stresses that trigger crack initiation and thus failure according to FFM prediction.

crack initiation. The net-section stresses $\sigma_y(x, 0)$ may open the crack and for its initiation, these stresses must be equal or larger a certain strength value. Since mode I occurring in a composite laminate is analysed in the course of this thesis its longitudinal plain strength X_T^L in tension is selected. Following a suggestion by Cornetti et al. (2006), the averaged stresses are evaluated and the stress criterion reads

$$\frac{1}{\Delta a} \int_R^{R+\Delta a} \sigma_y(x, 0) dx \geq X_T^L. \quad (2.36)$$

The energy criterion may also be expressed using stress intensity factors and relating these to the fracture toughness. For pure mode I crack opening and the overall hypothetical defect size $a = R + \Delta a$, this reads

$$\frac{1}{\Delta a} \int_R^{R+\Delta a} K_I^2(a) da \geq K_{Ic}^2. \quad (2.37)$$

Therein, K_I denotes the corresponding stress intensity factor and K_{Ic} the fracture toughness. In general, the determination of the critical load and the

corresponding crack length is done by solving an optimisation problem. With the failure load $\sigma_{0,F}$ and the external remote load σ_0 this reads

$$\sigma_{0,F} = \min_{\sigma_0, \Delta a} \left\{ \sigma_0 \mid \frac{1}{\Delta a} \int_R^{R+\Delta a} \sigma_y(x, 0) dx \geq X_T^L \quad \wedge \right. \\ \left. \frac{1}{\Delta a} \int_R^{R+\Delta a} K_I^2(a) da \geq K_{Ic}^2 \right\}. \quad (2.38)$$

In many cases, the stresses show a monotonic decrease and the energy release rate a monotonic increase. Such problems are also referred to as positive geometries (Bažant, 1984; Jenq and Shah, 1985; Bažant et al., 1991). Then, the coupled criterion further specialises to equalities and the optimisation simplifies. The corresponding solution procedure will be shown for the present bolted-joint problem in Sect. 5.1, for which these characteristics are true.

The FFM has been applied to many problems that involve brittle fracture. To name some, sharp V-notches are treated by Yosibash et al. (2006); Carpinteri et al. (2008) and Cornetti et al. (2013). Round U-notches are focus of Carpinteri et al. (2012) as well as Sapora et al. (2015). Adhesive joints are covered in Weißgraeber and Becker (2013); Hell et al. (2014); Weißgraeber et al. (2015b); Carrere et al. (2015); Stein et al. (2015) and Felger et al. (2018). Mixed-mode failure is considered by Cornetti et al. (2013); Felger et al. (2017a) and Talmon et al. (2017). Free-edge delamination is scope of Hebel et al. (2010); Martin et al. (2010); Dölling et al. (2020, 2021) as well as Frey et al. (2021a,b). For research that covers plate problems with an unloaded hole as well as bolted joints, refer to Sect. 1.2. A comprehensive FFM review can be found in Weißgraeber et al. (2015c).

Chapter 3

Stress analysis - Development of complex calculus

A methodology for the determination of the stress field of the bolted joint under bearing-bypass load interaction is to be developed. As outlined in Sect. 1.1, a linear 2D modelling approach as plate problem is chosen and a plane stress state is assumed. For the stress state representation of plates which can be made of orthotropic composite laminates, the complex potential method is employed. For isotropic plates and quasi-isotropic laminates, however, Airy stress functions are suggested. Special consideration is given to capture finite plate dimensions and their impact on the stress field and its concentrations. This is done since an assessment means for tension (or net-section) failure shall be developed, which likely occurs for narrow connections.

At first, the mechanical idealisation and the underlying assumptions, capabilities and limitations are explained in Sect. 3.1. Therein, a linear 2D modelling approach is introduced and the bolted joint under bearing-bypass load is treated as superposition of the open- and filled hole. Further, the stress boundary conditions (BCs) are defined. An overview of the overall calculus is given in Sect. 3.2. Then, the solutions of the infinite-domain open- and filled-hole problems are provided in Sect. 3.3. To take finite dimensions into account, three different types of auxiliary potentials and functions are introduced in Sects. 3.4-3.6. However, each of them addresses a certain set of stress BCs only and may interfere with others. To satisfy all BCs simultaneously nevertheless, the correction functions and potentials are applied iteratively until errors become negligibly small. The corresponding calculation procedure is explained in Sect. 3.7.

The content of this Chapter as well as the stress results discussed in Chap. 4 have been published in the following scientific articles. By using Airy stress functions, finite-sized isotropic plates are covered in Nguyen-Hoang and Becker (2020a) dealing with the single-fastener bolted joint idealised by a filled (or pin-loaded) hole. Therein, a preliminary stress calculation method is developed that only takes into account BCs with stress components showing in the load (or longitudinal) direction. This is enhanced by further considering stress

BCs in the lateral direction regarding the open-hole problem (Nguyen-Hoang and Becker, 2020b) and for single-fastener bolted joints (Nguyen-Hoang and Becker, 2021a). The bearing-bypass load case is analysed in Nguyen-Hoang and Becker (2021b). Orthotropic composite laminates are covered in Nguyen-Hoang and Becker (2022d) regarding open holes and in Nguyen-Hoang and Becker (2021d) concerning filled holes. Tailored for industry contexts, the stress methodology for orthotropic composite laminates is documented in LTH Composite Design Criteria (FL) covering open holes (Nguyen-Hoang and Becker, 2021h), filled holes (Nguyen-Hoang and Becker, 2021e) and the combined bearing-bypass load case (Nguyen-Hoang and Becker, 2022a). Furthermore, polynomial fitting functions for the isotropic pin-loaded-hole problem are provided in a HSB method sheet (Nguyen-Hoang and Becker, 2022c).

3.1 Mechanical idealisation

Generally, the structural situation of bolted joints is quite complex. For instance, the bearing load transfer involves a contact problem and actually a three-dimensional stress state. This refers to the in-plane stress components that may depend on the thickness direction but also to the out-of-plane stress components. In this situation, clamping pressure may be applied, which increases the contact area. Then, the stress concentrations are reduced leading to higher static failure loads. However, capturing all effects is rather expensive and not easily feasible when aiming to develop efficient analytical methods. Hence, a mechanical idealisation as 2D linear plane stress problem is suggested, which is capable of rendering the main mechanisms in the tension failure mode of bolted joints nevertheless. Particularly, the stress concentrations due to finite dimensions shall be accurately captured since fatal net-section failure is likely triggered for narrow connections. Once the developed methodology has proven to be feasible, other effects may be included. When choosing a linear 2D approach as plane plate problem, the engineer should be aware that contact elasticity, 3D effects as well as secondary bending are not covered. Then, referring to the latter, only connections with an overall symmetry with respect to the midplane are eligible for a plane stress model. In particular, this is true if the number of plates is uneven and the plate material without bending extension coupling. Then, symmetric layouts shall be chosen when use is made of composite laminates. See Fig. 3.1 and 3.2 for illustration of secondary bending effects.

For connections that can be treated as linear 2D plane stress problem, the following mechanical idealisation is selected as commonly suggested in the

3.1 Mechanical idealisation

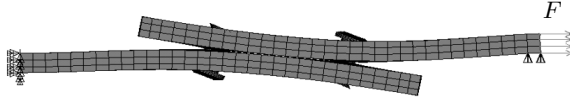


Fig. 3.1 FE model of single-lap shear joint with pronounced secondary bending.

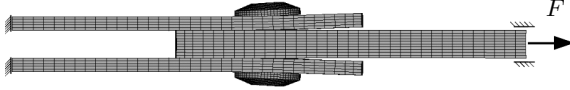


Fig. 3.2 FE model of double-lap shear joint with negligible secondary bending.

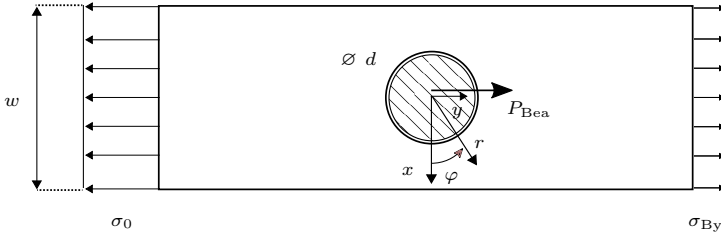


Fig. 3.3 Finite dimensions bolted joint under combined bearing-bypass load.

literature (Camanho and Lambert, 2006). The bolted joint under combined bearing-bypass load is modelled as a superposition of the open- and filled (or pin-loaded) hole in a plate with finite dimensions. Regarding the latter subproblem, a frictionless perfect fit of the fastener is assumed and the bolt contact is idealised by radial tractions of sinusoidal shape along half of the hole edge. That approach was addressed by Waszczak and Cruse (1971). Concerning the bypass load case, remote uniform tensile stresses are assumed. This is eligible for sufficient longitudinal bolt distance wider than ten times of the hole and bolt diameter. The 2D mechanical idealisation is shown in Fig. 3.3. Therein, the parameter w represents the finite plate width and d the hole diameter of the central, circular opening. Assuming a perfect fit of the bolt its diameter d_B equals that of the hole, $d_B = d$. The quantity σ_0 denotes the uniaxial far-field stress along $y \rightarrow -\infty$, which equilibrates both the bearing load P_{Bea} introduced by the bolt and the remaining remote bypass load $P_{By} = \sigma_{By} \cdot w$ at $y \rightarrow \infty$. The total force is $P = P_{Bea} + P_{By}$. Note that in this thesis, all forces are given per plate thickness. With the hole and bolt radius $R = d/2$, the stress BCs are as follows.

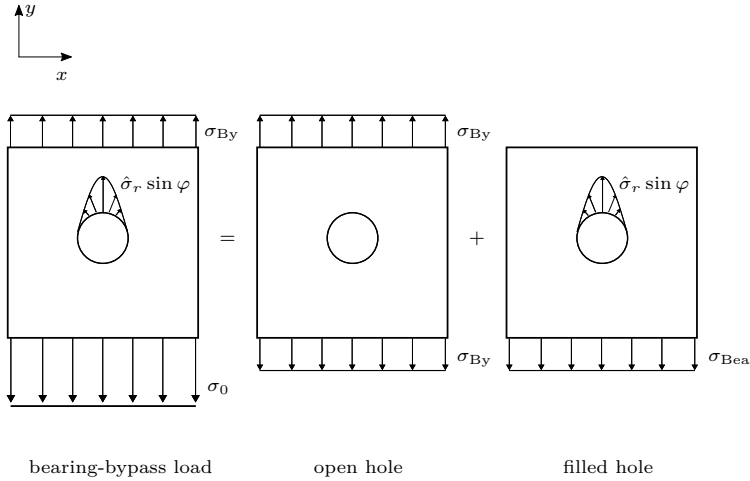


Fig. 3.4 Stress field determination by superposition of the open- and filled-hole problem. The amplitude of the radial hole tractions is $\hat{\sigma}_r = \frac{2 P_{\text{Bea}}}{\pi R}$.

Open hole:

$$\lim_{y \rightarrow \pm\infty} \sigma_y(x, y) = \sigma_{\text{By}}, \quad \sigma_r(R, \varphi) = \tau_{r\varphi}(R, \varphi) = 0, \quad (3.1)$$

$$\sigma_x(\pm w/2, y) = \tau_{xy}(\pm w/2, y) = 0. \quad (3.2)$$

Filled hole:

$$\sigma_r(R, \varphi) = \begin{cases} -\frac{2 P_{\text{Bea}}}{\pi R} \sin \varphi & \text{for } 0 \leq \varphi \leq \pi, \\ 0 & \text{for } \pi \leq \varphi \leq 2\pi, \end{cases} \quad (3.3)$$

$$\tau_{r\varphi}(R, \varphi) = 0 \quad \text{for } 0 \leq \varphi \leq 2\pi.$$

$$\sigma_x(\pm w/2, y) = \tau_{xy}(\pm w/2, y) = 0, \quad (3.4)$$

$$\sigma_y(x, e) = \tau_{xy}(x, e) = 0. \quad (3.5)$$

The filled-hole problem is an idealisation of a connection containing a single fastener with the geometrical properties finite width w and finite height (or end distance) e as shown in Fig. 3.5. By implementation of Eq. (3.4) and (3.5),



Fig. 3.5 Filled-hole problem.

the bolt load is directed towards the part $y \rightarrow -\infty$. Regarding the bolted joint under combined bearing-bypass load, the quantity e may be considered as a fictitious length. However, its implementation is vital to ensure that the bolt load is transferred towards $y \rightarrow -\infty$. Neglecting this condition would allow the bearing load's force flux to be also transferred towards $y \rightarrow \infty$, where the uniform bypass loading should be located only. Note that the end distance should be chosen sufficiently wide so that no further raising effects occur. For example, $e = 10d$ may be selected. Also note that regarding the filled-hole problem, a uniaxial stress state along $y \rightarrow -\infty$ is not achieved by defining a corresponding BC *a priori*, but eventually results as a reaction by fulfilling the BCs of the stress-free straight edges in Eq. (3.4) and (3.5).

In the context of the complex potential method, the hole tractions are typically applied using loading functions. This is of interest for the filled-hole problem containing a loaded hole edge. Let us first express its stress BCs in Eq. (3.3) using a Fourier series expansion. Normalised to the bearing stress $\sigma_d = P_{\text{Bea}}/d$, these read

$$\sigma_r(R, \varphi)/\sigma_d = -\frac{2}{\pi} \sin \varphi - \underbrace{\frac{4}{\pi^2} - \sum_{n=1}^N \frac{4}{\pi^2} \frac{1 + \cos 2n\pi}{1 - 4n^2}}_{\text{cosine Fourier series of } |-2/\pi \sin \varphi|} \cos 2n\varphi, \quad (3.6)$$

$$\tau_{r\varphi}(R, \varphi)/\sigma_d = 0.$$

Therein, the sum's number of terms N is determined by checking if the sinusoidal bolt load along just half of the hole edge is accurately represented. In doing so, the following convergence criteria are used.

$$\begin{aligned} \psi_{\sigma_r} &= \frac{R}{P_{\text{Bea}}} \int_{\pi}^{2\pi} \sqrt{\sigma_r(R, \varphi)^2} \sin \varphi \, d\varphi \leq 0.01, \\ \chi_{\sigma_r} &= \frac{R}{P_{\text{Bea}}} \left| \int_0^{\pi} \sigma_r(R, \varphi) \sin \varphi \, d\varphi \right| \quad \text{with } |\chi_{\sigma_r} - 1| \leq 0.01. \end{aligned} \quad (3.7)$$

Therein, the load transfer ratio ψ_{σ_r} enables the assessment if nonzero fluctuations exist along the lower hole edge. The quantity χ_{σ_r} checks if the external bolt load is fully introduced along the upper hole boundary. The defined convergence criteria turn out to be satisfied for $N \geq 7$. In complex potential method, the stress BCs in Eq. (3.6) are taken into account using the loading functions $p_x(\varphi)$ and $p_y(\varphi)$. These can be calculated by Eq. (2.30), (2.35) and may also be represented by Fourier series expansions of the general form

$$\begin{aligned}
 p_x(\varphi) &= \underbrace{-\frac{P_x}{2\pi} \varphi + H_0}_{=p_x^{\text{mv}}(\varphi)} + \underbrace{\sum_{n=1}^N \{H_n e^{in\varphi} + \bar{H}_n e^{-in\varphi}\}}_{=p_x^{\text{Fo,sv}}(\varphi)}, \\
 p_y(\varphi) &= \underbrace{+\frac{P_y}{2\pi} \varphi + G_0}_{=p_y^{\text{mv}}(\varphi)} + \underbrace{\sum_{n=1}^N \{G_n e^{in\varphi} + \bar{G}_n e^{-in\varphi}\}}_{=p_y^{\text{Fo,sv}}(\varphi)}.
 \end{aligned} \tag{3.8}$$

Therein, the linear terms in φ are multivalued along any path enclosing the external forces and hence enable to model any nonzero force resultants P_x, P_y . For the filled-hole problem, $P_x = 0$ and $P_y = P_{\text{Bea}}$. Contrary, for the open hole and in general for all doubly symmetric problems (Michell, 1899), the force resultants vanish. To further illustrate how the multivalued loading functions arise, let us analyse the filled hole's radial stresses, which introduce the bolt load P_{Bea} . The normalised radial hole tractions involve the term $-2/\pi \sin \varphi$ in Eq. (3.6), which inserted in the integration Eq. (2.35) yields a multivalued function $p_y^{\text{mv}}(\varphi)$. In particular, with the part $\sigma_r^{\text{mv}}(R, \varphi)/\sigma_d = -2/\pi \sin \varphi$, the corresponding loading function

$$\begin{aligned}
 p_y(\varphi) &= R \int_0^\varphi \left(\sigma_r^{\text{mv}}(R, \hat{\varphi}) \sin \hat{\varphi} + \underbrace{\tau_{r\varphi}^{\text{mv}}(R, \hat{\varphi}) \cos \hat{\varphi}}_{=0} \right) d\hat{\varphi} \\
 &= R \int_0^\varphi -\frac{2}{\pi} \sin \hat{\varphi}^2 d\hat{\varphi} \sigma_d = R (\sin \varphi \cos \varphi - \varphi) \frac{\sigma_d}{\pi}
 \end{aligned} \tag{3.9}$$

is multivalued due to the linear term in φ (Nguyen-Hoang and Becker, 2020a). The remaining quantities $p_x^{\text{Fo,sv}}(\varphi), p_y^{\text{Fo,sv}}(\varphi)$ in Eq. (3.8) denote Fourier series expansions that are capable of representing any periodic and single-valued loading function $p_x^{\text{sv}}(s), p_y^{\text{sv}}(s)$. With that both the open- and filled-hole problems are fully defined and ready to be treated by the complex potential method in the following Sections. The corresponding stress results superimposed then lead to the solution of the bolted joint under combined bearing-bypass load.

3.2 Overview of the calculus

At first, the complex potentials Φ_k^{inf} producing the stress fields of the infinite domain open- and filled-hole problem are determined. In doing so, only the stress BCs in Eq. (3.1) and (3.3), respectively, are considered. To obtain the stress field of the corresponding finite-domain problem, that of the infinite-domain setting is taken and three types of auxiliary functions and potentials are supplemented. These intend to additionally satisfy the BCs in Eq. (3.2) regarding the open hole as well as in Eq. (3.4) and Eq. (3.5) for the filled hole. Thus, finite plate dimensions are taken into account. The first type of the auxiliary functions is capable of cancelling the longitudinal nonzero tractions $\sigma_y(x, e)$, $\tau_{xy}(\pm w/2, y)$ along the straight edges. These affect the equilibrium in load direction and an accurate cancellation is essential to equilibrate the external load by the net-section stresses $\sigma_y(R, y)$ alone. The second type of the auxiliary functions is dedicated to eliminate the lateral nonzero stresses $\sigma_x(\pm w/2, y)$ and the third type mitigates erroneous hole BCs, which may arise due to the other two auxiliary functions. Note that regarding the filled hole, its traction-free condition $\tau_{xy}(x, e) = 0$ will not be covered. The reasons why and the slight impact on the stress results justifying this assumption will be discussed in Sect. 4.5.

3.3 Infinite-domain problem

This Section begins with an introduction of the general structure of complex potentials that are capable of modelling the open and filled hole in an infinite plate. Then, the particular potentials for these problem settings are determined.

3.3.1 General structure of complex potentials

Complex potentials Φ_k^{inf} capable of modelling the infinite open- and filled-hole problem shall be determined. In doing so, let us select complex potentials of the general form

$$\begin{aligned}\Phi_1^{\text{inf}}(z_1) &= A_1 z_1 + B_1 \ln \zeta_1 + \sum_{n=1}^N C_{1n} \zeta_1^{-n}, \\ \Phi_2^{\text{inf}}(z_2) &= A_2 z_2 + B_2 \ln \zeta_2 - \sum_{n=1}^N C_{2n} \zeta_2^{-n}.\end{aligned}\tag{3.10}$$

The coefficients A_k are present whenever BCs representing a uniform stress state shall be implemented. With the constants B_k the multivalued and with C_{kn} the single-valued part of any loading functions p_x, p_y can be modelled. To apply the hole tractions, use is made of the conformal mapping functions $\zeta_k(z_k)$ in Eq. (2.31). Therein, the sign is chosen such that stresses of the corresponding complex potentials with respect to $\zeta_k(z_k)$ are continuously differentiable along any path and yield physically meaningful values. For instance, the circumferential stresses of the open-hole problem under uniaxial tension shall be positive throughout the net-section plane $y = 0$. All in all, the following choice is made.

$$\zeta_j = \begin{cases} \zeta_k^+ & \text{for } 0 \leq \varphi \leq \pi/2 \quad \vee \quad 3/2\pi < \varphi \leq 2\pi, \\ \zeta_k^- & \text{for } \pi/2 < \varphi \leq 3/2\pi. \end{cases} \quad (3.11)$$

Furthermore, when intending to obtain stresses along the vertical edge $x = \pm w/2$ a change of sign needs to be taken into account if the coefficients α_k of the complex constants μ_k are nonzero. This occurs for $[\pm 45^\circ]_s$ -laminates for instance. The location of the change of sign y_k^* can be calculated by solving

$$\sqrt{(x + \mu_k y_k^*)^2 - R(1 + \mu_k^2)} \Big|_{x=\pm w/2} = 0. \quad (3.12)$$

With these fundamentals the complex potentials for the open and filled hole in an infinite plate can be determined.

3.3.2 Open hole

Let us begin with the determination of the stress field of the infinite open-hole problem. According to Lekhnitskii (1968) and Sadd (2005), the solution is of the form

$$\Phi_k^{\text{OH,inf}} = \Phi_k^{\text{OH-I,inf}} + \Phi_k^{\text{OH-II,inf}}, \quad (3.13)$$

Therein, the former first potentials represent the plain plate under uniform tension producing nonzero tractions along the hole boundary and the second enables their cancellation. Both potentials superimposed then satisfy the stress-free hole BCs in Eq. (3.1). In particular, the former potentials are of the general form

$$\Phi_k^{\text{OH-I,inf}}(z_k) = A_k z_k \quad (3.14)$$

and the complex constants $A_k = a_k + i b_k$ are obtained by the requirements

$$\lim_{y \rightarrow \pm\infty} \sigma_x(x, y) = \lim_{y \rightarrow \pm\infty} \tau_{xy}(x, y) = 0, \quad \lim_{y \rightarrow \pm\infty} \sigma_y(x, y) = \sigma_{By}. \quad (3.15)$$

3.3 Infinite-domain problem

Since the system of equations is underdetermined, $b_1 = 0$ is arbitrarily set, which yields

$$\begin{aligned} a_1 &= \frac{1}{2} \frac{\alpha_2^2 + \beta_2^2}{(\alpha_1 - \alpha_2)^2 - \beta_1^2 + \beta_2^2} \sigma_{\text{By}}, & a_2 &= \frac{1}{2} \frac{\alpha_1^2 - 2\alpha_1\alpha_2 - \beta_1^2}{(\alpha_1 - \alpha_2)^2 - \beta_1^2 + \beta_2^2} \sigma_{\text{By}}, \\ b_1 &= 0, & b_2 &= \frac{1}{2\beta_2} \frac{\alpha_2 [\alpha_1(\alpha_1 - \alpha_2) - \beta_1^2] + \alpha_1 \beta_2^2}{(\alpha_1 - \alpha_2)^2 - \beta_1^2 + \beta_2^2} \sigma_{\text{By}}. \end{aligned} \quad (3.16)$$

The corresponding hole tractions are single-valued and can be calculated using Eq. (2.28), which leads to

$$\sigma_r^{\text{OH-I,inf}}(R, \varphi) = \sigma_{\text{By}} \sin^2 \varphi, \quad \tau_{r\varphi}^{\text{OH-I,inf}}(R, \varphi) = \sigma_{\text{By}} \sin \varphi \cos \varphi. \quad (3.17)$$

These tractions shall be compensated by $\Phi_k^{\text{OH-II,inf}}$ and the potentials representing any nonzero and single-valued hole tractions are of the general form

$$\Phi_1^{\text{HBC,sv}}(z_1) = \sum_{n=1}^N C_{1n} \zeta_1^{-n}, \quad \Phi_2^{\text{HBC,sv}}(z_2) = - \sum_{n=1}^N C_{2n} \zeta_1^{-n}. \quad (3.18)$$

The corresponding complex coefficients C_{kn} are determined by calculating the loading functions produced by $\Phi_k^{\text{HBC,sv}}$ using Eq. (2.29) and equating them with the prescribed single-valued traction expressed using the Fourier series representations $p_x^{\text{Fo,sv}}, p_y^{\text{Fo,sv}}$ in Eq. (3.8). This eventually leads to

$$C_{1n} = \frac{\overline{H}_n - \mu_2 \overline{G}_n}{\mu_1 - \mu_2}, \quad C_{2n} = \frac{\overline{H}_n - \mu_1 \overline{G}_n}{\mu_1 - \mu_2}. \quad (3.19)$$

For the potentials $\Phi_k^{\text{OH-II,inf}}$ of the infinite open hole, we obtain

$$\Phi_1^{\text{OH-II,inf}}(z_1) = \frac{\sigma_{\text{By}} R}{2} \frac{\mu_2}{\mu_1 - \mu_2} \zeta_1^{-1}, \quad \Phi_2^{\text{OH-II,inf}}(z_2) = - \frac{\sigma_{\text{By}} R}{2} \frac{\mu_1}{\mu_1 - \mu_2} \zeta_2^{-1}. \quad (3.20)$$

The corresponding stresses vanish with increasing hole distance and the uniaxial stress state modelled by $\Phi_k^{\text{OH-I,inf}}$ is not disturbed. Both partial potentials superimposed satisfy the stress BCs of the infinite open-hole problem and its complex potentials representation is fully determined.

When quasi-isotropic laminates shall be calculated complex potentials can be still used. The complex constants then specialise to $\mu_k = \pm i$ and the arising singularity in the denominator of the mapping functions in Eq. (2.31) may be circumvented by introducing a small artificial anisotropy (Tung, 1987; Chue et al., 2001). However, this takes some effort and the author considers

using Airy stress functions for the stress state representation as more feasible. The corresponding infinite open-hole solution addressed by Kirsch (1898) reads

$$F^{\text{OH,inf}} = \overbrace{\frac{\sigma_{\text{By}}}{4} (r^2 + r^2 \cos 2\varphi)}^{F^{\text{OH,inf1}}} + \underbrace{\frac{\sigma_{\text{By}}}{4} \left(-2R^2 \ln \frac{r}{R} + \frac{R^4}{r^2} \cos 2\varphi - 2R^2 \cos 2\varphi \right)}_{F^{\text{OH,inf2}}}. \quad (3.21)$$

Therein, the first part $F^{\text{OH,inf1}}$ represents the uniform-tension stress state and $F^{\text{OH,inf2}}$ ensures stress-free hole BCs by eliminating violations due to the first stress function. The polar stress components can be derived by Eq. (2.22) and read

$$\sigma_r^{\text{OH,inf}} = \frac{\sigma_{\text{By}}}{2} \left[1 - \frac{R^2}{r^2} - \left(1 - 4 \frac{R^2}{r^2} + 3 \frac{R^4}{r^4} \right) \cos 2\varphi \right], \quad (3.22)$$

$$\sigma_\varphi^{\text{OH,inf}} = \frac{\sigma_{\text{By}}}{2} \left[1 + \frac{R^2}{r^2} + \left(1 + 3 \frac{R^4}{r^4} \right) \cos 2\varphi \right], \quad (3.23)$$

$$\tau_{r\varphi}^{\text{OH,inf}} = \sigma_{\text{By}} \left(-1 - 2 \frac{R^2}{r^2} + 3 \frac{R^4}{r^4} \right) \cos \varphi \sin \varphi. \quad (3.24)$$

Details in terms of derivation can be also taken from Timoshenko and Goodier (1951) as well as Sadd (2005).

3.3.3 Filled hole

Let us proceed to determine the complex potentials $\Phi_k^{\text{FH,inf}}$ which represent the infinite domain filled-hole problem. In doing so, complex potentials capable of producing multivalued loading functions of the form as expressed in Eq. (3.8) shall be found. These can be decomposed to a single-valued and a multivalued part, which may be modelled using potentials of the structure

$$\begin{aligned} \Phi_1^{\text{FH-inf}}(z_1) &= \Phi_1^{\text{HBC,mv}} + \Phi_1^{\text{HBC,sv}} = B_1 \ln \zeta_1 + \sum_{n=1}^N C_{1n} \zeta_1^{-n}, \\ \Phi_2^{\text{FH-inf}}(z_2) &= \Phi_2^{\text{HBC,mv}} + \Phi_2^{\text{HBC,sv}} = B_2 \ln \zeta_2 - \sum_{n=1}^N C_{2n} \zeta_2^{-n}. \end{aligned} \quad (3.25)$$

3.3 Infinite-domain problem

Therein, the series terms of $\Phi_k^{\text{HBC,sv}}$ represent the potentials that model the single-valued part of the loading functions and the free coefficients C_{kn} are determined in the same way as outlined for the potentials $\Phi_k^{\text{OH-II,inf}}$ of the infinite open-hole problem (Subsect. 3.3.2). The remaining logarithmic terms in $\Phi_k^{\text{HBC,mv}}$ produce the multivalued loading functions $p_x^{\text{mv}}(\varphi)$ and $p_y^{\text{mv}}(\varphi)$. The corresponding complex coefficients B_k are obtained in the same way as described by Lekhnitskii (1968). Taking into account that all forces are given per plate thickness in this thesis, the coefficients are derived by the requirements

$$\begin{aligned}
 B_1 + B_2 - \bar{B}_1 - \bar{B}_2 &= \frac{P_y}{2\pi i}, \\
 \mu_1 B_1 + \mu_2 B_2 - \bar{\mu}_1 \bar{B}_1 - \bar{\mu}_2 \bar{B}_2 &= -\frac{P_x}{2\pi i}, \\
 \mu_1^2 B_1 + \mu_2^2 B_2 - \bar{\mu}_1^2 \bar{B}_1 - \bar{\mu}_2^2 \bar{B}_2 &= -\frac{S_{16}}{S_{11}} \frac{P_x}{2\pi i} - \frac{S_{12}}{S_{11}} \frac{P_y}{2\pi i}, \\
 \frac{1}{\mu_1} B_1 + \frac{1}{\mu_2} B_2 - \frac{1}{\bar{\mu}_1} \bar{B}_1 - \frac{1}{\bar{\mu}_2} \bar{B}_2 &= \frac{S_{12}}{S_{22}} \frac{P_x}{2\pi i} + \frac{S_{26}}{S_{22}} \frac{P_y}{2\pi i}.
 \end{aligned} \tag{3.26}$$

Note that this system of equations may be given in the matrix form $\mathbf{A} \cdot \mathbf{x} = \mathbf{b}$ and the solution can be conveniently determined by inversion. For the present filled-hole problem, $P_x = 0$ and $P_y = P_{\text{Bea}}$. With that all means for the stress field determination of the open and filled hole in an infinite domain are provided.

As for the infinite open-hole problem, Airy stress functions for the pin-loaded hole in an infinite, isotropic plate shall be provided as done in Nguyen-Hoang and Becker (2020a, 2021a). The corresponding stress functions are of the form

$$F^{\text{FH,inf}} = F^{\text{FH,inf1}} + F^{\text{FH,inf2}}. \tag{3.27}$$

Therein, the quantity $F^{\text{FH,inf1}}$ produces a full sine along the entire hole edge and $F^{\text{FH,inf2}}$ models the Fourier series expansion of the full sine's magnitude. This enables cancellation along the lower hole edge as depicted in Fig. 3.6. According to Bickley (1928), the first stress function $F^{\text{FH,inf1}}$ is of the general structure

$$F^{\text{FH,inf1}} = a_{15} r \varphi \cos \varphi + b_{12} r \ln \frac{r}{R} \sin \varphi + b_{13} \frac{1}{r} \sin \varphi. \tag{3.28}$$

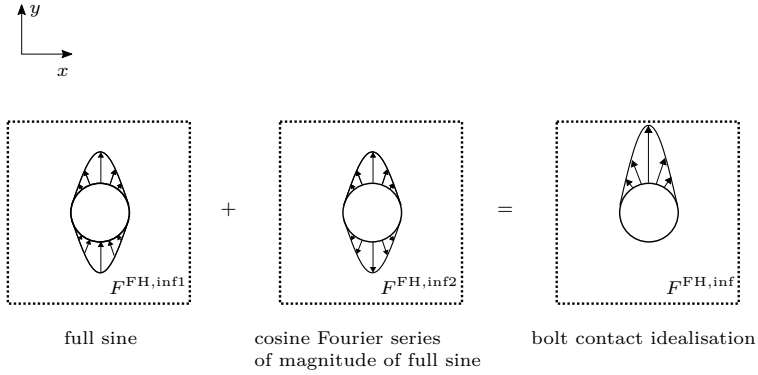


Fig. 3.6 Partial stress functions of the infinite filled-hole problem: radial hole tractions.

Note that the indices of the free coefficients are chosen as in Sadd (2005). The corresponding polar stress components can be derived using Eq. (2.22). With the reference bearing stress $\sigma_d = P_{\text{Bea}}/d$, these read

$$\sigma_r^{\text{FH,inf1}} = \left(-2a_{15} \frac{1}{r} + b_{12} \frac{1}{r} - 2b_{13} \frac{1}{r^3} \right) \sin \varphi \sigma_d, \quad (3.29)$$

$$\sigma_\varphi^{\text{FH,inf1}} = \left(b_{12} \frac{1}{r} + 2b_{13} \frac{1}{r^3} \right) \sin \varphi \sigma_d, \quad (3.30)$$

$$\tau_{r\varphi}^{\text{FH,inf1}} = \left(-b_{12} \frac{1}{r} + 2b_{13} \frac{1}{r^3} \right) \cos \varphi \sigma_d. \quad (3.31)$$

The free coefficients can be determined as follows. The condition

$$\frac{b_{12}}{a_{15}} = \frac{1}{2}(1 - \nu) \quad (3.32)$$

ensures single-valued circumferential displacements u_φ (Bickley, 1928; Timoshenko and Goodier, 1951), where the quantity ν denotes the Poisson's ratio of the (quasi-)isotropic plate. Further, by

$$\sigma_r^{\text{FH,inf1}}(R, \pi/2) = -\frac{1}{\pi} \frac{P_{\text{Bea}}}{R}, \quad (3.33)$$

half of the bolt (or bearing) load is introduced. Eventually,

$$\tau_{r\varphi}^{\text{FH,inf1}}(R, \varphi) = 0, \quad (3.34)$$

3.3 Infinite-domain problem

takes into account a frictionless and hence shear stress free bolt contact idealisation along the hole edge. Eventually, the first stress function is

$$F^{\text{FH,inf1}} = \frac{R}{\pi} \left[r\varphi \cos \varphi + \frac{1}{2}(1-\nu) r \ln \frac{r}{R} \sin \varphi + \frac{1}{4}(1-\nu) R^2 \frac{1}{r} \sin \varphi \right] \sigma_d. \quad (3.35)$$

Interestingly, the stress function $F^{\text{FH,inf1}}$ and thus its stress state depend on Poisson's ratio ν . This is actually true for any boundary value problem with a nonzero force resultant (Bickley, 1928) such as the present pin-loaded hole. To name a well known example, this finding can be also observed for the plate reacting to a single force (Timoshenko and Goodier, 1951; Becker and Gross, 2002; Sadd, 2005). The stress function of a problem with nonzero force resultant then contains first order terms of $\sin \varphi$ or $\cos \varphi$ so that at least one of the loading functions becomes multivalued. This has been shown for the filled hole in Eq. (3.9). However, in doubly symmetric problems the force resultants of the tractions vanish. If the plate material is isotropic then the stress function is independent of the elastic constants (Michell, 1899). This can be also observed for the infinite open-hole problem (see Eq. (3.21)).

The magnitude of the radial tractions $|\sigma_r^{\text{FH,inf1}}(R, \varphi)|$ is now expanded by a Fourier cosine series. In doing so, use is made of the stress function $F^{\text{FH,inf2}}$ with the general form

$$F^{\text{FH,inf2}} = R^2 \left[b_2 \ln \frac{r}{R} + \sum_{n=1}^N \left\{ A_{2,n} \left(\frac{R}{r} \right)^{2n} + B_{2,n} \left(\frac{R}{r} \right)^{2n-2} \right\} \cos 2n\varphi \right] \sigma_d. \quad (3.36)$$

Its polar stress components read

$$\sigma_r^{\text{FH,inf2}} = \left[b_2 \left(\frac{R}{r} \right)^2 - 2 \sum_{n=1}^N \left\{ n(2n+1) A_{2,n} \left(\frac{R}{r} \right)^{2n+2} + (n+1)(2n-1) B_{2,n} \left(\frac{R}{r} \right)^{2n} \right\} \cos 2n\varphi \right] \sigma_d, \quad (3.37)$$

$$\sigma_\varphi^{\text{FH,inf2}} = \left[-b_2 \left(\frac{R}{r} \right)^2 + 2 \sum_{n=1}^N \left\{ n(2n+1) A_{2,n} \left(\frac{R}{r} \right)^{2n+2} + (n-1)(2n-1) B_{2,n} \left(\frac{R}{r} \right)^{2n} \right\} \cos 2n\varphi \right] \sigma_d, \quad (3.38)$$

Chapter 3 Stress analysis - Development of complex calculus

$$\tau_{r\varphi}^{\text{FH,inf2}} = -2 \left[\sum_{n=1}^N \left\{ n(2n+1)A_{2,n} \left(\frac{R}{r}\right)^{2n+2} + n(2n-1)B_{2,n} \left(\frac{R}{r}\right)^{2n} \right\} \sin 2n\varphi \right] \sigma_d. \quad (3.39)$$

The amount $|\sigma_r^{\text{FH,inf1}}(R, \varphi)|$ is now expanded by the cosine Fourier series

$$\sigma_r^{\text{FH,inf2}}(R, \varphi)/\sigma_0 = \frac{f_{2,0}}{2} + \sum_{n=1}^{N^*} f_{2,n} \cos n\varphi, \quad (3.40)$$

$$\begin{aligned} \text{with } f_{2,n} &= \frac{1}{\pi} \frac{1}{\sigma_0} \int_0^{2\pi} \sigma_r^{\text{FH,inf1}}(R, \varphi) \cos n\varphi \, d\varphi \\ &= \begin{cases} -\frac{4}{\pi^2} \frac{1 + \cos n\pi}{1 - n^2} & \text{for even } n, \\ 0 & \text{for odd } n. \end{cases} \end{aligned} \quad (3.41)$$

Equating the coefficients of Eq. (3.37) and (3.40) as well as taking into account that uneven $f_{2,n}$ vanish reveals

$$b_2 = \frac{f_{2,0}}{2}, \quad (3.42)$$

$$-2[n(2n+1)A_{2,n} + (n+1)(2n-1)B_{2,n}] = f_{2,2n}. \quad (3.43)$$

Further, taking into account vanishing shear tractions $\tau_{r\varphi}^{\text{FH,inf2}}(R, \varphi) = 0$ in Eq. (3.39) leads to

$$(2n+1)A_{2,n} + (2n-1)B_{2,n} = 0. \quad (3.44)$$

The involved Airy stress coefficients can be derived using Eq. (3.43), (3.44) and finally

$$\begin{aligned} A_{2,n} &= -\frac{2n-1}{2n+1} B_{2,n}, \\ B_{2,n} &= \frac{1}{2} \frac{f_{2,2n}}{n(2n-1) - (n+1)(2n-1)}. \end{aligned} \quad (3.45)$$

Note that the stress function $F^{\text{FH,inf2}}$ is independent of the Poisson's ratio ν since the corresponding tractions along the hole edge yield vanishing force resultants. See Fig. 3.6 for further illustration. With that the stress solutions of the open- and filled-hole problem in an infinite domain are fully determined.

3.4 Cancellation of tractions parallel to the load direction

Both isotropic and orthotropic plate material is covered. To obtain the solution of corresponding finite-domain problems, auxiliary potentials and functions are superimposed such that the stress-free BCs along the straight edges are satisfied in addition. These are expressed in Eq. (3.2) for the open hole as well as in Eq. (3.4) and (3.5) for the filled hole. The development of the auxiliary potentials and functions is scope of the next Sections.

3.4 Cancellation of tractions parallel to the load direction

In this Section, auxiliary potentials of the first type are developed. These intend to eliminate nonzero tractions showing in load direction. The infinite domain complex potentials $\Phi_k^{\text{OH,inf}}$ and $\Phi_k^{\text{FH,inf}}$ produce the corresponding nonzero tractions $\tau_{xy}(\pm w/2, y)$ and $\sigma_y(x, e), \tau_{xy}(\pm w/2, y)$, respectively, which affect the equilibrium in load direction (Fig. 3.7). Hence, their elimination is crucial to transfer the external load by the net-section stresses $\sigma_y(x, 0)$ alone and a necessary condition to obtain an accurate solution. The following periodic arrangement technique shown in Fig. 3.8 provides a robust cancellation method for any plane problem which involves at least one symmetry axis. Let Φ_k^{inf} be the complex potentials representing the corresponding infinite-domain problem. Further, a symmetry to the y -axis is assumed and the stress-free edges $x = \pm w/2$ and $y = e$ shall be implemented. For convenience, let us express the infinite domain's stress field using its Airy stress function F^{inf} instead of the complex potentials Φ_k^{inf} , whose relationship is given by Eq. (2.26). To eliminate the nonzero tractions $\sigma_y(x, e), \tau_{xy}(\pm w/2, y)$ showing in load direction, virtual auxiliary plates are superimposed, which are created by shifting and periodically assembling the stress field of F^{inf} as depicted in Fig. 3.8. Therein, the infinite filled-hole problem's stress field is inserted for reasons of better illustration, $F^{\text{inf}} = F^{\text{FH,inf}}$. To eliminate the normal stresses $\sigma_y^-(x, e)$ along the horizontal edge $y = e$, F^{inf} is vertically copied, its sinusoidal traction reversed to tension and rotated by π along the hole boundary, thus creating the auxiliary plate F_{21}^{inf} . This step is omitted in doubly symmetric problems such as the orthotropic open-hole setting, which are not bounded by horizontal edges. To cancel the shear tractions $\tau_{xy}(\pm w/2, y)$ along the vertical edges $x = \pm w/2$, F_{11}^{inf} is copied and horizontally arranged creating F_{12}^{inf} and F_{13}^{inf} . Since the right auxiliary plate does not only cancel the shear stresses along $x = w/2$ but also affects those at the opposite boundary $x = -w/2$ and vice versa for the left auxiliary plate and its opposite edge at $x = w/2$, there will be residual shear tractions along both vertical edges. Their magnitudes depend on the number of horizontally aligned auxiliary

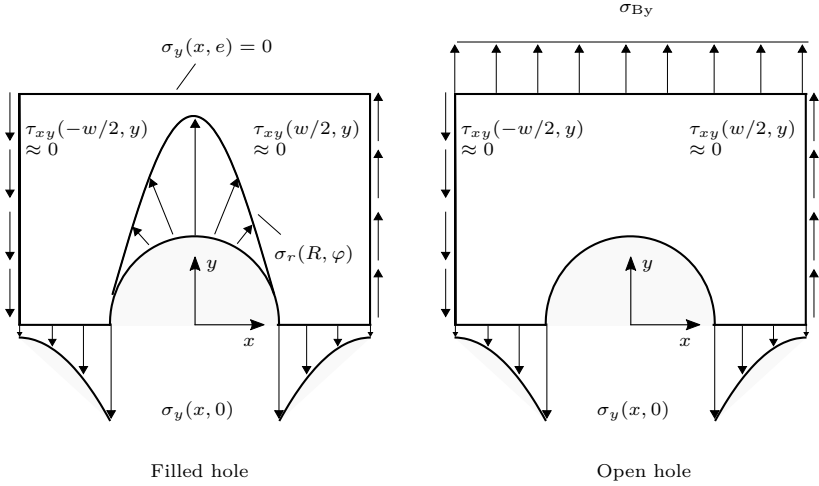


Fig. 3.7 Free form bodies, for which the tractions affecting the equilibrium in load/ y -direction are shown only. By means of the periodic arrangement technique, the shear stresses $\tau_{xy}(\pm w/2, y)$ become negligibly small such that external load is reacted by the net-section stresses $\sigma_y(x, 0)$ alone.

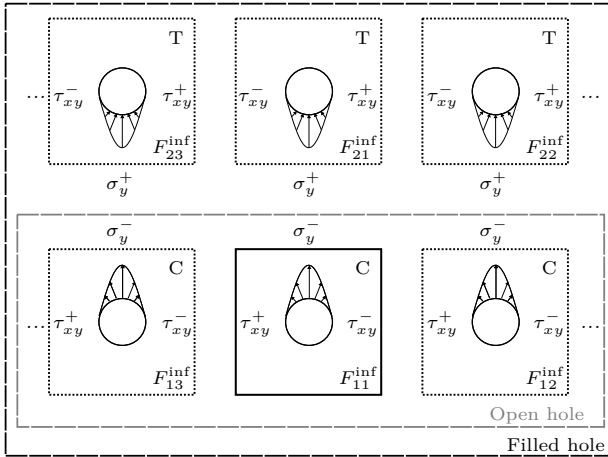


Fig. 3.8 Periodic arrangement to cancel nonzero tractions along straight edges in load direction. The plate drawn in solid lines $F^{inf} = F_{11}^{inf}$ represents the original, non-shifted infinite-domain solution, whereas those in dotted lines denote the auxiliary plates. The finite domain open-hole problem is just bounded by $x = \pm w/2$. Hence, only the lower auxiliary plates F_{1j} are required. For better illustration, the filled hole's stress field containing the sinusoidal bolt load along the hole edge is inserted. C $\hat{=}$ Compression, T $\hat{=}$ Tension.

3.4 Cancellation of tractions parallel to the load direction

plates in use and vanish if this number goes to infinity. Since the horizontal auxiliary plates cause additional normal stresses σ_y^- along $y = e$, they need to be vertically mirrored as performed for F_{11}^{inf} ensuring full elimination when a horizontal stress-free edge shall be modelled. The formulae to take into account the location of the auxiliary plates read

$$F_{ij}^{\text{inf}}(x, y) = \underbrace{(-1)^{i+1}}_{\substack{\text{Tension/} \\ \text{Compression}}} \cdot F^{\text{inf}}\left(\underbrace{(-1)^{i+1}x_j, (-1)^{i+1}y_i}_{\text{load shifting along hole}}\right), \quad (3.46)$$

$$\begin{aligned} \text{with } [x_j] &= [x_1 \quad x_2 \quad x_3 \quad x_4 \quad \dots] \\ &= [x \quad x - w \quad x + w \quad x - 2w \quad \dots], \end{aligned} \quad (3.47)$$

$$[y_i] = \begin{cases} [y] & \text{open hole,} \\ [y_1 \quad y_2] = [y \quad y - 2e] & \text{filled hole.} \end{cases} \quad (3.48)$$

Let n_x represent the number of horizontally and n_y the number of vertically aligned plates with

$$n_y = \begin{cases} 1 & \text{open hole,} \\ 2 & \text{filled hole.} \end{cases} \quad (3.49)$$

Then, the superposition of the auxiliary functions is performed using

$$\text{PA} \left(F^{\text{inf}} \right) = \sum_{i=1}^{n_y} \sum_{j=1}^{n_x} F_{ij}^{\text{inf}}, \quad (3.50)$$

where $\text{PA}(\square)$ represents the operator executing this arrangement for any infinite-domain stress field symmetric to the y -axis. In this thesis, n_x is considered as sufficiently large if there is an error smaller than 0.5 % in the load transfer due to remaining shear stresses along the vertical boundaries. These are produced by the superimposed periodic arrangement $\text{PA}(F^{\text{inf}})$. The corresponding inequalities read

$$\psi_{\tau_{xy}^{\text{inf}}} = \begin{cases} \left| \frac{4}{P_{\text{By}}} \left| \int_0^\infty \sum_{i=1}^{n_{x,\text{min}}} \tau_{xy,1j}^{\text{inf}}(\pm w/2, y) dy \right| \right| \leq 0.5 \% & \text{open hole,} \\ \left| \frac{2}{P_{\text{Bea}}} \left| \int_0^e \sum_{i=1}^{n_y} \sum_{j=1}^{n_{x,\text{min}}} \tau_{xy,ij}^{\text{inf}}(\pm w/2, y) dy \right| \right| \leq 0.5 \% & \text{filled hole} \end{cases} \quad (3.51)$$

and the smallest n_x obeying Eq. (3.51) yields $n_{x,\min}$. Also see Fig. 3.7 for illustration how to derive the integrals. Note that total effect of the shear stresses can be quickly determined by taking into account the pairwise cancellation. For instance, when assuming $n_x = 3$ the remaining shear tractions along the left edge $x = -w/2$ will be only due to F_{i2}^{inf} since those of F_{i1}^{inf} and F_{i3}^{inf} cancel each other (Fig. 3.8). For any value of n_x , the total effect of the shear stresses then simplifies to

$$\sum_{i=1}^{n_y} \sum_{j=1}^{n_x} \tau_{xy,ij}^{\text{inf}}(\pm w/2, y) = \sum_{i=1}^{n_y} \tau_{xy,i1}^{\text{inf}}(\pm n_x w/2, y). \quad (3.52)$$

With that the periodic arrangement technique for cancellation of the nonzero tractions $\tau_{xy}(\pm w/2, y)$ and $\sigma_y(x, e)$ along the free straight edges is fully determined. Note that problems symmetric to the x -axis may be treated by either rotating the whole setup by $\pi/2$ or by adapting the periodic arrangement's formulae. The author recommends the first approach since the effort is smaller.

3.5 Cancellation of tractions perpendicular to the load direction

Scope of this Section is the mitigation of the nonzero stresses $\sigma_x(\pm w/2, y)$ along the vertical edges, which arise due to the periodic auxiliary field applied to the infinite open- and filled-hole problem. This is achieved by the stress function $F_l^{\text{VE}\perp}$ expanding the undesirable violations in a Fourier series. Therein, the index l denotes a placeholder for any arbitrary stress function, for which those corresponding nonzero tractions need to be cancelled. Let us investigate the periodic arrangement in Fig. 3.8. Regarding the open hole, its superimposed stress field is symmetric to the x - and y -axis. Concerning that of the filled hole, a symmetry to the y -axis as well as an antisymmetry to the axis $y = e$ is given. Then, the stress deviations along the vertical edges fulfil the following symmetry characteristics.

$$\begin{aligned} \sigma_{x,l}^{\text{dev}}(\pm w/2, y) &= \sigma_{x,l}^{\text{dev}}(\pm w/2, -y) && \text{open hole,} \\ \sigma_{x,l}^{\text{dev}}(\pm w/2, y^*) &= -\sigma_{x,l}^{\text{dev}}(\pm w/2, -y^*) \quad \text{with } y^* = y - e && \text{filled hole.} \end{aligned} \quad (3.53)$$

Taking into account these symmetries simplifies the Fourier series expansions over the virtual wave length l_{F_0} as follows.

3.5 Cancellation of tractions perpendicular to the load direction

Open hole:

$$\sigma_{x,l}^{\text{VE}\perp}(\pm w/2, y)/\sigma_{\text{By}} = \sum_{n=1}^{N_l} f_{l,n}^{\sigma_x} \cos \alpha_n y \quad \text{with} \quad (3.54)$$

$$\alpha_n = \frac{2n\pi}{l_{\text{Fo}}}, \quad f_{l,n}^{\sigma_x} = \frac{2}{l_{\text{Fo}}} \int_0^{l_{\text{Fo}}} \sigma_{x,l}^{\text{dev}}(\pm w/2, y) \cos \alpha_n y \, dy. \quad (3.55)$$

Filled hole:

$$\sigma_{x,l}^{\text{VE}\perp}(\pm w/2, y^*)/\sigma_d = \sum_{n=1}^{N_l} g_{l,n}^{\sigma_x} \sin \alpha_n y^* \quad \text{with} \quad (3.56)$$

$$\alpha_n = \frac{2n\pi}{l_{\text{Fo}}}, \quad g_{l,n}^{\sigma_x} = \frac{2}{l_{\text{Fo}}} \int_0^{l_{\text{Fo}}} \sigma_{x,l}^{\text{dev}}(\pm w/2, y^*) \sin \alpha_n y^* \, dy^*. \quad (3.57)$$

Note that the stress deviations at the lower and upper bound of the integral are unequal, which is expressed by the inequalities

$$\begin{aligned} \sigma_{x,l}^{\text{dev}}(\pm w/2, y = 0) &\neq \sigma_{x,l}^{\text{dev}}(\pm w/2, y = l_{\text{Fo}}) && \text{open hole,} \\ \sigma_{x,l}^{\text{dev}}(\pm w/2, y^* = 0) &\neq \sigma_{x,l}^{\text{dev}}(\pm w/2, y^* = l_{\text{Fo}}) && \text{filled hole.} \end{aligned} \quad (3.58)$$

Then, Gibbs' phenomenon involving overshoots occurs in the corresponding Fourier series expansions. This is a discrepancy since the actual deviations should continuously decay with increasing hole distance. That is why the correction function of the type $F_l^{\text{VE}\perp}$ is regarded as less robust than the periodic arrangement technique and, hence, is not applied to simultaneously also eliminate the shear tractions $\tau_{xy}(\pm w/2, y)$. Be reminded that these shear tractions affect the load transfer through the net-section area and their cancellation is a necessary condition to obtain an accurate solution (Sect. 3.4). Moreover, the shear stresses elimination using stress functions of the type $F_l^{\text{VE}\perp}$ in addition would require another Fourier series expansion. That is more expensive than the periodic arrangement method, which only requires the translation (and rotation regarding filled holes) of stress fields. To mitigate any impact of periodicity and Gibbs' phenomenon on the characteristic stresses nearby the hole, the virtual wave length $l_{\text{Fo}} = 40d$ is chosen sufficiently large so that an undisturbed uniaxial stress state in the far-field $|y| \gg d$ can establish. Hence, by these measures, the correction function $F_l^{\text{VE}\perp}$ will not negatively affect the solution quality. This will be confirmed in Chap. 4 by comparing the results to Finite Element analyses.

Furthermore, the correction function must not produce any shear stresses along the vertical edges $x = \pm w/2$,

$$\tau_{xy,l}^{\text{VE}\perp}(\pm w/2, y) = 0. \quad (3.59)$$

The tractions of the open hole in Eq. (3.54), (3.59) can be modelled by the Airy stress function of the form (Lekhnitskii, 1963, 1968)

$$F_l^{\text{VE}\perp} / \sigma_{\text{By}} = a_l y^2 + \sum_{n=1}^{N_l} \phi_n(x) A_{l,n}^{\text{VE}\perp} \cos \alpha_n y, \quad (3.60)$$

and the tractions of the filled hole in Eq. (3.56), (3.59) by

$$F_l^{\text{VE}\perp} / \sigma_d = \sum_{n=1}^{N_l} \phi_n(x) A_{l,n}^{\text{VE}\perp} \sin \alpha_n y^*. \quad (3.61)$$

Therein, the entities $\phi_n(x)$ denote unknown functions with respect to x . For an orthotropic plate material, the governing equations can be reduced using the laminate's in-plane engineering constants $\hat{E}_x, \hat{E}_y, \hat{G}_{xy}, \hat{\nu}_{xy}$ and we obtain

$$\frac{d^4 \phi_n}{dx^4} - \left(\frac{\hat{E}_y}{\hat{G}_{xy}} - 2\hat{\nu}_{xy} \frac{\hat{E}_y}{\hat{E}_x} \right) \frac{d^2 \phi_n}{dx^2} + \frac{\hat{E}_y}{\hat{E}_x} \phi_n = 0. \quad (3.62)$$

The corresponding characteristic equation is

$$s^4 - \hat{E}_y \left(\frac{1}{\hat{G}_{xy}} - 2\frac{\hat{\nu}_{xy}}{\hat{E}_x} \right) s^2 + \frac{\hat{E}_y}{\hat{E}_x} = 0 \quad (3.63)$$

and for finite nonzero values of $\hat{E}_x, \hat{E}_y, \hat{G}_{xy}$, three different cases need to be considered:

- case I: The roots are real and equal, which occurs for quasi-isotropic laminates with $s = s_1 = s_2 = 1$.
- case II: The roots are real but not equal. For the laminates to be investigated in the present work, this occurs for the layups $[0^\circ]$, $[0^\circ/90^\circ]_s$ and $[0^\circ/\pm 45^\circ/90^\circ]_s$ (50%/40%/10%).
- case III: The roots are complex and of the form $h_s \pm t_s i, -h_s \pm t_s i, \{h_s, t_s\} \in \mathbb{R}$. This occurs for angle-ply laminates.

The general solution for the differential Eq. (3.62) is given by the ansatz

$$\begin{aligned} \phi_n^{\text{I}} &= C_1^{\phi_n} \cosh \alpha_n x + C_2^{\phi_n} \sinh \alpha_n x + \\ &\quad C_3^{\phi_n} x \cosh \alpha_n x + C_4^{\phi_n} x \sinh \alpha_n x, \\ \phi_n^{\text{II}} &= C_1^{\phi_n} \cosh s_1 \alpha_n x + C_2^{\phi_n} \sinh s_1 \alpha_n x + \\ &\quad C_3^{\phi_n} \cosh s_2 \alpha_n x + C_4^{\phi_n} \sinh s_2 \alpha_n x, \\ \phi_n^{\text{III}} &= (C_1^{\phi_n} \cosh h_s \alpha_n x + C_2^{\phi_n} \sinh h_s \alpha_n x) \cos t_s \alpha_n x + \\ &\quad (C_3^{\phi_n} \cosh h_s \alpha_n x + C_4^{\phi_n} \sinh h_s \alpha_n x) \sin t_s \alpha_n x. \end{aligned} \quad (3.64)$$

3.5 Cancellation of tractions perpendicular to the load direction

The stress components of $F_l^{\text{VE}\perp}$ are calculated using Eq. (2.21) yielding

Open hole:

$$\sigma_{x,l}^{\text{VE}\perp} / \sigma_{\text{By}} = 2a_l - \sum_{n=1}^{N_l} \alpha_n^2 \phi_n(x) A_{l,n}^{\text{VE}\perp} \cos \alpha_n y, \quad (3.65)$$

$$\sigma_{y,l}^{\text{VE}\perp} / \sigma_{\text{By}} = \sum_{n=1}^{N_l} \frac{d^2 \phi_n}{dx^2} A_{l,n}^{\text{VE}\perp} \cos \alpha_n y, \quad (3.66)$$

$$\tau_{xy,l}^{\text{VE}\perp} / \sigma_{\text{By}} = \sum_{n=1}^{N_l} \alpha_n \frac{d\phi_n}{dx} A_{l,n}^{\text{VE}\perp} \sin \alpha_n y. \quad (3.67)$$

Filled hole:

$$\sigma_{x,l}^{\text{VE}\perp} / \sigma_d = - \sum_{n=1}^{N_l} \alpha_n^2 \phi_n(x) A_{l,n}^{\text{VE}\perp} \sin \alpha_n y^*, \quad (3.68)$$

$$\sigma_{y,l}^{\text{VE}\perp} / \sigma_d = \sum_{n=1}^{N_l} \frac{d^2 \phi_n}{dx^2} A_{l,n}^{\text{VE}\perp} \sin \alpha_n y^*, \quad (3.69)$$

$$\tau_{xy,l}^{\text{VE}\perp} / \sigma_d = - \sum_{n=1}^{N_l} \alpha_n \frac{d\phi_n}{dx} A_{l,n}^{\text{VE}\perp} \cos \alpha_n y. \quad (3.70)$$

The derivatives of ϕ_n are

$$\begin{aligned} \frac{d\phi_n^{\text{I}}}{dx} &= \alpha_n \left(C_1^{\phi_n} \sinh \alpha_n x + C_2^{\phi_n} \cosh \alpha_n x \right) + \\ & C_3^{\phi_n} \left(\alpha_n x \sinh \alpha_n x + \cosh \alpha_n x \right) + \\ & C_4^{\phi_n} \left(\alpha_n x \cosh \alpha_n x + \sinh \alpha_n x \right), \end{aligned} \quad (3.71)$$

$$\begin{aligned} \frac{d^2 \phi_n^{\text{I}}}{dx^2} &= \alpha_n^2 \left(C_1^{\phi_n} \cosh \alpha_n x + C_2^{\phi_n} \sinh \alpha_n x \right) + \\ & C_3^{\phi_n} \left(\alpha_n^2 x \cosh \alpha_n x + 2\alpha_n \sinh \alpha_n x \right) + \\ & C_4^{\phi_n} \left(\alpha_n^2 x \sinh \alpha_n x + 2\alpha_n \cosh \alpha_n x \right), \end{aligned} \quad (3.72)$$

$$\frac{d\phi_n^{\text{II}}}{dx} = \alpha_n \left(s_1 C_1^{\phi_n} \sinh s_1 \alpha_n x + s_1 C_2^{\phi_n} \cosh s_1 \alpha_n x + s_2 C_3^{\phi_n} \sinh s_2 \alpha_n x + s_2 C_4^{\phi_n} \cosh s_2 \alpha_n x \right), \quad (3.73)$$

$$\frac{d^2\phi_n^{\text{II}}}{dx^2} = \alpha_n^2 \left(s_1^2 C_1^{\phi_n} \cosh s_1 \alpha_n x + s_1^2 C_2^{\phi_n} \sinh s_1 \alpha_n x + s_2^2 C_3^{\phi_n} \cosh s_2 \alpha_n x + s_2^2 C_4^{\phi_n} \sinh s_2 \alpha_n x \right), \quad (3.74)$$

$$\begin{aligned} \frac{d\phi_n^{\text{III}}}{dx} = \alpha_n \left\{ \cosh h_s \alpha_n x \left[(C_2^{\phi_n} h_s + C_3^{\phi_n} t_s) \cos t_s \alpha_n x + (C_4^{\phi_n} h_s - C_1^{\phi_n} t_s) \sin t_s \alpha_n x \right] + \sinh h_s \alpha_n x \left[(C_1^{\phi_n} h_s + C_4^{\phi_n} t_s) \cos t_s \alpha_n x + (C_3^{\phi_n} h_s - C_2^{\phi_n} t_s) \sin t_s \alpha_n x \right] \right\}, \end{aligned} \quad (3.75)$$

$$\begin{aligned} \frac{d^2\phi_n^{\text{III}}}{dx^2} = \alpha_n^2 \left\{ \cosh h_s \alpha_n x \left[(2C_4^{\phi_n} h_s t_s + C_1^{\phi_n} (h_s + t_s) (h_s - t_s)) \cos t_s \alpha_n x + (C_3^{\phi_n} (h_s + t_s) (h_s - t_s) - 2C_2^{\phi_n} h_s t_s) \sin t_s \alpha_n x \right] + \sinh h_s \alpha_n x \left[(C_2^{\phi_n} (h_s + t_s) (h_s - t_s) + 2C_3^{\phi_n} h_s t_s) \cos t_s \alpha_n x + (C_4^{\phi_n} (h_s + t_s) (h_s - t_s) - 2C_1^{\phi_n} h_s t_s) \sin t_s \alpha_n x \right] \right\}. \end{aligned} \quad (3.76)$$

The coefficients $C_i^{\phi_n}$ are determined by

$$\phi_n(\pm w/2) = 1, \quad (3.77)$$

$$\tau_{xy,l}^{\text{SE}\perp}(\pm w/2, y) = 0 \quad \Rightarrow \quad \left. \frac{d\phi_n}{dx} \right|_{x=\pm w/2} = 0. \quad (3.78)$$

3.5 Cancellation of tractions perpendicular to the load direction

Note that Eq. (3.77) is set to unity only for computational convenience and eventually for case I

$$\begin{aligned} C_1^{\phi_n} &= \frac{2 \sinh w/2 \alpha_n + \alpha_n w \cosh w/2 \alpha_n}{\sinh w \alpha_n + w \alpha_n}, \\ C_2^{\phi_n} &= C_3^{\phi_n} = 0, \\ C_4^{\phi_n} &= -\frac{2 \alpha_n \sinh w/2 \alpha_n}{\sinh w \alpha_n + w \alpha_n}, \end{aligned} \quad (3.79)$$

for case II

$$\begin{aligned} C_1^{\phi_n} &= \frac{s_2}{s_2 \cosh s_1 w/2 \alpha_n - s_1 \coth s_2 w/2 \alpha_n \sinh s_1 w/2 \alpha_n}, & C_2^{\phi_n} &= 0, \\ C_3^{\phi_n} &= \frac{s_1}{s_2 \coth s_1 w/2 \alpha_n \sinh s_2 w/2 \alpha_n - s_1 \cosh s_2 w/2 \alpha_n}, & C_4^{\phi_n} &= 0 \end{aligned} \quad (3.80)$$

and for case III

$$\begin{aligned} C_1^{\phi_n} &= \frac{4h_s \cosh h_s w/2 \alpha_n \sin t_s w/2 \alpha_n + 2t_s \cos t_s w/2 \alpha_n \sinh h_s w/2 \alpha_n}{h_s \sin t_s w/2 \alpha_n + t_s \cosh h_s w/2 \alpha_n}, \\ C_2^{\phi_n} &= C_3^{\phi_n} = 0, \\ C_4^{\phi_n} &= \frac{2t_s \cosh h_s w/2 \alpha_n \sin t_s w/2 \alpha_n - 2h_s \cos t_s w/2 \alpha_n \sinh h_s w/2 \alpha_n}{h_s \sin t_s w/2 \alpha_n + t_s \sinh h_s w/2 \alpha_n}. \end{aligned} \quad (3.81)$$

Equating the coefficients of Eq. (3.54), (3.65) as well as those of Eq. (3.56), (3.68), respectively, and taking into account Eq. (3.77) leads to

$$a_l = \frac{f_{l,0}^{\sigma_x}}{4}, \quad A_{l,n}^{\text{VE}\perp} = \begin{cases} -\frac{f_{l,n}^{\sigma_x}}{\alpha_n^2} & \text{open hole,} \\ -\frac{g_{l,n}^{\sigma_x}}{\alpha_n^2} & \text{filled hole.} \end{cases} \quad (3.82)$$

With this the stress function $F_l^{\text{VE}\perp}$ that mitigates the tractions $\sigma_x(\pm w/2, y)$ is fully determined. However, regarding the filled-hole problem bounded by the horizontal edge $y = e$, the tractions $\tau_{xy}(x, e)$ perpendicular to the load direction are still nonzero. The filled-hole problem and its stress functions are symmetric with respect to the y -axis. Due to Eq. (2.21), the corresponding shear stresses involve the antisymmetry $\tau_{xy}(x, y) = -\tau_{xy}(-x, y)$. Their

Fourier series representation may be performed by adapting the ansatz of $F_l^{\text{VE}\perp}$ in Eq. (3.61) yielding the stress function of the general form

$$F_l^{\text{HE}\perp}/\sigma_d = \sum_{l=1}^{N_l} \varrho_n(y) A_{l,n}^{\text{HE}\perp} \sin \beta_n x, \quad (3.83)$$

where the entity $\varrho_n(y)$ is of the same form as $\phi_n(x)$ in Eq. (3.64) and therefore produces unbounded stresses with increasing hole distance $|y| \rightarrow \infty$. Hence, the stress-free vertical edges would be seriously disrupted and the stress BC $\tau_{xy}(x, e) = 0$ shall not be covered by the present calculus. Their slight impact on the characteristic stresses in the hole vicinity for most of the relative finite dimensions $w/d, e/d$ will be discussed in Chap. 4.

3.6 Cancellation of violated hole boundary conditions

The periodic arrangement technique as well as the stress function $F_l^{\text{VE}\perp}$ only address the straight edges. However, hole tractions to be rendered are neglected. Hence, the superposition of these correction functions and potentials with the infinite open- or filled-hole problem will yield erroneous hole BCs. These can be eliminated by superimposing additional complex potentials $\Phi_k^{\text{HBC,sv}}$ with the general form as in Eq. (3.18). The free coefficients shall be then determined such that the produced loading functions capture the Fourier series expansion of the violations, which are of the general structure as in Eq. (3.8). Refer to Sect. 3.3 for further details.

When quasi-isotropic laminates or isotropic plates are treated Airy stress functions should be employed. These are provided in the following. Again, the index l denotes any arbitrary stress field. Its hole tractions $\sigma_{r,l}^{\text{dev}}(R, \varphi)$ and $\tau_{r\varphi,l}^{\text{dev}}(R, \varphi)$ deviate from the desired hole BCs expressed by Eq. (3.1) for the open hole and by Eq. (3.3) for the filled hole. The deviating hole BCs can be expanded by the Fourier series

$$\sigma_{r,l}^{\text{HBC}}(R, \varphi)/\sigma_0 = \frac{f_{l,0}^{\sigma_r}}{2} + \sum_{n=1}^N f_{l,n}^{\sigma_r} \cos n\varphi + \sum_{n=1}^N g_{l,n}^{\sigma_r} \sin n\varphi, \quad (3.84)$$

$$\tau_{r\varphi,l}^{\text{HBC}}(R, \varphi)/\sigma_0 = \frac{f_{l,0}^{\tau_{r\varphi}}}{2} + \sum_{n=1}^N f_{l,n}^{\tau_{r\varphi}} \cos n\varphi + \sum_{n=1}^N g_{l,n}^{\tau_{r\varphi}} \sin n\varphi. \quad (3.85)$$

3.6 Cancellation of violated hole boundary conditions

Note that the stress deviations may also be normalised to the bearing stress σ_d when treating the filled hole. The Fourier coefficients can be calculated using

$$\begin{aligned}
 f_{l,n}^{\sigma_r} &= \frac{1}{\pi} \frac{1}{\sigma_0} \int_0^{2\pi} \sigma_{r,l}^{\text{dev}}(R, \varphi) \cos n\varphi \, d\varphi, \\
 g_{l,n}^{\sigma_r} &= \frac{1}{\pi} \frac{1}{\sigma_0} \int_0^{2\pi} \sigma_{r,l}^{\text{dev}}(R, \varphi) \sin n\varphi \, d\varphi, \\
 f_{l,n}^{\tau_{r\varphi}} &= \frac{1}{\pi} \frac{1}{\sigma_0} \int_0^{2\pi} \tau_{r\varphi,l}^{\text{dev}}(R, \varphi) \cos n\varphi \, d\varphi, \\
 g_{l,n}^{\tau_{r\varphi}} &= \frac{1}{\pi} \frac{1}{\sigma_0} \int_0^{2\pi} \tau_{r\varphi,l}^{\text{dev}}(R, \varphi) \sin n\varphi \, d\varphi.
 \end{aligned} \tag{3.86}$$

For problems symmetric to the y -axis as the filled hole, only the even quantities $f_{l,n}^{\sigma_r}, g_{l,n}^{\tau_{r\varphi}}$ and the uneven quantities $g_{l,n}^{\sigma_r}, f_{l,n}^{\tau_{r\varphi}}$ are nonzero. Then, the general form for the Airy stress function F_l^{HBC} capable of producing those Fourier expansions in Eq. (3.84) and (3.85) is given by

$$\begin{aligned}
 F_l^{\text{HBC}} &= R^2 \left[b_l^{\sigma_r} \ln \frac{r}{R} + c_l^{\sigma_r} \frac{r}{R} \varphi \cos \varphi + d_l^{\sigma_r} \frac{r}{R} \ln \frac{r}{R} \sin \varphi + d_l^{\tau_{r\varphi}} \frac{R}{r} \sin \varphi + \right. \\
 &\quad \left. + \sum_{n=1}^N \left\{ A_{l,n} \left(\frac{R}{r} \right)^{2n} + B_{l,n} \left(\frac{R}{r} \right)^{2n-2} \right\} \cos 2n\varphi + \right. \\
 &\quad \left. + \sum_{n=1}^N \left\{ C_{l,n} \left(\frac{R}{r} \right)^{2n+1} + D_{l,n} \left(\frac{R}{r} \right)^{2n-1} \right\} \sin(2n+1)\varphi \right] \sigma_0.
 \end{aligned} \tag{3.87}$$

Its polar stress components are

$$\begin{aligned}
 \sigma_{r,l}^{\text{HBC}} &= \left[b_l^{\sigma_r} \left(\frac{R}{r} \right)^2 - \left(2c_l^{\sigma_r} - d_l^{\sigma_r} \right) \frac{R}{r} \sin \varphi - 2d_l^{\tau_{r\varphi}} \left(\frac{R}{r} \right)^3 \sin \varphi - \right. \\
 &\quad \left. - 2 \sum_{n=1}^N \left\{ n(2n+1) A_{l,n} \left(\frac{R}{r} \right)^{2n+2} + \right. \right. \\
 &\quad \left. \left. + (n+1)(2n-1) B_{l,n} \left(\frac{R}{r} \right)^{2n} \right\} \cos 2n\varphi - \right. \\
 &\quad \left. - 2 \sum_{n=1}^N \left\{ (2n+1)(n+1) C_{l,n} \left(\frac{R}{r} \right)^{2n+3} + \right. \right.
 \end{aligned}$$

$$+ n(2n + 3) D_{l,n} \left(\frac{R}{r} \right)^{2n+1} \left. \right\} \sin(2n + 1) \varphi \left. \right] \sigma_0, \quad (3.88)$$

$$\begin{aligned} \sigma_{\varphi,l}^{\text{HBC}} = & \left[-b_l^{\sigma_r} \left(\frac{R}{r} \right)^2 + d_l^{\sigma_r} \frac{R}{r} \sin \varphi + 2d_l^{\tau_r \varphi} \left(\frac{R}{r} \right)^3 \sin \varphi + \right. \\ & + 2 \sum_{n=1}^N \left\{ n(2n + 1) A_{l,n} \left(\frac{R}{r} \right)^{2n+2} + \right. \\ & + (n - 1)(2n - 1) B_{l,n} \left(\frac{R}{r} \right)^{2n} \left. \right\} \cos 2n\varphi + \\ & + 2 \sum_{n=1}^N \left\{ (2n + 1)(n + 1) C_{l,n} \left(\frac{R}{r} \right)^{2n+3} + \right. \\ & + n(2n - 1) D_{l,n} \left(\frac{R}{r} \right)^{2n+1} \left. \right\} \sin(2n + 1) \varphi \left. \right] \sigma_0, \quad (3.89) \end{aligned}$$

$$\begin{aligned} \tau_{r\varphi,l}^{\text{HBC}} = & \left[-d_l^{\sigma_r} \frac{R}{r} \cos \varphi + 2d_l^{\tau_r \varphi} \left(\frac{R}{r} \right)^3 \cos \varphi - \right. \\ & - 2 \sum_{n=1}^N \left\{ n(2n + 1) A_{l,n} \left(\frac{R}{r} \right)^{2n+2} + \right. \\ & + n(2n - 1) B_{l,n} \left(\frac{R}{r} \right)^{2n} \left. \right\} \sin 2n\varphi + \\ & + 2(2n + 1) \sum_{n=1}^N \left\{ (n + 1) C_{l,n} \left(\frac{R}{r} \right)^{2n+3} + \right. \\ & + n D_{l,n} \left(\frac{R}{r} \right)^{2n+1} \left. \right\} \cos(2n + 1) \varphi \left. \right] \sigma_0. \quad (3.90) \end{aligned}$$

The free coefficients are determined as follows. Let us equate the Fourier series coefficients in Eq. (3.84), (3.85) with those of the Airy stress components in Eq. (3.88), (3.90), respectively. Furthermore, let us take into account single-valued displacements when required⁵, which is expressed by

$$\frac{d_l^{\sigma_r}}{c_l^{\sigma_r}} = \frac{1}{2}(1 - \nu). \quad (3.91)$$

⁵ See Sect. 3.3 or Bickley (1928); Timoshenko and Goodier (1951).

3.7 Overall iterative calculation procedure

Then, the free coefficients can be calculated by

$$b_l^{\sigma_r} = \frac{1}{2} f_{l,0}^{\sigma_r}, \quad c_l^{\sigma_r} = -\frac{1}{2} (f_{l,1}^{\tau_{r\varphi}} + g_{l,1}^{\sigma_r}), \quad d_l^{\sigma_r} = \frac{1}{2} (1 - \nu) c_l^{\sigma_r}, \quad (3.92)$$

$$d_l^{\tau_{r\varphi}} = \frac{1}{2} (f_{l,1}^{\tau_{r\varphi}} + d_l^{\sigma_r}),$$

$$A_{l,n} = -\frac{1}{n(2n+1)} \left[\frac{1}{2} g_{l,2n}^{\tau_{r\varphi}} + n(2n-1) B_{l,n} \right],$$

$$B_{l,n} = \frac{1}{2} \frac{g_{l,2n}^{\tau_{r\varphi}} - f_{l,2n}^{\sigma_r}}{2n-1}, \quad C_{l,n} = \frac{1}{n+1} \left[\frac{f_{l,2n+1}^{\tau_{r\varphi}}}{2(2n+1)} - n D_{l,n} \right], \quad (3.93)$$

$$D_{l,n} = -\frac{1}{4n} (g_{l,2n+1}^{\sigma_r} + f_{l,2n+1}^{\tau_{r\varphi}}).$$

For doubly symmetric settings as the open-hole problem, only the coefficients $b_l^{\sigma_r}, A_{l,n}, B_{l,n}$ are nonzero and the remaining others vanish. With that all means to address the straight edges as well as the hole boundary are provided. However, each of the correction functions and potentials only addresses a certain set of tractions along the boundaries and even may interfere with the others. This is further discussed in the next Section and an iterative calculation procedure is developed to nevertheless take into account all edges simultaneously.

3.7 Overall iterative calculation procedure

The capability of each correction function which BCs they address as well as which they may interfere is listed in Table 3.1. To simultaneously satisfy all addressed BCs, the correction functions are applied iteratively until the remaining errors become negligibly small. The flowchart in Fig. 3.9 illustrates this procedure. After implementing the periodic arrangement for the infinite

Table 3.1

Overview of correction functions. The operator $\text{PA}(\square)$ implementing the periodic arrangement is applied to the stress functions F^{inf} modelling the infinite domain open/filled hole as well as to F_l^{HBC} mitigating deviations along the hole edge.

	treats	interferes with
$\text{PA}(\square)$	$\tau_{xy}(\pm w/2, y) = 0$ $\sigma_y(x, e) = 0$	Hole BCs, $\sigma_x(\pm w/2, y) = 0$ $\tau_{xy}(x, e) = 0$
$F_l^{\text{VE}\perp}$	$\sigma_x(\pm w/2, y) = 0$	Hole BCs, $\tau_{xy}(x, e) = 0$
F_l^{HBC}	Hole BCs	all BCs along straight edges

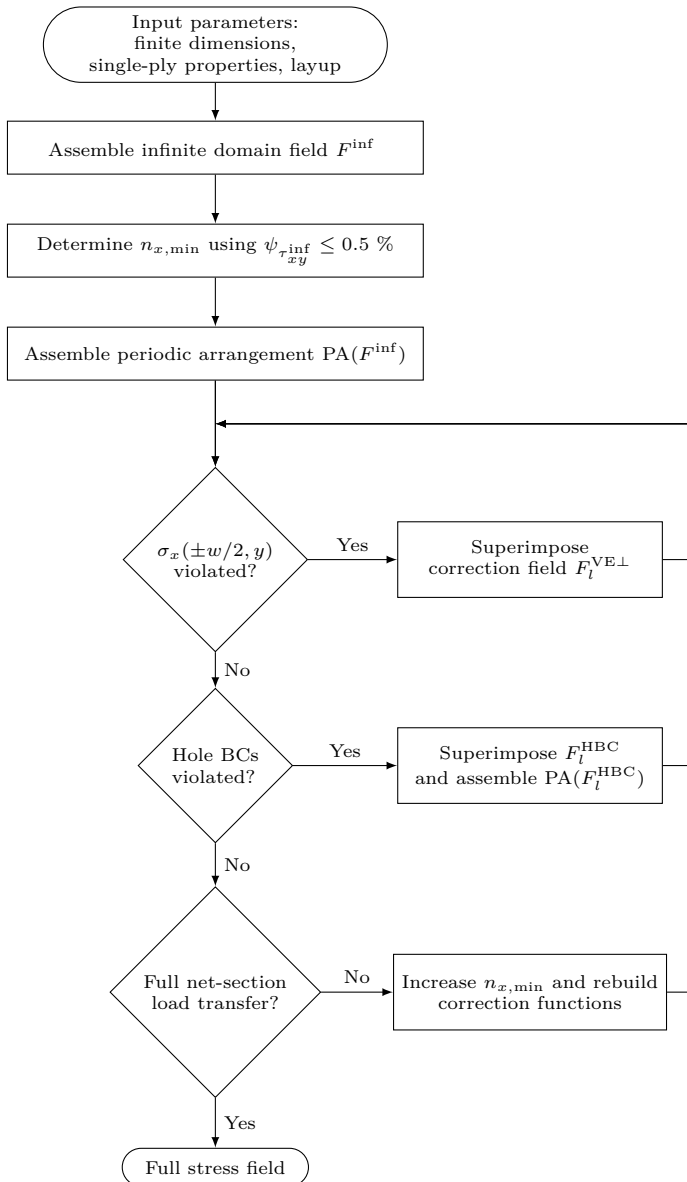


Fig. 3.9 Flowchart of the present stress calculus.

3.7 Overall iterative calculation procedure

domain problem using the operator $\text{PA}(F_{\text{inf}})$, the correction function $F_l^{\text{VE}\perp}$ is applied. Both yield deviations in the hole tractions, which requires to apply the stress function F_l^{HBC} for correction. Since this function is in conflict with the stress-free conditions of the straight edges, violations along these arise. This is mitigated by periodically arranging the stress field produced by F_l^{HBC} as implemented for F_{inf} and then by superimposing another correction function $F_{l+1}^{\text{VE}\perp}$ to cancel the newly produced stresses $\sigma_x(\pm w/2, y)$ along the vertical edges. That will slightly interfere with the hole BCs again. Note that the function of the type $F_l^{\text{VE}\perp}$ is not required to be periodically assembled since the condition in Eq. (3.59) already employs vanishing shear stresses $\tau_{xy}(\pm w/2, y)$. Further, regarding finite-domain problems bounded by the horizontal edge $y = e$ as the filled hole, the stress-free condition $\sigma_y(x, e) = 0$ is not interfered. This is due to the fact that the stress function $F_l^{\text{VE}\perp}$ is chosen such that the antisymmetry to the axis $y = e$ has been employed (see Sect. 3.5). This has been implemented since the periodic auxiliary field also contains this antisymmetry (Fig. 3.8). Hence, the tractions $\sigma_y^{\text{VE}\perp}(x, e)$ along the symmetry axis $y = e$ vanish. Iterating this procedure enables to simultaneously fulfil the addressed BCs and the stress function of the full finite-domain solution is given by

$$F = \underbrace{\sum_{i=1}^{n_y} \sum_{j=1}^{n_{x,\min}} F_{ij}^{\text{inf}}}_{\text{periodic field of } F^{\text{inf}}} + \sum_{l=1}^L \left\{ F_l^{\text{VE}\perp} + \underbrace{\sum_{i=1}^{n_y} \sum_{j=1}^{n_{x,\min}} F_{l,ij}^{\text{HBC}}}_{\text{periodic field of } F_l^{\text{HBC}}} \right\}. \quad (3.94)$$

Therein, the quantity L represents the number of iterations yielding sufficiently fulfilled BCs. This can be quantitatively ensured by the following load transfer values and convergence criteria.

Open hole:

$$\begin{aligned}
 \psi_{\sigma_r} &= \frac{R}{P_{By}} \int_0^{2\pi} \sqrt{\sigma_r(R, \varphi)^2} \sin \varphi \, d\varphi && \leq 0.01, \\
 \psi_{\tau_{r\varphi}} &= \frac{R}{P_{By}} \int_0^{2\pi} \sqrt{\tau_{r\varphi}(R, \varphi)^2} \cos \varphi \, d\varphi && \leq 0.01, \\
 \psi_{\sigma_x} &= \frac{4}{P_{By}} \int_0^{l_{F0}/2} \sqrt{\sigma_x(\pm w/2, y)^2} \, dy && \leq 0.01, \\
 \psi_{\tau_{xy}} &= \frac{4}{P_{By}} \int_0^\infty \sqrt{\tau_{xy}(\pm w/2, y)^2} \, dy && \leq 0.01, \\
 \psi_{\sigma_y^{\text{inf}}} &= \frac{2}{P_{By}} \int_0^{w/2} \sqrt{(\sigma_y(x, \pm l_{F0}/2) - \sigma_0)^2} \, dx && \leq 0.01, \\
 \chi_{\sigma_y} &= \frac{2}{P_{By}} \int_R^{w/2} \sigma_y(x, 0) \, dx, && \text{with } |\chi_{\sigma_y} - 1| \leq 0.01. \quad (3.95)
 \end{aligned}$$

Filled hole:

$$\begin{aligned}
 \psi_{\sigma_r} &= \frac{R}{P_{Bea}} \int_\pi^{2\pi} \sqrt{\sigma_r(R, \varphi)^2} \sin \varphi \, d\varphi && \leq 0.01, \\
 \psi_{\tau_{r\varphi}} &= \frac{R}{P_{Bea}} \int_0^{2\pi} \sqrt{\tau_{r\varphi}(R, \varphi)^2} \cos \varphi \, d\varphi && \leq 0.01, \\
 \psi_{\sigma_x} &= \frac{2}{P_{Bea}} \int_{-l_{F0}/2}^0 \sqrt{\sigma_x(\pm w/2, y^*)^2} \, dy^* && \leq 0.01, \\
 \psi_{\tau_{xy}} &= \frac{2}{P_{Bea}} \int_{-l_F/2}^e \sqrt{\tau_{xy}(\pm w/2, y)^2} \, dy && \leq 0.01, \\
 \chi_{\sigma_r} &= \frac{R}{P_{Bea}} \left| \int_0^\pi \sigma_r(R, \varphi) \sin \varphi \, d\varphi \right|, && \text{with } |\chi_{\sigma_r} - 1| \leq 0.01 \\
 \chi_{\sigma_y} &= \frac{2}{P_{Bea}} \int_R^{w/2} \sigma_y(x, 0) \, dx, && \text{with } |\chi_{\sigma_y} - 1| \leq 0.01. \quad (3.96)
 \end{aligned}$$

Excessive values of ψ_{σ_r} , $\psi_{\tau_{r\varphi}}$, ψ_{σ_x} , $\psi_{\tau_{xy}}$ indicate deviations in the corresponding stress-free BC, which can be cured by increasing the number of iterations L . For the relative dimensions $w/d \geq 3$, $e/d \geq 3$ treated in this thesis, $L = 3$ has revealed to be sufficient. As the stresses $\sigma_x(\pm w/2, y)$ are eliminated using periodic Fourier series expansion, the upper/lower boundary of the integral in ψ_{σ_x} is chosen $y = \pm l_{F0}/2$ conservatively assuming that along half of the wave length l_{F0} , Gibbs' phenomenon has a negligible impact and an unperturbed uniaxial stress state can establish therein. Regarding the filled hole, be

3.7 Overall iterative calculation procedure

Table 3.2

Overview of the correction function input.

stress function	corrects deviations by
$F_1^{\text{VE}\perp}$	$\text{PA}\left(F^{\text{inf}}\right)$
F_1^{HBC}	$\text{PA}\left(F^{\text{inf}}\right) + F_1^{\text{VE}\perp}$
$F_{l>1}^{\text{VE}\perp}$	$\text{PA}\left(F^{\text{inf}}\right) + \sum_{l^*=1}^{l-1} F_{l^*}^{\text{VE}\perp} + \sum_{l^*=1}^{l-1} \text{PA}\left(F_{l^*}^{\text{HBC}}\right)$
$F_{l>1}^{\text{HBC}}$	$\text{PA}\left(F^{\text{inf}}\right) + \sum_{l^*=1}^l F_{l^*}^{\text{VE}\perp} + \sum_{l^*=1}^{l-1} \text{PA}\left(F_{l^*}^{\text{HBC}}\right)$

reminded that the coordinate $y^* = y - e$ has been introduced such that the antisymmetry is along $y^* = 0$, from which Fourier series expansion can be conveniently performed. Inaccurate load transfer ratios $\chi_{\sigma_y}, \chi_{\sigma_r}$ are due to an excessive force flux through the hole edge or excessive shear stresses along the vertical boundaries $x = \pm w/2$. The former is cured by applying further correction functions F_l^{HBC} and the latter by increasing the minimum total number of plates $n_{x,\text{min}}$. The correction functions then shall be recalculated since the arising stress errors are affected by the number of plates $n_{x,\text{min}}$ in use. Table 3.2 provides an overview concerning the correction functions of an iteration step from which the stress deviations to cancel originate.

Chapter 4

Stress analysis - Discussion of the results

In this Chapter, the stress results of the present complex calculus are discussed and validated against Finite Element (FE) analyses. The implementation of the corresponding FE model is described in Sect. 4.1. The effect of the periodic arrangement technique (Sect. 3.4) is demonstrated by plotting the force flux of the open- and filled-hole problem in Sect. 4.2. This enables to qualitatively assess if the stress-free finite boundaries are captured adequately. Furthermore, the influence of finite plate dimensions on the number of auxiliary plates required to obtain an accurate solution is shown in Sect. 4.3. For quantitative assessment, the circumferential and net-section stresses are investigated for some commonly used layups enabling to analyse the effect of material orthotropy on these characteristic stresses. Moreover, effects by finite plate dimensions are studied by varying the plate geometry. The analysis starts with the open hole in Sect. 4.4, followed by the filled (or pin-loaded) hole in Sect. 4.5. Then, the superposition of the corresponding stress fields in Sect. 4.6 enables the investigation of the bolted joint under combined bearing-bypass load. Besides validation against FE analyses, the performance of the present calculus is compared against heuristic approaches. These are given by the well known Tan solutions for the open hole (Tan, 1988; Tan and Kim, 1990; Tan, 1994).

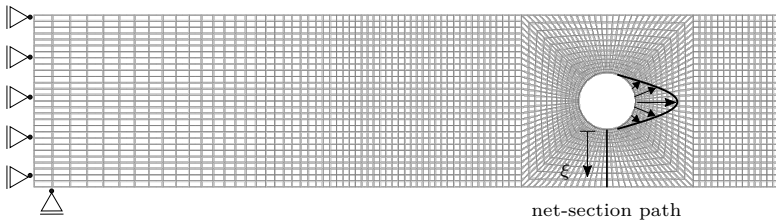


Fig. 4.1 Finite Element model of the filled hole with $w/d = 3$, $e/d = 3$.

4.1 Finite Element model for validation

For validation of the present calculus, a Finite Element model has been built in ABAQUS. Concerning its mesh, CPS8 continuum plane stress elements containing 8 nodes are used. Radial hole tractions with sinusoidal shape as bolt contact idealisation are applied to model the filled hole as expressed by Eq. (3.3). Regarding the open hole, uniform tension is applied in sufficiently large hole distance $y = \pm 20d$. Fig. 4.1 exemplarily shows the FE model for the filled-hole problem. Concerning an extensive convergence study, refer to Nguyen-Hoang and Becker (2021d). Therein, it is concluded that at least 72 elements shall be located along the hole edge to achieve the same accuracy as the FE values published by Catalanotti and Camanho (2013).

4.2 Investigation of force flux

To qualitatively analyse the compatibility of all correction functions and potentials with the stress boundary conditions and the overall load transfer, let us calculate the force flux using the stress vector

$$\mathbf{t}_y = \begin{bmatrix} \sigma_x & \tau_{xy} \\ \tau_{xy} & \sigma_y \end{bmatrix} \begin{bmatrix} 0 \\ n_y \end{bmatrix} = n_y \begin{bmatrix} \tau_{xy} \\ \sigma_y \end{bmatrix} \quad \text{with} \quad n_y = \begin{cases} 1 & \text{open hole,} \\ -1 & \text{filled hole.} \end{cases} \quad (4.1)$$

Regarding the filled hole, $n_y = -1$ is chosen only for cosmetic reasons. Then, the corresponding force flux is introduced along the upper half of the hole edge, which is further led through the plate's net-section plane towards the clamp. Fig. 4.2 and 4.3 exemplarily show the flux for the open and filled hole both in a quasi-isotropic laminate. The force fluxes of the finite-domain problems derived using the present calculus are tangent to the straight edges as in the FE reference and thus provide a physically meaningful load transfer. This qualitatively confirms the present method. Further quantitative approval is given by the load transfer ratios in Eq. (3.95) and (3.96) staying within the defined limits. Note that the force flux of the open hole in an infinite domain is dominated by the stress component σ_y and only slight shear tractions along the vertical edges $x = \pm w/2$ need to be mitigated. Hence, the impact of the auxiliary plates can be hardly noticed when modelling the force flux of the finite open-hole problem. Nevertheless, for high precision in the overall solution, their presence is essential. The investigation of the force fluxes enables an insight into the tractions (normal or shear tractions) that dominate the load transfer mechanism. This will be vital for the scope of the next Section.

4.3 Influence of finite dimensions on number of required auxiliary plates

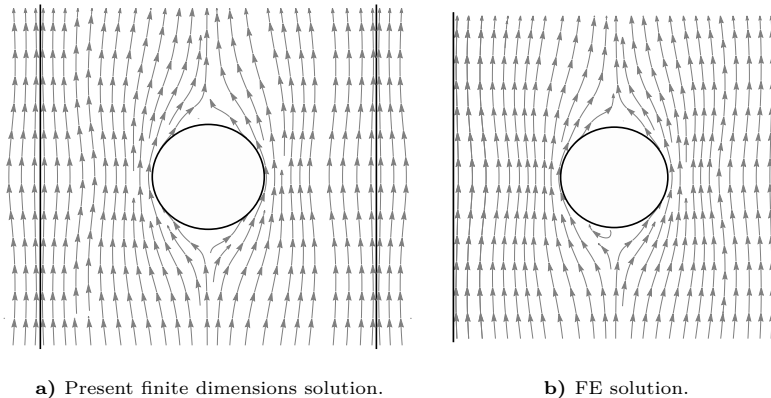
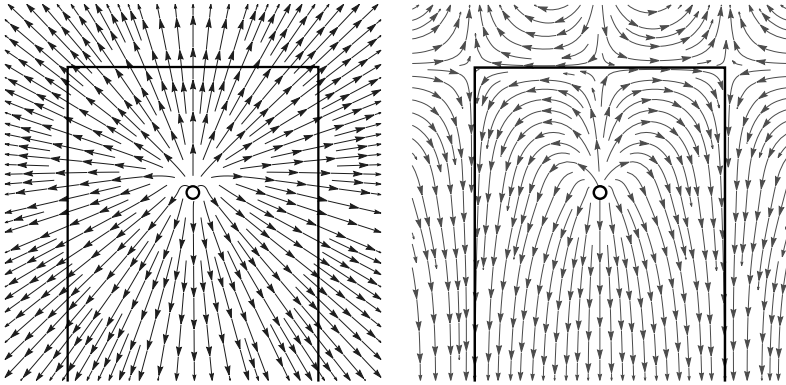


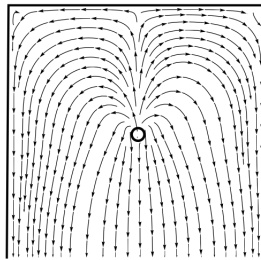
Fig. 4.2 Flux of the stress vectors \mathbf{t}_y for the open hole in a quasi-isotropic laminate of the finite width $w/d = 3$. The force flux of the infinite open-hole problem is not shown yielding almost no difference to that of the open hole in a finite domain. According to $n_y = 1$ in Eq. (4.1), vectors pointing in positive y -/upward direction indicate normal stresses in tension. Negative y -/downward direction indicates normal stresses in compression. Horizontal vectors indicate a pure shear stress state.

4.3 Influence of finite dimensions on number of required auxiliary plates

To investigate the effect of finite dimensions on the minimum number of auxiliary plates $n_{x,\min}$ that lead to sufficiently eliminated shear tractions $\tau_{xy}(\pm w/2, y)$, let us exemplarily take the filled-hole problem with quasi-isotropic plate material and calculate its corresponding values $n_{x,\min}$ shown in Fig. 4.4. Therein, the minimum numbers of auxiliary plates that lead to a sufficiently small load transfer value $\psi_{\tau_{xy}}^{\text{inf}}$ with respect to finite-dimensions properties w/d and e/d are plotted. Setting $\psi_{\tau_{xy}}^{\text{inf}}$ is generally a trade-off between accuracy of the solution and required computational cost. To demonstrate the capabilities of the present calculation method, a rather small value of $\psi_{\tau_{xy}}^{\text{inf}} \leq 0.5\%$ has been selected in Eq. (3.51). The minimum number of horizontal plates $n_{x,\min}$ increases with a decreasing value w/d as the shear stress decay is more restricted than in wider connections. Hence, shear tractions of larger magnitude need to be eliminated, which requires additional horizontal auxiliary plates. Further, the quantity $n_{x,\min}$ increases with the relative end distance e/d . A high ratio of e/d means that the load transfer ratio $\psi_{\tau_{xy}}^{\text{inf}}$ in



a) Load introduction through infinite plate. b) Present finite dimensions solution.



c) FE solution.

Fig. 4.3 Force flux of stress vectors \mathbf{t}_y for the filled hole in a quasi-isotropic laminate bounded by $w/d = 20$, $e/d = 10$. According to $n_y = -1$ in Eq. (4.1), vectors pointing in negative y -southern direction indicate normal stresses in tension. Positive y -northern direction indicates normal stresses in compression. Horizontal vectors indicate a pure shear stress state.

Eq. (3.51) needs to be calculated by integration over a length which is longer than for connections with small end distance. This then yields higher remaining integrated shear tractions to be eliminated. Also see Fig. 3.7 and 3.8 for further illustration. For the finite boundaries $w/d \geq 3$, $e/d \geq 3$ investigated in this work, $L = 3$ iterations have revealed to yield sufficiently fulfilled BCs. This quantity generally increases when reducing the dimensions w/d , e/d and vice versa. Note that halving $\psi_{\tau_{xy}}^{\text{inf}}$ approximately doubles $n_{x,\text{min}}$. This inversely linear relationship $\psi_{\tau_{xy}}^{\text{inf}} \sim 1/n_{x,\text{min}}$ is due to the fact that the leading

4.3 Influence of finite dimensions on number of required auxiliary plates

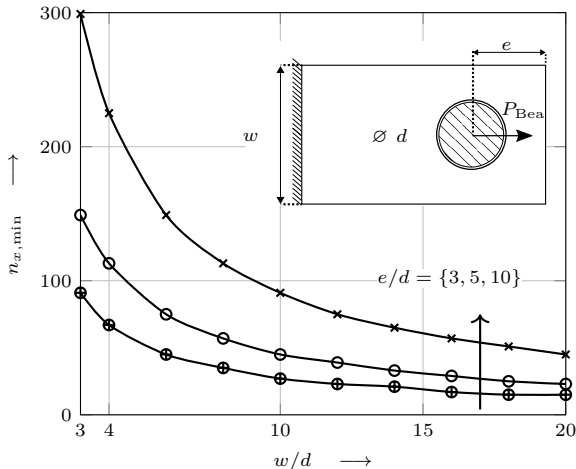


Fig. 4.4 Filled hole: minimum number of horizontal plates $n_{x,\min}$ enabling vanishing shear stresses along the vertical boundaries with a load transfer ratio of $\psi_{\tau_{xy}^{LI}} \leq 0.5\%$. This is shown for quasi-isotropic laminates. For the orthotropic case, the qualitative behaviour is the same.

term of the stresses is of the order $1/r$. This is produced by the logarithmic terms $B_k \ln \zeta_k$ in the complex potentials in Eq. (3.25) representing the infinite domain filled-hole problem. These terms are required to model the nonzero force resultant P_{Bea} . The stresses then can be derived using Eq. (2.27), (2.28) containing the complex potentials' first derivative. Hence, the stresses are of the leading order $1/r$. For open holes, contrary, this relationship is quadratic with $\psi_{\tau_{xy}^{inf}} \sim 1/n_{x,\min}^2$ because the stresses of the doubly-symmetric open-hole problem with vanishing force resultants have the leading term $1/r^2$.

Furthermore, the minimum plate number of the open hole is quite small in comparison to those of the filled hole. For instance, $n_{x,\min} \leq 10$ regarding $w/d = 3$ and a quasi-isotropic material. To better understand this difference of the plate numbers, let us investigate the integration of the shear tractions in Eq. (3.51), by which $n_{x,\min}$ is derived. Although the integration boundaries involved in the open hole are significantly wider, the integrated shear stresses are smaller leading to a low minimum number of plates. This matter why the corresponding shear tractions are differently pronounced shall be further analysed by heuristically investigating the following characteristics of the open- and filled-hole problem. First, the remaining area on which the external

load is concentrated. Generally, it can be expected that a smaller remaining area relative to the total area yields higher stress concentrations. Second, the decay of the stress concentrations and third, the stress components that dominate the load transfer mechanism. Regarding the infinite open-hole problem, uniform tension is applied at infinity. This pure force flux in load direction is disturbed by the hole, where the loading is distributed and concentrated to an area only reduced by the hole diameter d and the area reduction is relatively slight. Hence, its effects of changing the load transfer mechanism dominated by the stress component σ_y are rather small and locally concentrated in the hole vicinity. Only near its boundary but hardly along the straight edges, stress vectors with horizontal part indicating shear tractions are present (Fig. 4.2). Further, the decay of the stress concentrations is of the order $1/r^2$ due to the double symmetry. Regarding the filled hole in an infinite domain, the bolt load is introduced along half of the circumference length of the hole πR , and distributed in all directions through the entire plate. The area per plate thickness which is available for load transfer decreases as follows:

$$w \rightarrow \pi R \quad \text{for filled hole,} \quad w \rightarrow w - d \quad \text{for open hole.} \quad (4.2)$$

Hence, the area reduction of the filled hole is more significant than that of the open hole. This is even more pronounced the wider the plate width w . That is why the filled hole can be considered as the more critical load case and its stress concentrations are expected to be generally higher than those of the open hole. This matter will be quantitatively discussed in Sect. 4.6 by comparing the corresponding characteristic stress data. Moreover, for the filled hole, the decay of the stress concentrations is weaker (filled hole: $1/r$ vs. open hole: $1/r^2$). Concerning the load transfer mechanism of the filled-hole problem, the load distribution mainly occurs by radial tractions (Fig. 4.3). Using stress transformation these then yield high shear stresses $\tau_{xy}(\pm w/2, y)$ to eliminate, which require a high minimum number of auxiliary plates.

In the next Sections, the characteristic stresses are analysed for some common layups and the impact of finite dimensions is discussed. Further, the present stress results are validated using FE analyses and compared against heuristic approaches. First, open holes are treated followed by filled holes and then by bolted joints under combined bearing-bypass load.

4.4 Analysis of characteristic stresses: Open hole

Table 4.1

Elastic ply properties of Hexcel IM7-8552 (Camanho et al., 2012). In this thesis, the orientation of a ply is counted anti-clockwise with $[0^\circ]$ parallel to the y -axis.

	$[0^\circ]$	$[\pm 45^\circ]_s$	$[0^\circ/90^\circ]_s$	$[0^\circ/\pm 45^\circ/90^\circ]_s$ (50%/40%/10%)	quasi-isotropic
\hat{E}_x in GPa	9.10	17.75	90.60	39.52	64.52
\hat{E}_y in GPa	171.40	17.75	90.60	100.05	64.52
\hat{E}_y/\hat{E}_x	18.84	1.00	1.00	2.53	1.00
\hat{G}_{xy} in GPa	5.30	36.51	5.30	20.77	24.64
$\hat{\nu}_{xy}$	0.016	0.775	0.030	0.169	0.309

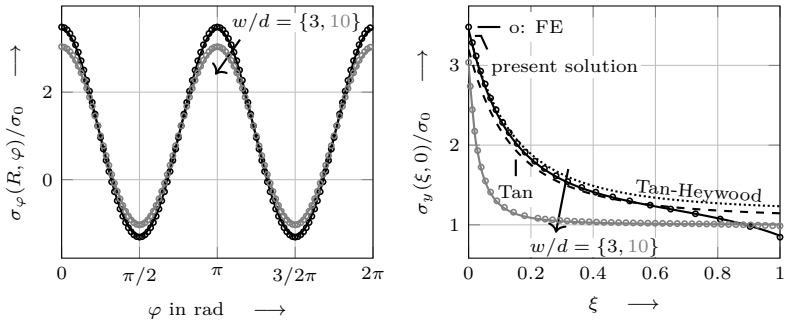
4.4 Analysis of characteristic stresses: Open hole

Let us investigate the circumferential and the net-section stresses for different layups and a geometry ratio of $w/d = \{3, 10\}$ in Fig. 4.5. The latter dimension is chosen such that finite-width effects have rather decayed and the corresponding infinite-domain solution by Lekhnitskii (1968) may be used as a good approximation. For convenience, the dimensionless coordinate

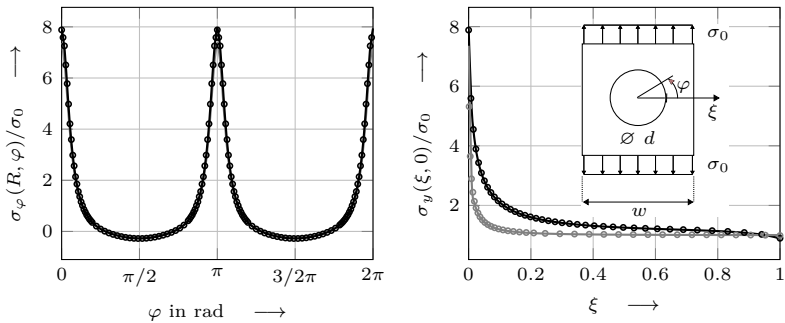
$$\xi = \frac{x - R}{w/2 - R}, \quad (4.3)$$

with $\xi = 0$ at the hole edge and $\xi = 1$ at the free straight boundary is used. See the pictograms in Fig. 4.5 for illustration. Note that all stresses shown refer to a plate model of a laminate with the smeared effective in-plane engineering constants $\hat{E}_x, \hat{E}_y, \hat{G}_{xy}, \hat{\nu}_{xy}$. The corresponding values of the laminates investigated are listed in Table 4.1. The stresses of a ply may be calculated using the strains and the corresponding reduced stiffness matrix in the context of Classical Laminate Theory (see Subsect. 2.1.5 or Halpin (1992); Becker and Gross (2002); Schürmann (2007) and Tsai (2008)). In general, the maximum of the net-section stresses $\sigma_y(\xi, 0)$ is directly located at the hole edge except for the $[\pm 45^\circ]_s$ -laminate, where it can be found at some hole distance. For the laminates $[0^\circ/90^\circ]_s$ involving a low shear modulus \hat{G}_{xy} and $[0^\circ]$ characterised by both low \hat{G}_{xy} and high orthotropy degree \hat{E}_y/\hat{E}_x (see Table 4.1), very high stress concentrations $\sigma_{y,\max}$ for both narrow and wide plates $w/d = \{3, 10\}$ arise. Finite-width effects then are rather small and the shapes of the circumferential stresses are hardly changed. Contrary, for the remaining laminates $[\pm 45^\circ]_s, [0^\circ/\pm 45^\circ/90^\circ]_s$ (50%/45%/10%) and quasi-isotropic with low orthotropy degree and higher shear modulus, the net-section stress concentrations are generally lower. Further, more significant finite-width effects occur. This is observable by a more pronounced raise of the stress concentrations when reducing the plate dimension w/d . Moreover,

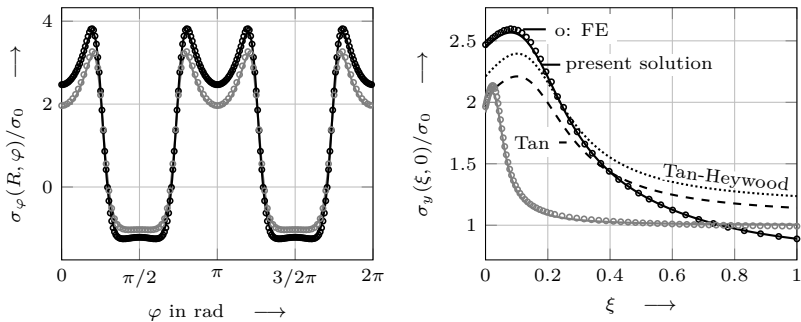
Chapter 4 Stress analysis - Discussion of the results



a) Quasi-isotropic laminate.

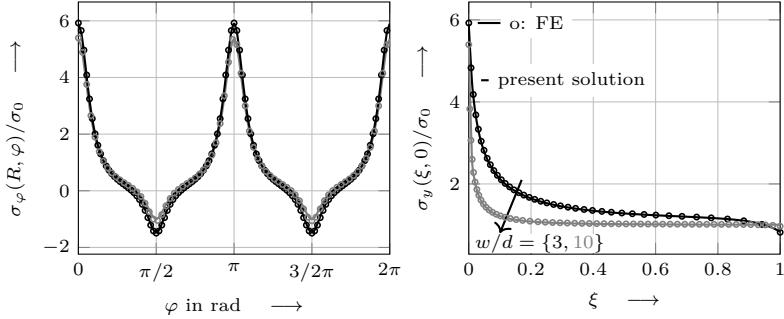


b) $[0^\circ]$ -laminate. For reasons of clear view, the following stresses are not shown: FE values of the circumferential stresses for $w/d = 10$ almost coinciding with solution for $w/d = 3$ due to slight finite-width effect and net-section stresses by Tan and Tan-Heywood yielding good correlation to FE.

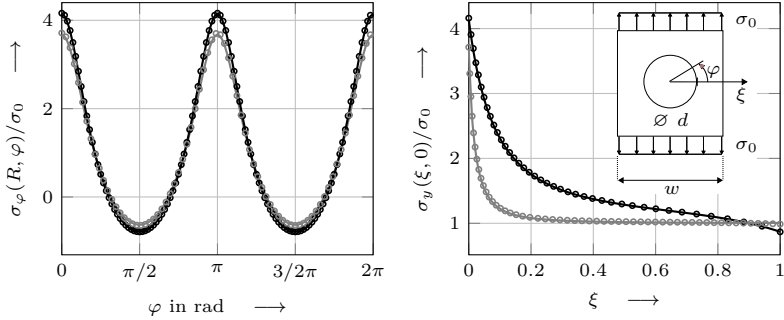


c) $[\pm 45^\circ]_s$ -laminate.

4.4 Analysis of characteristic stresses: Open hole



d) $[0^\circ/90^\circ]_s$ -laminate. Net-section stresses by Tan and Tan-Heywood yield good correlation to FE and are not shown for reasons of clear view.



e) $[0^\circ/\pm 45^\circ/90^\circ]_s$ (50%/40%/10%)-laminate. Net-section stresses by Tan and Tan-Heywood yield good correlation to FE and are not shown for reasons of clear view.

Fig. 4.5 Circumferential and net-section stresses of the laminate's idealisation as an orthotropic plate with smeared stiffnesses. For $w/d = 10$, finite-width effects have decayed and the infinite-domain solution by Lekhnitskii (1968) can be used. Note that the fibre orientation ϑ is counted anti-clockwise with $\vartheta = 0^\circ$ parallel to the y -axis/direction of the external load.

the circumferential stresses $\sigma_\varphi(R, \varphi)$ yield values in compression along the parts of the hole edge that face towards the uniaxial remote load introduction at $\varphi = \{\pi/2, 3/2\pi\}$. These minima are more pronounced for laminates with higher lateral stiffness \hat{E}_x , for instance $[0^\circ/90^\circ]_s$ and quasi-isotropic layup.

The present calculus yields excellent agreement with a maximum error magnitude of 1.4 %, which occurs in the net-section stresses of the $[\pm 45^\circ]_s$ -laminate. Note that its peak $\sigma_{\varphi, \max}$ does not lie in the net-section

area $\varphi = \{0, \pi\}$ but is slightly shifted along the hole boundary in the circumferential direction. The performance of the present methodology shall be also compared to the commonly used heuristic net-section stress approximations documented in Tan (1988); Tan and Kim (1990) as well as Tan (1994). Be reminded that these are based on two concepts: Firstly, the Tan approach in which the net-section stresses of the infinite open-hole problem are scaled such that their integration along the width of the actual finite-domain problem equilibrates the external load and secondly, the enhanced Tan-Heywood approach (Tan-HW). Therein, the stresses are adapted to the Heywood formula (Heywood, 1952) based on photoelasticity. Let K_{t0} be the stress concentration factor⁶ (SCF) at the hole edge with

$$K_{t0} = \frac{\sigma_y(\xi = 0, y = 0)}{\sigma_0}. \quad (4.4)$$

Then, the finite-width correction factor $K_{t0}^{\text{Tan}}/K_{t0}^{\text{inf}}$ of the Tan approach is derived by

$$\begin{aligned} \sigma_y^{\text{Tan}}(x, 0) &= \frac{K_{t0}^{\text{Tan}}}{K_{t0}^{\text{inf}}} \sigma_y^{\text{inf}}(x, 0), \\ 2 \frac{K_{t0}^{\text{Tan}}}{K_{t0}^{\text{inf}}} \int_R^{w/2} \sigma_y^{\text{inf}}(x, 0) dx &= \sigma_0 \cdot w. \end{aligned} \quad (4.5)$$

For $\sigma_y^{\text{inf}}(x, 0)$, the corresponding infinite domain open-hole stresses shall be taken. Regarding the enhanced Tan-Heywood approach, the finite-width correction factor $K_{t0}^{\text{Tan-HW}}/K_{t0}^{\text{inf}}$ is determined by

$$\begin{aligned} K_{t0}^{\text{Tan-HW}}/K_{t0}^{\text{inf}} &= \\ &= \left[\frac{3(1-d/w)}{2+(1-d/w)^3} + \frac{1}{2} \left(\frac{d}{w} M \right)^6 (K_{t0}^{\text{inf}} - 3) \left\{ 1 - \left(\frac{d}{w} M \right)^2 \right\} \right]^{-1} \end{aligned} \quad (4.6)$$

with

$$\begin{aligned} M^2 &= \left\{ \sqrt{1 - 8 \left[\frac{3(1-d/w)}{2+(1-d/w)^3} - 1 \right]} - 1 \right\} \cdot \frac{1}{2(d/w)^2}, \\ K_{t0}^{\text{inf}} &= 1 + \sqrt{\frac{2}{A_{11}} \left(\sqrt{A_{11}A_{22}} - A_{12} + \frac{A_{11}A_{22} - A_{12}^2}{2A_{66}} \right)} \\ &= \sigma_y^{\text{inf}}(R, 0)/\sigma_0. \end{aligned} \quad (4.7)$$

⁶ For disambiguation: stress concentrations normalised to a certain reference value shall be called stress concentration factors.

4.4 Analysis of characteristic stresses: Open hole

Therein, the quantities A_{ij} denote the in-plane stiffnesses of a laminate that can be calculated using Classical Laminate Theory (Tsai (2008); Halpin (1992) or Sect. 2.1.5). Note that the formula for K_{t0}^{inf} is adapted to the nomenclature of the present thesis with a fibre orientation $\vartheta = 0^\circ$ parallel to the y -axis. For the quasi-isotropic case, the correction factors specialise to

$$\begin{aligned} K_{t0}^{\text{Tan}}/K_{t0}^{\text{inf}} &= \frac{2}{2 - (d/w)^2 - (d/4)^4}, \\ K_{t0}^{\text{Tan-HW}}/K_{t0}^{\text{inf}} &= \frac{2 + (1 - d/w)^3}{3(1 - d/w)}. \end{aligned} \quad (4.8)$$

Let us assess the net-section stresses derived by the Tan formulae. When comparing the entire net-section plane $0 \leq \xi \leq 1$ and assessing the highest error magnitude, deviations for all heuristic approaches are quite high as summarised in Table 4.2. However, Whitney and Nuismer (1974); Taylor (2007, 2008); Camanho et al. (2012); Nguyen-Hoang and Becker (2022d) as well as Sect. 5.2 of the present work reveal that nonlocal failure concepts require the stress evaluation in the vicinity of the hole edge when assessing a technically relevant hole diameter not smaller than a few millimetres. Hence, the range of interest is limited, which shall be roughly assumed to lie within $0 \leq \xi \leq 0.2$. Therein, both the Tan and Tan-Heywood approaches perform better than along $\xi > 0.2$. Their solution quality depends on how pronounced the finite-width effect of a laminate is. As a reminder, it is slight for $[0^\circ]$, $[0^\circ/90^\circ]_s$ as well as $[0^\circ/\pm 45^\circ/90^\circ]_s$ (50%/40%/10%)-laminates and their stress concentrations are mainly due to the material anisotropy. These only slightly increase with decreasing w/d . For these laminates, the approaches by Tan and Tan-Heywood yield good approximations within $0 \leq \xi \leq 0.2$ and are not further shown in Fig. 4.5 for reasons of limited space. Contrary, $[\pm 45^\circ]_s$ and quasi-isotropic laminates show pronounced finite-width effects and the errors of the heuristic approaches are larger within $0 \leq \xi \leq 0.2$ except for the Tan-HW concept yielding excellent results for

Table 4.2
Maximum error magnitudes of heuristically determined stresses.

	$0 \leq \xi \leq 1$		$0 \leq \xi \leq 0.2$	
	Tan	Tan-HW	Tan	Tan-HW
quasi-isotropic	36 %	46 %	-8 %	2 %
$[\pm 45^\circ]_s$	28 %	39 %	-17 %	-10 %
$[0^\circ]$	26 %	33 %	-2 %	5 %
$[0^\circ/90^\circ]_s$	39 %	48 %	-3 %	-5 %
$[0^\circ/\pm 45^\circ/90^\circ]_s$ (50%/40%/10%)	31 %	41 %	-6 %	4 %

quasi-isotropic laminates. However, for the remaining cases, the stresses derived by solving the actual boundary value problem should be taken, especially when each percent accuracy matters in lightweight optimal design. Concerning $[\pm 45^\circ]_s$ -laminates treated by both the Tan and Tan-Heywood approach as well as regarding the quasi-isotropic laminate by Tan approach, their net-section stresses in the critical range $\xi \leq 0.2$ underestimate the FE solution and therefore can be regarded as nonconservative approximations. Further, the net-section stresses by Tan-Heywood violate the equilibrium. In particular, their integral along the width of the finite problem unphysically yields an excessive load transfer value of up to $\chi_{\sigma_y} = 1.08$ although a value of 1 should be obtained.

With this the stress results of the open-hole problem derived by the present calculus are validated. Hence, it can be regarded as a reliable means to treat any other doubly symmetric finite-domain problem.

4.5 Analysis of characteristic stresses: Filled hole

The stress results for single-fastener connections of the geometrical properties $w/d = \{3, 20\}$, $e/d = \{3, 10\}$ are presented. The second ratios $w/d = 20$ and $e/d = 10$ are chosen in such a way that the corresponding finite dimensions effect has decayed. The following layups commonly used in composite bolted joints shall be analysed: quasi-isotropic, $[0^\circ]$, $[0^\circ/90^\circ]_s$ and $[0^\circ/\pm 45^\circ/90^\circ]_s(50\%/40\%/10\%)$ -laminate. Let us investigate the circumferential and net-section stresses relevant for the crack initiation assessment in Fig. 4.6-4.9. Therein, the stresses are normalised to the bearing stress $\sigma_d = P_{\text{Bea}}/d$. In general, the shape of characteristic stresses as well as their stress concentrations are strongly affected by the material orthotropy \hat{E}_y/\hat{E}_x and the shear modulus \hat{G}_{xy} . The effective in-plane constants for each laminate are shown in Table 4.1. The following observations can be made for all geometry properties $w/d, e/d$ and both results of FE and the present calculus. The most orthotropic $[0^\circ]$ -laminate with $\hat{E}_y/\hat{E}_x = 18.84$ leads to the highest stress concentration $\sigma_\varphi(R, 0)$. This implies that a high stiffness ratio \hat{E}_y/\hat{E}_x leads to a pronounced peak in the circumferential stresses. However, the concentration of the $[0^\circ/\pm 45^\circ/90^\circ]_s(50\%/40\%/10\%)$ -laminate is lower than that of the $[0^\circ/90^\circ]_s$ -laminate although the orthotropy degree of the first layup ($\hat{E}_y/\hat{E}_x = 2.53$) is higher than that of the second ($\hat{E}_y/\hat{E}_x = 1$). This is due to their different shear modulus \hat{G}_{xy} , for which a low value as for the $[0^\circ]$ - and $[0^\circ/90^\circ]_s$ -laminate raises the stress concentration at $\varphi = \{0, \pi\}$. This is further confirmed when comparing the quasi-isotropic and the $[0^\circ/90^\circ]_s$ -laminate both yielding a ratio $\hat{E}_y/\hat{E}_x = 1$ but different shear moduli. The

4.5 Analysis of characteristic stresses: Filled hole

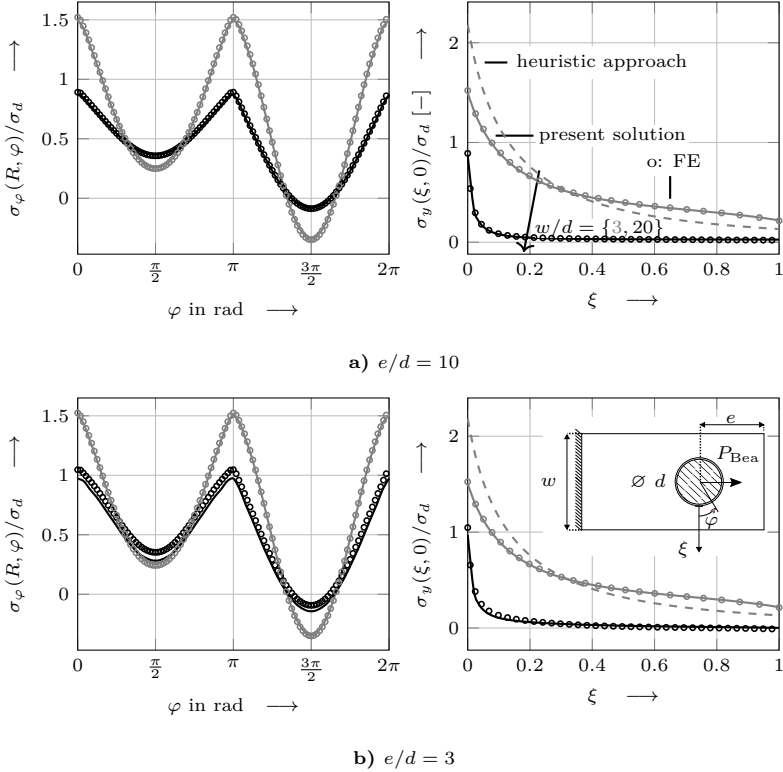


Fig. 4.6 Circumferential and net-section stresses of quasi-isotropic laminate.

value of the $[0^\circ/90^\circ]_s$ -laminate is lower leading to the higher stress concentration. To conclude, an interaction between \hat{E}_y/\hat{E}_x and \hat{G}_{xy} is decisive for the peak of the circumferential stresses that is located in the net-section plane $\varphi = \{0, \pi\}$. Regarding the extremum at $\varphi = \pi/2$, the peak is dominantly affected by \hat{G}_{xy} . The quasi-isotropic laminate is characterised by the highest shear modulus in this study and its local extremum is a local minimum. All other laminates have a smaller value of the shear stiffness \hat{G}_{xy} and a local maximum, contrary. The highest peaks $\sigma_\varphi(R, \pi/2)$ can be found in the $[0^\circ]$ and $[0^\circ/90^\circ]_s$ -laminate with the smallest shear modulus. However, the peak of latter layout is higher than that of the former. This is due the

Chapter 4 Stress analysis - Discussion of the results

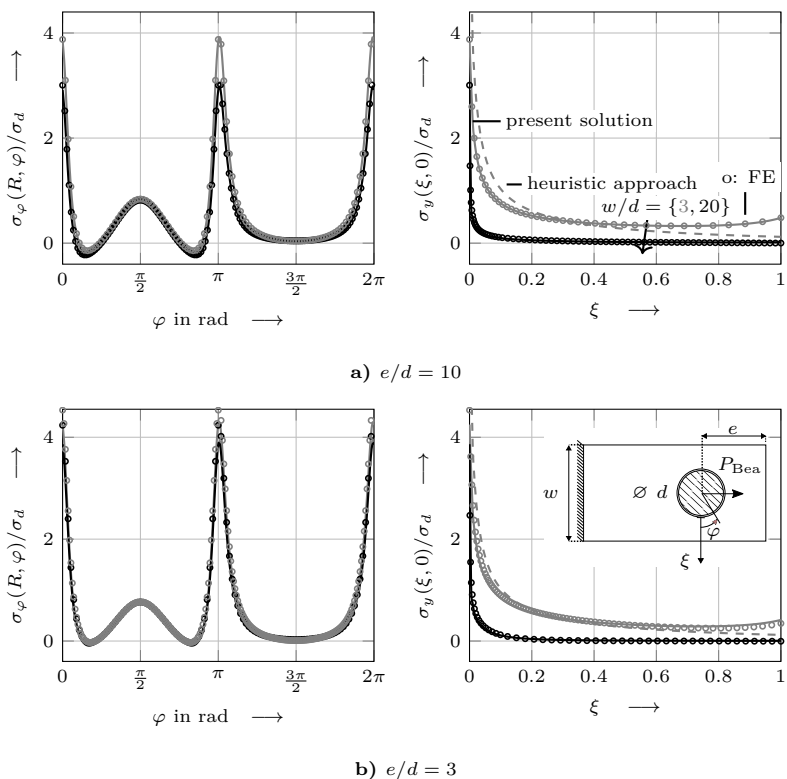


Fig. 4.7 Circumferential and net-section stresses of $[0^\circ]$ -laminates.

different lateral stiffnesses \hat{E}_x , for which a significantly higher value belongs to the $[0^\circ/90^\circ]_s$ -laminates further raising the stress concentration $\sigma_\varphi(R, \pi/2)$. Contrary to $\sigma_\varphi(R, \pi/2)$, the peak at $\varphi = 3/2\pi$ stays a local minimum for all laminates investigated.

Let us proceed with analysing the effect by finite dimensions. In general, the raise of the stress concentrations as well as the change of the shape of the circumferential stresses when reducing the relative dimensions $w/d, e/d$ is more significant the smaller the orthotropy degree. For instance, the effect due to finite dimensions is the most pronounced in the quasi-isotropic laminate ($\hat{E}_y/\hat{E}_x = 1$) with a stress concentration raise of 71 % when shortening the

4.5 Analysis of characteristic stresses: Filled hole

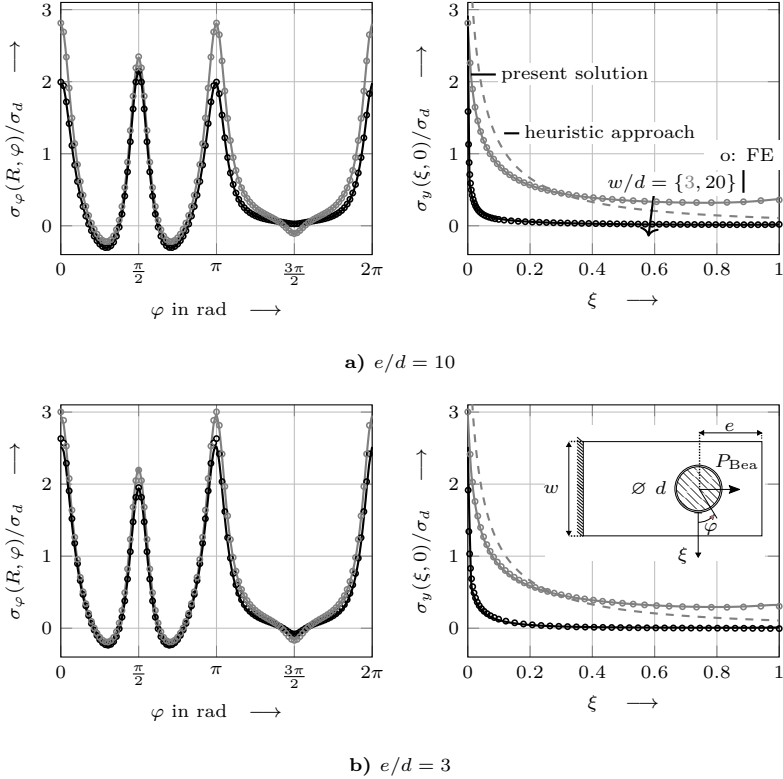


Fig. 4.8 Circumferential and net-section stresses of $[0^\circ/90^\circ]_s$ -laminate.

relative dimensions $w/d = 20$, $e/d = 10$ to $w/d = 3$, $e/d = 3$. Further, the shape of the circumferential stresses changes significantly. By contrast, laminates with strong orthotropy degree (e.g. $[0^\circ]$ -laminate) or small shear modulus relative to \hat{E}_y, \hat{E}_x (e.g. $[0^\circ/90^\circ]_s$ -laminate) yield a less pronounced effect due to finite dimensions. The stress concentration rises by 51 % for the first laminate and by 34 % for the second. Moreover, the shape of the circumferential stresses only slightly changes. Note that the corresponding FE stress concentrations have been taken to determine the percentage increases.

The performance of the present calculus shall be now assessed. In general, finite dimensions are captured with satisfactory accuracy. However, regarding

Chapter 4 Stress analysis - Discussion of the results

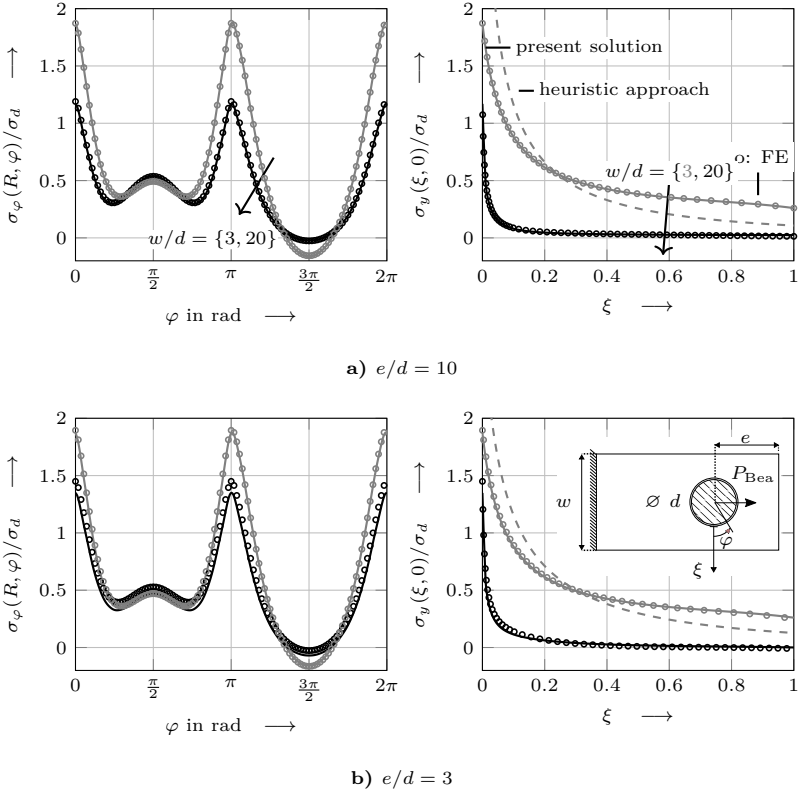


Fig. 4.9 Circumferential and net-section stresses of $[0^\circ / \pm 45^\circ / 90^\circ]_s$ (50%/40%/10%) - laminate.

geometry properties for which the effect by finite dimensions is dominantly or even only caused by a small end distance as for $w/d = 20$, $e/d = 3$, slight deviations are observable in the characteristic stresses of all laminates in the present study. This is due to the remaining shear stresses $\tau_{xy}(x, e)$ along the horizontal boundary $y = e$, which are not covered by the present methodology. Note that setups with large width and small end distance as $w/d = 20$, $e/d = 3$ triggering shear-out failure instead of the fail-safe bearing failure mode are quite unlikely to be designed. Hence, investigating these configurations is rather to better understand the effects of finite dimensions

4.5 Analysis of characteristic stresses: Filled hole

Table 4.3

Maximum error magnitudes of net-section stresses for $w/d = 3, e/d = 3$.

	$0 \leq \xi \leq 1$		$0 \leq \xi \leq 0.2$	
	present solution	heuristic approach	present solution	heuristic approach
Quasi-isotropic	2 %	-41 %	-1 %	43 %
$[0^\circ]$	20 %	-65 %	-7 %	52 %
$[0^\circ/90^\circ]_s$	6 %	-65 %	-2 %	56 %
$[0^\circ/\pm 45^\circ/90^\circ]_s$ (50%/40%/10%)	4 %	53 %	-2 %	53 %

and to demonstrate the limits of the present method than of interest in engineering applications. For $w/d = 3, e/d = 3$ of the $[0^\circ]$ -layup, the nonzero shear tractions are also leading to deviating peaks in the circumferential stresses at $\varphi = \{0, \pi\}$. Let us quantitatively assess the performance of the present calculus regarding the net-section stresses, which are relevant in tension failure analysis. This shall be done for the smallest configuration $w/d = 3, e/d = 3$ involving the most pronounced effects by finite dimensions in this thesis. Table 4.3 lists the relative errors along the entire net-section path $0 \leq \xi \leq 1$. Therein, except for the $[0^\circ]$ -laminates yielding deviations up to 20 %, results with errors not higher than 6 % and hence acceptable accuracy can be observed. However, failure analyses which are typically conducted by means of nonlocal criteria have shown that the stress evaluation occurs along some rather small hole distance (Whitney and Nuismer (1974); Taylor (2007, 2008); Camanho et al. (2012); Nguyen-Hoang and Becker (2022d) regarding open holes and Catalanotti and Camanho (2013); Nguyen-Hoang and Becker (2020a) concerning filled holes). When again roughly estimating this distance to lie within $0 \leq \xi \leq 0.2$, then the maximum error magnitude therein further reduces to a few percent for the quasi-isotropic layup, $[0^\circ/90^\circ]_s$ as well as $[0^\circ/\pm 45^\circ/90^\circ]_s$ (50%/40%/10%) and 7 % for the $[0^\circ]$ -laminates. Therefore, the present methodology leads to results with excellent accuracy in most cases. Then, regarding the analysis of tensile failure which likely occurs for $w/d \leq 4$, the predicted failure loads based on the stresses of the present method are expected to be of the same accuracy as by FE studies.

The performance of the heuristic approach shall now be analysed. This concept requires to scale the net-section stresses $\sigma_y^{\text{inf}}(x, 0)$ of the infinite-domain problem such that its integration along the width of the actual

finite-domain problem equilibrates the external load. In doing so, the stresses of the heuristic approach are calculated by

$$\sigma_y^{\text{HA}}(x, 0) = \frac{K_{t0}^{\text{HA}}}{K_{t0}^{\text{inf}}} \sigma_y^{\text{inf}}(x, 0) \quad \text{with} \quad 2 \frac{K_{t0}^{\text{HA}}}{K_{t0}^{\text{inf}}} \int_R^{w/2} \sigma_y^{\text{inf}}(x, 0) dx = P_{\text{Bea}}. \quad (4.9)$$

For the quantity $\sigma_y^{\text{inf}}(x, 0)$, the stress decay of the infinite filled-hole problem shall be taken. Table 4.3 shows excessive relative errors for all laminates investigated. Also note that the effect of a finite end distance e/d cannot be captured by this heuristic approach. The fact that this concept applied to open holes by Tan (1988, 1994) yields acceptable results is rather coincidental than physically motivated. The infinite open-hole problem (Kirsch, 1898; Lekhnitskii, 1968) is described by Airy stress functions or complex potentials with a few coefficients. Particularly, $\Phi_k^{\text{OH,inf}}$ is described by a sum with 2 terms⁷. The corresponding quantities of the present infinite bolted joint problem, however, require many coefficients. The complex potentials $\Phi_k^{\text{FH,inf}}$ contain sums with at least 8 coefficients⁸. Equally scaling the corresponding coefficients is unlikely to coincide with that of the actual finite boundary value problem. Further improving this approach is hard to implement since the solution is not known *a priori*. The present calculus, however, provides a robust and physically motivated means to model stress-free edges within a finite domain, no matter how complex the corresponding infinite problem is.

4.6 Analysis of characteristic stresses: Bearing-bypass interaction

Having gained a sound understanding of the structural mechanisms which occur in the open- and filled-hole problem, the bolted joint under combined bearing-bypass load shall be now analysed. The bearing-bypass load case is determined by the following superposition. Let F^{OH} and F^{FH} be the Airy stress functions of the open- and filled-hole problem, respectively. With the total introduced force $P = P_{\text{Bea}} + P_{\text{By}}$, the stress function for the bolted joint under bearing-bypass load then reads

$$F^{\text{BBI}} = (1 - \beta)F^{\text{OH}} + \beta F^{\text{FH}} \quad \text{with the load factor } \beta = \frac{P_{\text{Bea}}}{P}. \quad (4.10)$$

The special cases are given by the load factors $\beta = 0$, for which F^{BBI} specialises to the open-hole problem and $\beta = 1$ representing the filled hole.

⁷ See Eq. (3.13), (3.14), (3.20) regarding complex potentials and Eq. (3.21)-(3.24) regarding Airy stress functions and its stress components.

⁸ See Eq. (3.10) and Eq. (3.6) for the stress BCs.

4.6 Analysis of characteristic stresses: Bearing-bypass interaction

Note that regarding the latter setting, a geometry ratio of $e/d = 10$ is chosen such that there are no increased stresses due to a short end distance. However, the implementation of a finite large end distance of $e/d \geq 10$ is essential to ensure that the bolt load of the filled-hole problem is transferred towards $y \rightarrow -\infty$ and a uniaxial stress state along $y \rightarrow \infty$ can establish only due to the impact of the open hole (see Sect. 3.1). The characteristic stresses are now investigated in Fig. 4.10. Concerning the circumferential stresses therein, only an excerpt in between $\pi/2 \leq \varphi \leq 3/2\pi$ is plotted. For reasons of symmetry to the y -axis, the stresses along $-\pi/2 \leq \varphi \leq \pi/2$ are the same as those shown. For all investigated laminates, the curves of the characteristic stresses lie in between the special cases of open and filled holes. In general, the latter is the more critical load case yielding higher stress concentrations as heuristically outlined in Sect. 4.3. Hence, it can be expected that the failure stresses of the pin-loaded hole are lower than these of the open hole. To assess the increased criticality of the filled-hole problem, let us compare the stress concentration factors (SCFs) $K_{t0} = \sigma_y(\xi = 0, y = 0)/\sigma_0$. These are listed in Table 4.4. Note that the FE reference values have been taken. Also note that the stresses of the filled hole (e.g. in Fig. 4.6-4.9) are commonly normalised to the bearing stress $\sigma_d = P_{\text{Bea}}/d$. However, for reasons of better comparison of the special cases of the open and filled hole, their stresses shall be now normalised to the corresponding far-field stress σ_0 . Conversion can be done as follows. Be reminded that all forces are given per plate thickness in this thesis and with

$$P_{\text{Bea}} = \sigma_0 \cdot w = \sigma_d \cdot d, \quad (4.11)$$

the net-section stresses normalised to σ_0 , e.g., may be calculated by the conversion

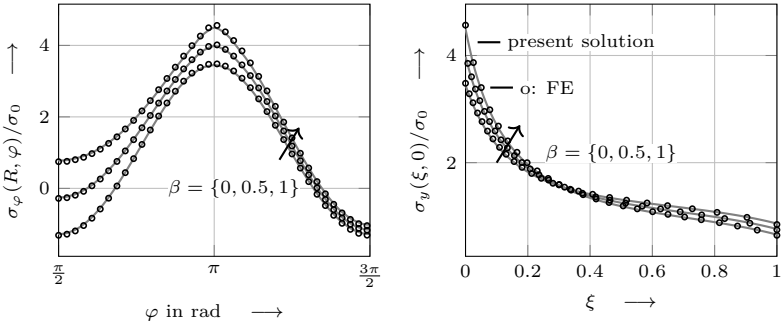
$$\frac{\sigma_y}{\sigma_0} = \frac{\sigma_y}{\sigma_d} \cdot \frac{w}{d}. \quad (4.12)$$

Furthermore, let us normalise the SCF of the filled hole to that of the open hole using

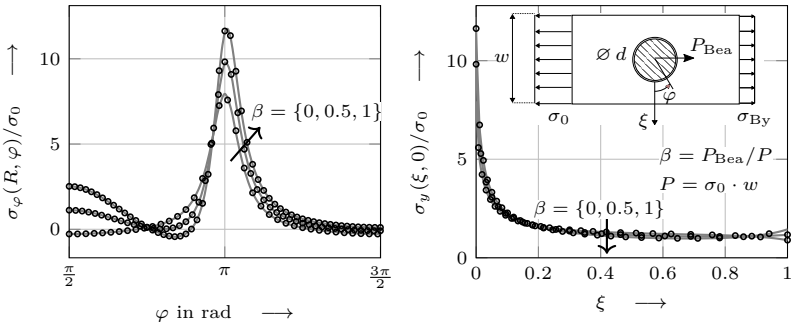
$$\kappa_{\beta=1} = \frac{K_{t0}(\text{Filled Hole})}{K_{t0}(\text{Open Hole})}. \quad (4.13)$$

This ratio shall serve as measure to quantify an increased criticality of the filled-hole problem relative to the open hole. The corresponding values of the laminates covered in this thesis are shown in Table 4.5a for $w/d = \{3, 20\}$. Generally, the wider w/d the higher the normalised SCF $\kappa_{\beta=1}$. Hence, the filled-hole problem is even more critical than the open hole for plates with larger ratio w/d . This applies for all laminates investigated. To better understand these findings, let us analyse the area reduction involved in the

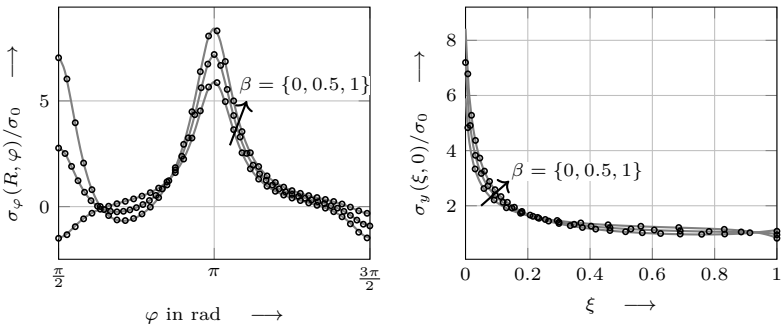
Chapter 4 Stress analysis - Discussion of the results



a) Quasi-isotropic laminate



b) $[0^0]$ -laminate



c) $[0^0/90^0]_s$ -laminate

4.6 Analysis of characteristic stresses: Bearing-bypass interaction

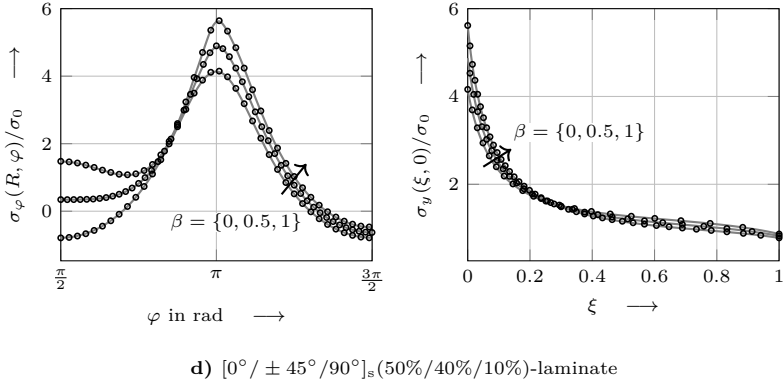


Fig. 4.10 Circumferential and net-section stresses of the bolted joint under bearing-bypass load. The relative plate width is $w/d = 3$.

open- and filled-hole problem. Let A_{tot} be the total area where the remote load σ_0 is introduced. Further, A_{red} denotes the reduced area to which the load is concentrated. Moreover, all areas shall be given per plate thickness. This yields the area reduction factors

$$\text{Open hole: } A_{\text{tot}} = w, \quad A_{\text{red}} = w - d \quad \rightarrow \quad \frac{A_{\text{red}}}{A_{\text{tot}}} = 1 - \frac{1}{w/d}, \quad (4.14)$$

$$\text{Filled hole: } A_{\text{tot}} = w, \quad A_{\text{red}} = \pi \frac{d}{2} \quad \rightarrow \quad \frac{A_{\text{red}}}{A_{\text{tot}}} = \frac{\pi}{2} \frac{1}{w/d}. \quad (4.15)$$

The area reduction factors $A_{\text{red}}/A_{\text{tot}}$ are plotted with respect to the width-to-diameter ratio w/d in Fig. 4.11. Generally, the higher $A_{\text{red}}/A_{\text{tot}}$, the larger the remaining area in which the external load is concentrated and vice versa. For the open hole, the remaining area is higher for wider w/d . Contrary, regarding the filled hole, the remaining area is higher for narrow connections. Interestingly, when $w/d \rightarrow \infty$ is due to a vanishing hole diameter $d \rightarrow 0$ the open-hole problem specialises to the plain plate under uniform tension and the filled-hole problem to the plain plate reacting to a single force. However, when $w/d \rightarrow \infty$ but the hole diameter stays nonzero the stress fields are those of the corresponding infinite-domain problem. In particular, the open hole is then described by the Kirsch (1898) solution regarding isotropic plates and by complex potentials addressed by Lekhnitskii (1968) for anisotropic plates. The filled hole is then represented by its infinite-domain solution, which can be found in Subsect. 3.3.3. Let us now investigate the area reduction

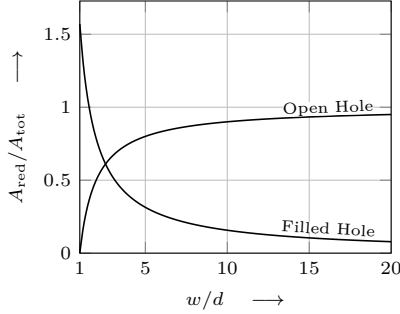


Fig. 4.11 Area reduction of the open- and filled-hole problem.

for a finite and nonzero width-to-hole diameter in Fig. 4.11. Regarding the open hole, the surface reduction factor converges to 1 with increasing w/d . For the filled hole, however, $A_{\text{red}}/A_{\text{tot}}$ approaches zero. Hence, the wider w/d the more significant its surface reduction factor, which eventually yields high values for K_{t0} and $\kappa_{\beta=1}$. These quantities also depend on the plate material. A high orthotropy degree or a low shear stiffness correlate with a higher sensitivity to a bearing (or bolt) load. This can be observed by a more significant increase of $\kappa_{\beta=1}$. For instance, the $[0^\circ]$ -laminates with the highest ratio $\hat{E}_y/\hat{E}_x = 18.84$ and a low shear modulus \hat{G}_{xy} yields the most pronounced factor $\kappa_{\beta=1}$. That is followed by the $[0^\circ/90^\circ]_s$ -layup with a low orthotropy degree $\hat{E}_y/\hat{E}_x = 1$ and the same shear stiffness as the $[0^\circ]$ -laminates. See Table 4.1 for an overview of the effective stiffness values. For bolted joints under combined bearing-bypass load ($0 < \beta < 1$), the normalised SCF is a linear function with respect to β ,

$$\kappa_\beta = 1 + \underbrace{\frac{\kappa_{\beta=1}}{\kappa_{\beta=0}}}_{=1} \cdot \beta \quad \text{with} \quad 1 < \kappa_\beta < \kappa_{\beta=1}. \quad (4.16)$$

This is due to the fact that the corresponding stress field is determined by superposition of the open- and filled-hole problem as expressed in Eq. (4.10).

The finite-width effects are now assessed. As quantitative measure, let us suggest the normalised SCFs

$$\kappa_{w/d} = \begin{cases} \frac{K_{t0}(w/d = 3)}{K_{t0}(w/d = 20)} & \text{for open holes,} \\ \frac{K_{td}(w/d = 3)}{K_{td}(w/d = 20)} & \text{for filled holes.} \end{cases} \quad (4.17)$$

4.6 Analysis of characteristic stresses: Bearing-bypass interaction

Table 4.4

Stress concentration factors for the special cases of bolted joint under bearing bypass load. The FE reference data is shown only. Regarding the filled hole, an end distance $e/d = 10$ is chosen. See Sect. 3.1 for further explanations.

(a) Quasi-isotropic laminate

	$w/d = 3$		$w/d = 20$	
	K_{td}	K_{t0}	K_{td}	K_{t0}
Open Hole	-	3.48	-	3.00
Filled Hole	1.50	4.50	0.87	17.40

(b) $[0^\circ]$ -laminate

	$w/d = 3$		$w/d = 20$	
	K_{td}	K_{t0}	K_{td}	K_{t0}
Open Hole	-	7.89	-	7.36
Filled Hole	3.88	11.64	3.01	60.20

(c) $[0^\circ/90^\circ]_s$ -laminate

	$w/d = 3$		$w/d = 20$	
	K_{td}	K_{t0}	K_{td}	K_{t0}
Open Hole	-	5.92	-	5.40
Filled Hole	2.81	8.43	1.99	39.80

(d) $[0^\circ/\pm 45^\circ/90^\circ]_s$
(50%/40%/10%)-laminate

	$w/d = 3$		$w/d = 20$	
	K_{td}	K_{t0}	K_{td}	K_{t0}
Open Hole	-	4.16	-	3.67
Filled Hole	1.87	5.61	1.19	23.80

Table 4.5

Normalised stress concentration factors (SCFs).

(a) $\kappa_{\beta=1}$

	$w/d = 3$	$w/d = 20$
QI	1.30	5.78
$[0^\circ]$	1.46	8.18
$[0^\circ/90^\circ]_s$	1.42	7.37
$[0^\circ/\pm 45^\circ/90^\circ]_s$ (50%/40%/10%)	1.35	6.49

(b) $\kappa_{w/d}$

	Open hole	Filled hole
QI	1.16	1.72
$[0^\circ]$	1.07	1.29
$[0^\circ/90^\circ]_s$	1.10	1.41
$[0^\circ/\pm 45^\circ/90^\circ]_s$ (50%/40%/10%)	1.13	1.57

These measures are summarised in Table 4.5b. Therein, it can be observed that finite-width effects are generally more significant for the filled hole. Moreover, the impact of finite width is more pronounced for laminates with a low orthotropy degree or a rather high shear modulus as the quasi-isotropic or $[0^\circ/\pm 45^\circ/90^\circ]_s$ (50%/40%/10%)-layup. For the bearing-bypass load case, the finite-width effect is lying in between the special cases and the degree depends on the actual load factor β .

Regarding the assessment of the performance of the present stress calculus, the results for the bearing-bypass load case stay within the small error ranges of the open and filled hole since the solution is obtained by superposition of these two special cases. Be reminded that the largest stress errors within the hole vicinity $0 \leq \xi \leq 0.2$ relevant for crack initiation assessment occur in

the filled hole for the plate dimensions of $w/d = e/d = 3$. These arise due to the nonzero shear tractions $\tau_{xy}(x, e)$, which are not covered by the present method. See Sect. 3.5 for details. The corresponding relative errors are listed in Table 4.3 and amount $|\epsilon| \leq 7\%$ regarding the $[0^\circ]$ -layup and $|\epsilon| \leq 2\%$ concerning the remaining laminates. However, this discrepancy does not apply to the bearing-bypass load case since the stress field of the filled-hole problem with a large end distance $e/d = 10$ is superimposed. Hence, the impact of nonzero shear tractions $\tau_{xy}(x, e)$ on the characteristic stresses is less significant. The stress results of all investigated laminates then have relative error magnitudes around $|\epsilon| = 1\%$ along $\xi \leq 0.2$. Therefore, the performance of the present stress calculus can be regarded as sufficiently accurate for the assessment of safety-critical structures in the context of lightweight design. With that the stress analysis is completed and the next step in structural assessment, failure analysis, can be done.

4.7 Interpolation formulae for quasi-isotropic laminates

In industry contexts, time constraints may require to quickly deliver the results of the stresses. Regarding the pin-loaded hole in a finite plate, a quite high number of auxiliary plates is needed due to large shear tractions to be eliminated (see Sect. 4.3). For the quasi-isotropic case, the stress field depends on the parameters $w/d, e/d$ and ν . However, the latter only slightly varies for common isotropic plate materials. In addition, the general influence of ν on the stresses is rather small (Bickley, 1928) and may be neglected in engineering applications. Then, only the plate dimensions shall be considered when deriving the stresses. For instantaneous determination of the stress decay along the net section as well as its concentration, polynomial fitting functions⁹ are suggested in Nguyen-Hoang and Becker (2021a, 2022c). These have been derived for a ratio of $e/d = 3$. For the connections with larger end distance, the derived fitting functions can be conservatively taken. Furthermore, when the primary effect of finite plate dimensions is due to a narrow width the impact of the end distance is small as discussed in Sect. 4.5. Regarding the stress concentration factor $K_{td} = \sigma_y(R, 0)/\sigma_d$, the corresponding fit shall be compared to the values documented in the well known Peterson's stress concentrations handbook (Pilkey and Pilkey, 2008), which is commonly used in industry contexts. With $\sigma_d = P_{\text{Bea}}/d$, the fitting functions of the SCFs read as follows.

⁹ Again, special thanks to Dr. J. Broede from the IASB working group for providing these functions.

4.7 Interpolation formulae for quasi-isotropic laminates

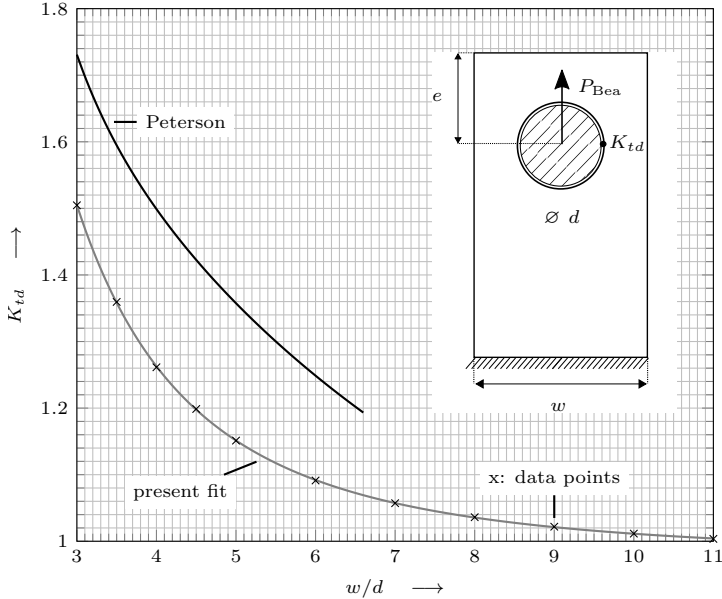


Fig. 4.12 Stress concentration factors for the pin-loaded hole in a quasi-isotropic laminate.

Present stress solution:

$$K_{td}(w/d) = 0.890684 + \frac{8.27509}{(w/d)^{3/2}} - \frac{4.78027}{w/d} + \frac{1.06557}{\sqrt{w/d}}, \quad (4.18)$$

Peterson's stress concentration:

$$K_{td, \text{Peterson}}(w/d) = 0.2880 + 8.820 \cdot \frac{1}{w/d} - 23.196 \cdot \frac{1}{(w/d)^2} + 29.167 \cdot \frac{1}{(w/d)^3}$$

$$\text{only valid for } 1.33 \leq w/d \leq 6.67, \quad e/w \geq 1. \quad (4.19)$$

In Fig. 4.12, the approximations are shown in a grid plot, which enables the graphical determination of the SCFs. The formula labelled with „Peterson“ was derived based on the works by Theocaris (1956) as well as Hill (1969), who actually treat a contact elasticity problem using Airy stress functions and test data, respectively. Modelling a contact even with perfect fit, which means

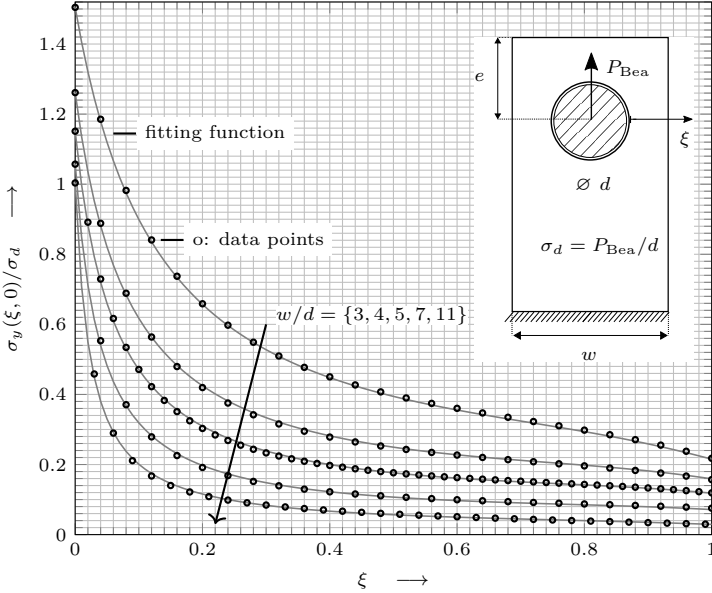


Fig. 4.13 Fit for the net-section stresses.

that the hole and bolt diameters are equal, leads to a contact area which is slightly smaller than that of the present idealisation with a contact area along the half of the hole edge (Crews et al., 1981; Camanho and Matthews, 1997). Hence, the stress concentrations $K_{td, \text{Peterson}}$ are higher than those of the present formula. However, for assessment of static net-tension failure, the overall modelling approach including the bolt contact idealisation has revealed good agreement to failure loads determined by experiments (Catalanotti and Camanho, 2013). Therefore, the stress results including the SCFs based on the present mechanical idealisation can be taken for further steps in the structural assessment.

4.7 Interpolation formulae for quasi-isotropic laminates

Regarding the net-section stresses, the following fitting function is suggested.

$$\begin{aligned}\sigma_y(\xi, w/d)/\sigma_d &= \frac{1}{C_0(w/d) + C_1(w/d) \cdot \xi + C_2(w/d) \cdot \xi^2 + C_3(w/d) \cdot \xi^8}, \\ C_0(w/d) &= \frac{1 + 1.368 \cdot (w/d)^{2.22}}{9.85 + 1.33 \cdot (w/d)^{2.22}}, \\ C_1(w/d) &= -3.087 + 1.13 \cdot w/d + (0.752 \cdot w/d)^2 - (0.301 \cdot w/d)^3, \\ C_2(w/d) &= 6.505 - 2.785 \cdot w/d + (0.1173 \cdot w/d)^8, \\ C_3(w/d) &= 0.97 + (0.1762 \cdot w/d)^{2.5} + (0.09415 \cdot w/d)^{20}.\end{aligned}\tag{4.20}$$

The results are shown in Fig. 4.13 revealing excellent agreement to the data points of the present stress calculus. Regarding open holes, the development of corresponding polynomial fitting functions is part of ongoing work.

Chapter 5

Failure analysis

Based on the present stress results, a failure analysis is conducted with the goal to predict the minimal external loads that yield crack initiation along the net-section area. This fatal failure mode likely occurs for narrow bolted joints with a finite width of $w/d \leq 4$ (Hart-Smith, 1980). The failure analysis is conducted using the nonlocal criteria of Finite Fracture Mechanics (FFM) and the Theory of Critical Distances (TCD), which are capable of capturing the hole size effect. First, a methodology for the derivation of the failure loads in the present bolted-joint context is introduced in Sect. 5.1. Regarding FFM, this involves the determination of the energy release rates. Concerning the TCD, use is made of experimental failure data to obtain the required characteristic distance. Second, the predicted failure stresses are validated against experimental results published in the literature. For the filled hole, this is exemplarily done using a single test set. Regarding the open hole, multiple test sets with different hole diameters are available. This enables the validation of the hole size effect. Concerning the joint under combined bearing-bypass load, unfortunately, there are no experiments available for validation of the hole size effect, according to the author's knowledge. The test data of the open and filled hole as well as the complete failure analysis are valid for quasi-isotropic laminates. Third, by means of FFM, the size effect is extensively studied. This includes the analysis of the failure load reduction with increasing hole and bolt diameter. Moreover, the influence of the finite plate width on the failure load reduction is investigated. Furthermore, the applicability of the TCD is assessed by comparing its results to those of FFM. The three steps are done separately beginning with the special cases of open holes (Sect. 5.2) and filled holes (Sect. 5.3), followed by bolted joints under bearing-bypass load (Sect. 5.4). Some parts of this Chapter have been already published in the literature. In particular, the TCD and FFM are employed in Nguyen-Hoang and Becker (2020a) to predict tension failure in single-fastener bolted joints based on a preliminary stress calculus. Further, a comprehensive assessment framework of tension failure of open holes is provided in Nguyen-Hoang and Becker (2022d). The publication of the results

for the combined load case in scientific journals as well as in LTH Design Criteria is part of ongoing work.

5.1 Failure load determination

First, a methodology for the determination of the failure stresses using FFM is introduced. Special focus is given to the calculation of the required quantities, especially the energy release rates involved in the coupled criterion. The corresponding quantities of the open- and filled-hole problems are taken from the literature, which are then superimposed in order to treat the combined load case. Second, the approach for the derivation of the failure stresses using the TCD is summarised in brief. This includes the selection of the characteristic distances.

Finite Fracture Mechanics

The present bolted-joint problem is characterised by a monotonic decrease of the stresses and a monotonic increase of the energy release rate with respect to the crack length Δa (see pictogram in Fig. 5.1). According to Weißgraeber et al. (2015c), the corresponding coupled criterion can then be specialised to the conditions

$$\frac{1}{\Delta a} \int_R^{R+\Delta a} \sigma_y(x, 0) dx = X_T^L \wedge \frac{1}{\Delta a} \int_R^{R+\Delta a} K_I^2(a) da = \int_R^{R+\Delta a} K_{Ic}^2(a) da. \quad (5.1)$$

Therein, for the R-curve $K_{Ic}(a)$, a Gompertz function is chosen, which enables the modelling of a crack length dependence of the fracture toughness as done by Catalanotti and Camanho (2013) for filled holes. This is vital for crack lengths of the same order as the process zone¹⁰, which particularly occurs for small defect sizes. The R-curve reads

$$K_{Ic}(\Delta a) = K_{Ic}^p \exp \left(\ln \frac{K_{Ic}^i}{K_{Ic}^p} \exp(b\Delta a) \right). \quad (5.2)$$

¹⁰The process zone is considered as the region close to the crack tip, in which complex separation mechanisms occur on a microscopic level. By classical continuum mechanics, such events cannot be captured. However, if that means shall be employed to describe fracture of the whole solid body the process zone should be small in comparison to its macroscopic dimensions. This commonly applies for brittle materials. In the context of linear elastic fracture mechanics, the entire body is considered as linear elastic and inelastic processes must be restricted to a small region. Refer to the textbooks Cherepanov (1979); Kanninen and Popelar (1985); Broberg (1999); Anderson (2005); Gross and Seelig (2016) regarding the field of fracture mechanics.

5.1 Failure load determination

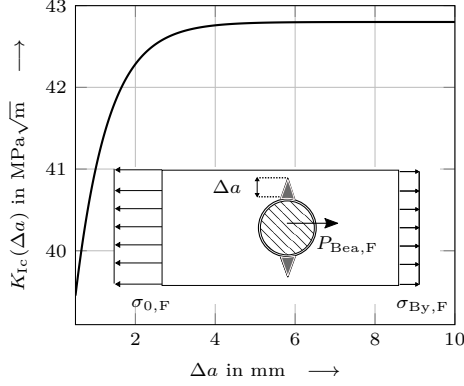


Fig. 5.1 R-curve for Hexcel IM7-8552 carbon epoxy unidirectional prepreg material.

Therein, the quantities $K_{Ic}^i = 36.7 \text{ MPa}\sqrt{\text{m}}$ and $K_{Ic}^p = 42.8 \text{ MPa}\sqrt{\text{m}}$ denote the initiation and propagation values of the fracture toughness, respectively. These parameters can be regarded as lower and upper limits of the fracture toughness. Moreover, the quantity $b = -1.27 \text{ mm}^{-1}$ is an experimental fitting parameter. The given numbers are valid for the quasi-isotropic composite laminate with the layup $[90^\circ/0^\circ/\pm 45^\circ]_{3s}$ made of Hexcel IM7-8552 carbon epoxy unidirectional prepreg material (Catalanotti and Camanho, 2013). The plain longitudinal tensile strength of this laminate is $X_T^L = 845.1 \text{ MPa}$. The corresponding effective failure stresses shall be derived in the present thesis. This is done since the experimental data taken for validation purposes are based on such a setting. The R-curve of the selected material system is shown in Fig. 5.1. Therein, the loads are indexed with „F“ indicating that these shall trigger net-section failure and a crack of the finite length Δa initiates. However, for open holes only, the fracture toughness is assumed to be constant, $K_{Ic} = 42.8 \text{ MPa}$. This is done as in Camanho et al. (2012) since the present results of the open holes shall be compared to those of the cited article. The net-section stresses $\sigma_y(x, 0)$ and the stress intensity factor $K_I(a)$ are derived by a superposition of the corresponding quantities of the open and filled hole. In particular,

$$\begin{aligned}
 \sigma_y(x, 0) &= (1 - \beta) \sigma_y^{\text{OH}}(x, 0) + \beta \sigma_y^{\text{FH}}(x, 0), \\
 K_I(a) &= (1 - \beta) K_I^{\text{OH}}(a) + \beta K_I^{\text{FH}}(a) \\
 \beta &= \frac{P_{\text{Bea}}}{P}, \quad P = P_{\text{Bea}} + P_{\text{By}}, \quad P_{\text{By}} = \sigma_{\text{By}} \cdot w.
 \end{aligned} \tag{5.3}$$

For the stresses, the results of the present calculus are inserted. Regarding the stress intensity factor of the quasi-isotropic open-hole problem, closed-form approximations from the literature shall be selected as done by Camanho et al. (2012). With the uniaxial far-field stress σ_{By} and the overall defect size $a = R + \Delta a$ (see pictogram in Fig. 5.5), the stress intensity factor reads

$$\begin{aligned}
 K_I^{\text{OH}}(a) &= \sigma_{By} F_h(a) F_w(a) \sqrt{\pi a}, \\
 F_h(a) &= \sqrt{1 - \frac{R}{a}} f_n(a), \\
 f_n(a) &= 1 + 0.358\lambda + 1.425\lambda^2 - 1.578\lambda^3 + 2.156\lambda^4, \quad \lambda = R/a, \\
 F_w(a) &= \sqrt{\sec \frac{\pi R}{w} \sec \frac{\pi a}{w}}
 \end{aligned} \tag{5.4}$$

and were determined by fitting to the results of Newman (1971) as well as Shivakumar and Forman (1980). The first work deals with finite and the second with infinite dimensions. Both contributions are based on the complex potential formulation by Muskhelishvili (1977). Note that the stress intensity factor is affected by the material orthotropy (Bao et al., 1992), which should be taken into account when extending the methodology.

Concerning the stress intensity factor of the quasi-isotropic filled-hole problem K_I^{FH} , a polynomial fitting function published by Catalanotti and Camanho (2013) is taken. This has been derived using FE analyses. With the dimensionless crack length $\Delta\xi$ the fitting function is

$$\begin{aligned}
 K_I^{\text{FH}}(\Delta\xi) &= \sqrt{d} \sigma_d \psi(\Delta\xi, w/d) \quad \text{with} \quad \sigma_d = w/d \cdot \sigma_{\text{Bea}}, \\
 \psi(\Delta\xi, w/d) &= \frac{\sqrt{\Delta\xi}}{1 - \Delta\xi} \sum_{i=1}^I \sum_{j=1}^J \Psi_{ij} (w/d)^{j-1} \Delta\xi^{i-1}.
 \end{aligned} \tag{5.5}$$

Therein, the quantity Ψ_{ij} represents the coefficient matrix of the polynomial fitting function. Its entries can be found in the cited article. Be reminded that the bearing stress introduced into the bolt is normalised to the hole diameter, $\sigma_d = P_{\text{Bea}}/d$. Further, the bolt force is reacted by the far-field stress $\sigma_{\text{Bea}} = P_{\text{Bea}}/w$ (Fig. 3.4). The absolute crack length Δa can be calculated using

$$\Delta a = d/2 (w/d - 1) \Delta\xi. \tag{5.6}$$

With that all required quantities involved in the coupled criterion Eq. (5.1) are determined. To obtain the far-field stress leading to failure, let us take the quantities $\tilde{\sigma}_y(x, 0)$ and $\tilde{K}_I(a)$ which are produced by the unit far-field

5.1 Failure load determination

stress $\sigma_0 = 1$ MPa for a given load factor $0 \leq \beta \leq 1$. Then, scaling $\tilde{\sigma}_y(x, 0)$ and $\tilde{K}_I(a)$ with the unknown far-field failure stress $\sigma_{0,F}$ and eliminating it in the coupled criterion Eq. (5.1) leads to

$$\frac{\frac{1}{\Delta a} \left[\int_R^{R+\Delta a} \tilde{\sigma}_y(x, 0) dx \right]^2}{\int_R^{R+\Delta a} \tilde{K}_I^2(a) da} = \frac{(X_T^L)^2}{\int_R^{R+\Delta a} K_{Ic}^2(a) da}. \quad (5.7)$$

Solving this equation yields Δa and back substitution in either the stress or the energy criterion reveals $\sigma_{0,F}$.

Theory of Critical Distances

In the context of the Theory of Critical Distances, the net-section stresses are evaluated at a certain characteristic distance. Using line method, the average net-section stresses

$$\bar{\sigma}_y(\tilde{r}_c) = \frac{1}{\tilde{r}_c} \int_0^{\tilde{r}_c} \sigma_y(x^*, 0) dx^* \quad \text{with } x^* = x - R \quad (5.8)$$

are investigated, where \tilde{r}_c denotes an arbitrary hole distance. Failure is postulated if the average net-section stresses within the characteristic hole distance $\tilde{r}_c = r_c$ equal the longitudinal tensile strength X_T^L of the plain laminate,

$$\bar{\sigma}_y(r_c) = X_T^L. \quad (5.9)$$

When employing the TCD, Taylor (2004, 2007, 2008, 2011) suggested the following value for the characteristic distance:

$$r_{c,T} = \frac{2}{\pi} \left(\frac{K_{Ic}}{X_T^L} \right)^2 = 1.632 \text{ mm}, \quad (5.10)$$

where the fracture toughness of the laminate is $K_{Ic} = 42.8 \text{ MPa}\sqrt{\text{m}}$ and its plain longitudinal strength in tension amounts $X_T^L = 845.1 \text{ MPa}$. The same length is taken no matter what particular structural problem is treated (open or filled hole, bolted joint under combined bearing-bypass load). Then, the failure stresses of the different problems investigated may differ only due to other distributions of the corresponding net-section stresses. Concerning the TCD using the calibrated characteristic distance $r_{c,clb}$, the failure load determined by experiments is required to obtain $r_{c,clb}$ (Whitney and Nuismer, 1974). The particular derivation is given in the following Sects. 5.2-5.4, treating the results of open and filled holes as well as bolted joints under bearing-bypass

load, respectively. Once the characteristic distance is determined, the failure load is derived as follows. With the normalised characteristic distance

$$\xi_{r_c} = \frac{2r_c}{(w/d - 1)d}, \quad (5.11)$$

the failure stresses by TCD using line method are

$$\sigma_{F,TCD} = \frac{X_T^L}{\frac{1}{\xi_{r_c}} \int_0^{\xi_{r_c}} \sigma_y(\xi, 0) \big|_{\sigma_0=1} d\xi}. \quad (5.12)$$

Therein, the net-section stresses that react the unit remote load $\sigma_0 = 1$ MPa shall be inserted. The TCD is based on characteristic distances, which are assumed to be invariant to the defect size. This is the hole and bolt diameter in the present bolted-joint context. However, the characteristic distance has been identified as a structural and not as a material parameter (Awerbuch and Madhukar, 1985; Pipes et al., 1979; Tan, 1987; Srivastava and Kumar, 2002; Camanho and Lambert, 2006) since it actually depends on geometrical properties as w/d but also on the absolute value of d itself. Therefore, the calibrated characteristic distance is in general not applicable to other configurations, though it may apply to some extent. This matter will be further analysed in Sects. 5.2-5.4, which is of interest when more experiments for calibration are not affordable. In doing so, the failure prediction concept of Finite Fracture Mechanics serves as reference since there is no additional experimental data available to the author. Moreover, FFM is generally the superior failure prediction model since it is purely based on physical input parameters.

5.2 Discussion of the results: Open hole

First, failure load predictions for open holes derived by TCD and FFM are validated against experimental data published in Camanho et al. (2012). This is done for the quasi-isotropic layup $[90^\circ/0^\circ/\pm 45^\circ]_{3s}$ weakened by a centred hole of the different diameters $d = \{2 \text{ mm}, 4 \text{ mm}, \dots, 10 \text{ mm}\}$. Thus, the size effect shall be modelled and validated. The relative plate width amounts $w/d = 6$. Then, the influence of the finite plate width w/d on the failure load reduction in the context of the size effect is extensively analysed by investigating configurations with $w/d = \{3, 6, 10\}$. Furthermore, the results of the TCD approaches are compared to those of FFM. This enables the assessment to which extent the TCD concepts may be used.

5.2 Discussion of the results: Open hole

Table 5.1

Open hole failure stresses for $[90^\circ/0^\circ/\pm 45^\circ]_{3s}$ -laminate with $w/d = 6$. The experimental failure stresses (Exp) are taken from Camanho et al. (2012).

d in mm ↓		TCD-CLB	TCD-T	FFM	Exp
2	σ_F in MPa →	573.0	555.3	560.4	555.7
	ϵ	3.1 %	-0.1 %	0.9 %	-
4	σ_F in MPa	475.7	459.3	470.2	480.6
	ϵ	-1.0 %	-4.4 %	-2.2 %	-
6	σ_F in MPa	425.1	411.1	420.6	438.7
	ϵ	-3.1 %	-6.3 %	-4.1 %	-
8	σ_F in MPa	394.3	382.4	390.1	375.7
	ϵ	5.0 %	1.8 %	3.8 %	-
10	σ_F in MPa	373.7	363.5	369.6	373.7
	ϵ	-	-2.7 %	-1.1 %	-

5.2.1 Validation to experiment

In the context of FFM, the coupled criterion reveals the crack length Δa to be dependent on the hole diameter d (Fig. 5.2). Therein, with increasing d , approximately for $d \geq 5$ mm, the crack length rapidly reaches a plateau where it can be approximated by a constant value. If the TCD approaches are based on characteristic distances that lie nearby or within this plateau these concepts should yield similar results as FFM. This is true for the TCD approach by Taylor (TCD-T) with $r_{c,T} = 1.632$ mm according to Eq. (5.10). The failure stresses are accurately predicted with relative error magnitudes of $|\epsilon| \leq 6.3$ % compared to the test data listed in Table 5.1. The FFM approach achieves accurate results with $|\epsilon| \leq 4.1$ %, which is visualised in Fig. 5.3. Therein, the markers „x“ denote the normalised experimental failure stresses for a plate of the width $w/d = 6$. Be reminded that the fracture toughness is assumed to be constant with $K_{Ic} = 42.8 \text{ MPa}\sqrt{\text{m}}$ as in Camanho et al. (2012). This is done for reasons of better comparison to those failure loads determined in the cited article. Note that the assumption is made for open holes only. Regarding the TCD using calibrated characteristic distances (TCD-CLB), the value of $r_{c,clb}$ depends on the particular test set that is chosen for calibration. As possible configurations the experimental results in Table 5.1 are taken. These involve plates of the same relative width $w/d = 6$ but different hole diameter d . In general, larger hole diameters should be selected so that the plateau area of Δa is reached. However, different values of calibrated

Chapter 5 Failure analysis

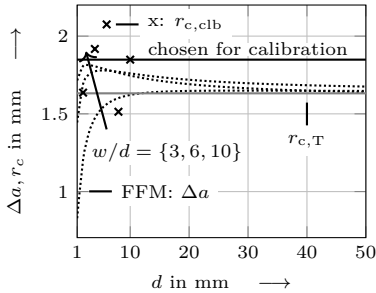


Fig. 5.2 Crack length Δa at failure.

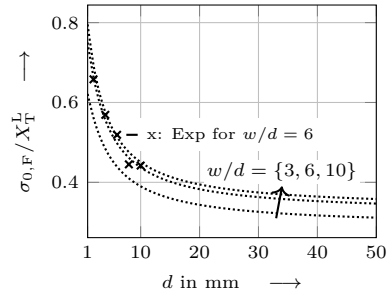


Fig. 5.3 Normalised failure loads by FFM with $X_T^L = 845.1$ MPa.

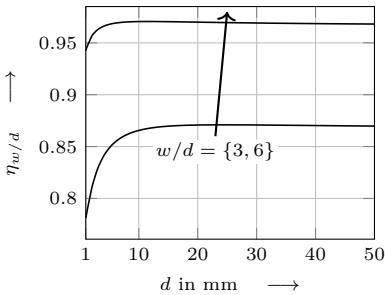


Fig. 5.4 Reduction factor describing finite-width effect on the FFM failure load.

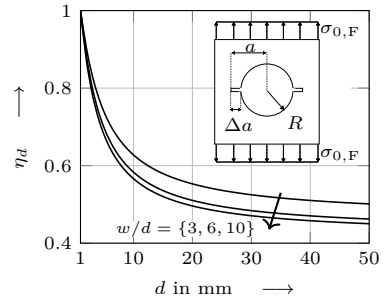


Fig. 5.5 Reduction factor describing size effect on the FFM failure load derived.

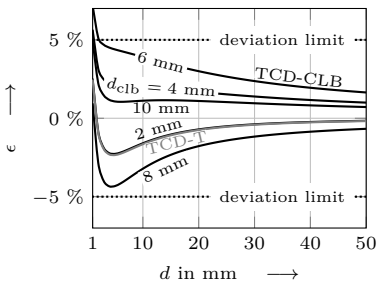


Fig. 5.6 Normalised deviations to FFM failure load for $w/d = 6$: TCD-CLB approach with respect to the calibration diameter d_{clb} and TCD-T concept.

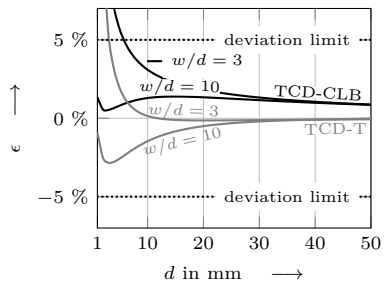


Fig. 5.7 Normalised deviations to FFM failure loads. For the calibrated characteristic distance, the configuration with $d = 10$ mm and $w/d = 6$ is chosen.

5.2 Discussion of the results: Open hole

characteristic distances $r_{c,clb}$ with respect to the their corresponding hole diameter d are shown in Fig. 5.2 by the markers „x“ and convergence to a constant value is yet not observable. Nevertheless, the test set with the largest diameter shall be chosen for calibration leading to $r_{c,clb} = 1.849$ mm. This is determined by using Eq. (5.11) and (5.12). Note that the selection of the particular test set for calibration is rather insignificant for the present open-hole problem since Δa rapidly reaches a plateau value. Further, failure stresses have been derived by the TCD-CLB method using all available test sets with $d = \{2 \text{ mm}, \dots, 10 \text{ mm}\}$ for calibration. For this whole test set, a maximum error magnitude of $|\epsilon| \leq 5 \%$ beyond $d \geq 2$ mm compared to FFM (Fig. 5.6¹¹) and of $|\epsilon| \leq 8 \%$ compared to the experiment has been revealed. To limit the amount of data, only the deviations of the TCD-CLB approach with the chosen calibration distance of $d_{clb} = 10$ mm are listed in Table 5.1. To conclude, all used brittle failure prediction concepts yield failure loads with acceptable error magnitude and thus can be considered as reliable assessment means for open holes. Furthermore, the proximity of the plateau value of Δa to $r_{c,clb}$ can be interpreted as follows. The calibrated characteristic distance may be regarded as experimentally determined crack length and since the corresponding quantity by the FFM concept lies nearby it, this crack initiation model can be seen as further confirmed. Note that the present FFM results are actually the same as those by Camanho et al. (2012), which are based on net-section stresses derived using the enhanced heuristic Tan-Heywood approach (Tan, 1988). This is due to the fact that for $w/d = 6$ rather slight finite-width effects occur and the stresses along the net-section plane of the actual boundary value problem are almost the same as those of the heuristic approach. However, for small w/d -ratios it is recommended to use the stress solution of the finite boundary value problem instead of heuristic approaches. This especially applies for quasi-isotropic and $[\pm 45^\circ]_s$ -laminates, which involve pronounced finite-width effects as discussed in Sect. 4.4.

5.2.2 Hole size effect

Let us investigate the failure stresses normalised to the plain strength of the laminate X_T^L in Fig. 5.3. These are derived by means of FFM. In order to capture the size effect, the hole diameter is varied in between $1 \text{ mm} \leq d \leq 50 \text{ mm}$. This is done for the different relative plate widths of $w/d = \{3, 6, 10\}$, which enables the investigation of finite-width effects. A significant decrease of the failure load with converging behaviour is observable. Particularly, for $d \rightarrow \infty$

¹¹Some figures are intentionally not placed in the order as mentioned in the text. This is also done for layout reasons.

nonlocal criteria coincide with local criteria and the net-section stresses can be evaluated directly at the hole edge. This is due to the crack length Δa , which reaches a plateau. Taking into account Eq. (5.6), the relative crack length approaches zero for $d, w \rightarrow \infty, w/d = \text{constant}$. Then, the failure load specialises to

$$\sigma_{0,F}(d \rightarrow \infty) = X_T^L/K_{t0}, \quad \text{with} \quad K_{t0} = \sigma_y(R, 0)/\sigma_0. \quad (5.13)$$

For instance, we can observe that for the plate bounded by $w/d = 10$, which may be treated as within an infinite domain (see Sect. 4.4), the normalised failure load $\sigma_{0,F}/X_T^L$ approaches $1/3$. This is the inverse value of the stress concentration factor $K_{t0} = 3$ for the infinite isotropic open-hole problem solved by Kirsch (1898). For the other special case of a vanishing hole diameter $d \rightarrow 0$, the failure stress coincides with the plain material strength X_T^L . With this the failure stresses of open holes lie in the range

$$\underbrace{\frac{X_T^L}{K_{t0}}}_{d \rightarrow \infty} \leq \underbrace{\sigma_{0,F}}_{d \text{ finite sized}} \leq \underbrace{X_T^L}_{d \rightarrow 0} \Leftrightarrow \frac{1}{K_{t0}} \leq \frac{\sigma_{0,F}}{X_T^L} \leq 1. \quad (5.14)$$

Generally, predictions based on local concepts deviate most from nonlocal criteria when assessing the special case of a vanishing hole diameter $d \rightarrow 0$. Predictions by local concepts underestimate the failure stresses, which leads to oversized and heavy designs. This matter shall be further quantified for technical structures with a finite-sized hole diameter by the example of the open hole-problem. In doing so, let $\sigma_{0,F}^{\text{local}}$ be the failure stress by local concepts and $\sigma_{0,F}^{\text{FFM}}$ that by FFM. Then, the failure load deviation normalised to FFM predictions reads

$$\chi_{\sigma_{0,F}} = \frac{\overbrace{\sigma_{0,F}^{\text{local}}}^{=X_T^L/K_{t0}} - \sigma_{0,F}^{\text{FFM}}}{\sigma_{0,F}^{\text{FFM}}} = \frac{1/K_{t0} - \sigma_{0,F}^{\text{FFM}}/X_T^L}{\sigma_{0,F}^{\text{FFM}}/X_T^L}. \quad (5.15)$$

Its amount is shown in Fig. 5.8 revealing that even for finite-sized hole diameters, a significant lightweight potential is not exploited when designing according to local criteria. Thus, it is strongly recommended to employ nonlocal concepts such as FFM. The deviation is larger for smaller hole diameters. For the special case of a vanishing hole diameter, the failure stress derived by FFM equals the plain strength of the material. Then, the deviation $\chi_{\sigma_{0,F}}$ specialises to

$$\lim_{d \rightarrow 0} \chi_{\sigma_{0,F}} = \left. \frac{1/K_{t0} - \sigma_{0,F}^{\text{FFM}}/X_T^L}{\sigma_{0,F}^{\text{FFM}}/X_T^L} \right|_{\sigma_{0,F}^{\text{FFM}}=X_T^L} = \frac{1}{K_{t0}} - 1. \quad (5.16)$$

5.2 Discussion of the results: Open hole

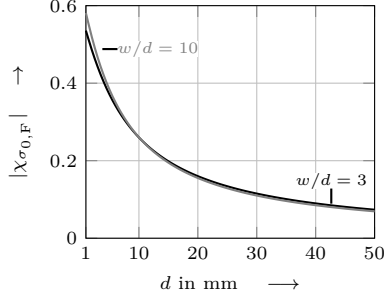


Fig. 5.8 Deviations of failure loads by local concepts normalised to FFM predictions.

For instance, concerning the plate of the relative width $w/d = 10$, the corresponding problem can be treated as within an infinite domain and the amount of the deviation specialises to $|\chi_{\sigma_{0,F}}| = 1 - 1/K_{t0} = 1 - 1/3 = 2/3 \approx 0.67$. The value of the deviation for the unit diameter $d = 1$ mm is not far from this special case. Furthermore, finite-width effects on the measure $\chi_{\sigma_{0,F}}$ are quite small. For all aspect ratios w/d and $d \rightarrow \infty$, the normalised deviation $\chi_{\sigma_{0,F}}$ vanishes since local concepts coincide with nonlocal criteria.

Of interest might be the determination of an analytical expression for the effective failure stress with respect to the hole diameter. In doing so, let us consider the net-section stresses. These may be written in the general form

$$\sigma_y(r, 0) = \left(C_0 + C_1 \frac{R}{r} + C_2 \frac{R}{r^2} + \dots + C_N \frac{R^N}{r^N} \right) \sigma_{By} = \sum_{n=0}^N C_n \frac{R^n}{r^n} \sigma_{By}, \quad (5.17)$$

where the coefficients C_n depend on the actual boundary value problem treated. To determine the failure loads, the net-section stresses shall be evaluated along the crack length and $r = d/2 + \Delta a$ is inserted. With $R = d/2$, the stresses can be expressed by

$$\sigma_y(d/2 + \Delta a, 0) = \sum_{n=0}^N \frac{C_n d^n \sigma_{By}}{2^n \left(\frac{d}{2} + \Delta a \right)^n} = \sum_{n=0}^N 2^{-n} C_n d^n \left(\frac{d}{2} + \Delta a \right)^{-n} \sigma_{By}. \quad (5.18)$$

Let us consider the stress criterion using point method,

$$\sigma_{0,F} \cdot \sigma_y(d/2 + \Delta a, 0)|_{\sigma_{By}=1} = X_T^L \quad (5.19)$$

Chapter 5 Failure analysis

The failure stress with respect to the hole diameter d is then of the form

$$\sigma_{0,F} = \frac{X_T^L}{\sum_{n=0}^N 2^{-n} C_n d^n \left(\frac{d}{2} + \Delta a\right)^{-n}}. \quad (5.20)$$

Regarding the open-hole problem and in general for doubly symmetric settings, uneven coefficients C_n vanish. For finite-sized diameters of about $d \geq 5$ mm (Fig. 5.2), the crack length Δa may be approximated by a constant. Then, we may investigate the special case of

$$\lim_{d \rightarrow \infty} \sigma_{0,F} / X_T^L = \lim_{d \rightarrow \infty} \frac{1}{\sum_{n=0}^N 2^{-n} C_n d^n \left(\frac{d}{2} + \Delta a\right)^{-n}} = \sum_{n=0}^N \frac{1}{C_n}. \quad (5.21)$$

For a relative width of $w/d \geq 10$, the solution by Kirsch (1898) can be taken and the corresponding net-section stresses read

$$\sigma_\varphi(r, 0) = \sigma_y(r, 0) = \frac{1}{2} \left(\frac{3R^4}{r^4} + \frac{R^2}{r^2} + 2 \right) \sigma_{By} \quad (5.22)$$

and the limit in Eq. (5.21) approaches $1/3$. This is the reverse value of the corresponding SCF. Note that any problem whose stress decay can be described by the general form in Eq. (5.18) involves a hole size effect of the structure as expressed by Eq. (5.20).

To investigate the interaction in between finite width and defect size on the failure stresses, let us analyse the reduction factors

$$\eta_{w/d} = \frac{\sigma_{0,F}(w/d = \{3, 6\}, d)}{\sigma_{0,F}(w/d = 10, d)}, \quad \eta_d = \frac{\sigma_{0,F}(w/d, d)}{\sigma_{0,F}(w/d, d = 1 \text{ mm})}. \quad (5.23)$$

Regarding the ratio $\eta_{w/d}$, the failure stress of $w/d = 10$ is selected as reference since finite-width effects have decayed for this configuration. In Fig. 5.4, the quantity $\eta_{w/d}$ reveals a converging behaviour similar to the crack length Δa . The finite-width influence on the failure stress reduction is higher the smaller the defect size. Moreover, the family of curves of η_d in Fig. 5.5 shows that the hole size effect is affected by the degree of finite width. In particular, the failure stress decrease is more significant for wider relative plate widths w/d and larger hole diameters d .

5.2.3 Performance of the TCD concepts

Next, the performance of the TCD concepts is compared against FFM. The crack length Δa derived by the latter approach is shown in Fig. 5.2 with respect to d for the aspect ratios of $w/d = \{3, 6, 10\}$. Herein, the corresponding plateau values are quite similar and lie near both characteristic distances $r_{c,clb}$ and $r_{c,T}$. Hence, it can be expected that the TCD approaches are acceptable assessment means for the defect sizes that yield a crack length extension Δa within or nearby the plateau. However, below $d < 10$ mm the quantity Δa shows a certain spread for the different geometry ratios treated. To assess if the TCD approaches are applicable nevertheless, their deviations normalised to FFM are calculated and shown in Fig. 5.6 and 5.7. Therein, the deviations are within a tolerable limit. Note that in the first Fig. 5.6, only the curve labelled with $d_{clb} = 10$ mm is now of interest since this value has been selected for calibration in the TCD-CLB approach. For the present open-hole problem, the larger the hole diameter the smaller the errors of the TCD concepts. For the open hole with $w/d = 10$, both the TCD-CLB and the TCD-T concepts yield error magnitudes $|\epsilon| < 3\%$ along the entire diameter range and regarding $w/d = 3$, the former approach leads to inaccuracies $|\epsilon| < 5\%$ for $d \geq 6$ mm and the latter concept for $d \geq 3$ mm. The following can be hence concluded for the present open-hole problem with quasi-isotropic laminate. The use of a single characteristic distance is sufficient to adequately capture the hole size effect without the necessity to model the crack length dependence for both small and large finite geometry values w/d within a wide hole diameter range. This even applies for the characteristic distance by Taylor, although the length parameter $r_{c,T}$ is not related to the open-hole problem but to $r_p = r_{c,T}/4$, the effective crack length of the mode I through crack in an infinite isotropic plate (Tada et al., 2000). This problem and the open hole have the external uniform loading in common. Moreover, both problems are doubly symmetric and involve area reductions that can be regarded as similar (area reduction by crack length or by hole diameter). The only difference lies in their shapes. Since $r_{c,T}$ can be used as an approximation to model Δa of both the finite and infinite dimensions open-hole problem it may be concluded that the considered shape of the defect (crack vs. circular hole) as well as finite-width effects have a less significant impact on the crack length $\Delta a(d)$ and on the failure stress prediction. Having gained a fundamental understanding how a finite plate width affects failure stresses of open holes and their reduction with increasing hole diameter in the context of the hole size effect, let us proceed with analysing the pin-loaded hole.

Table 5.2

Failure stresses for the filled-hole problem with $w/d = 2$, $e/d = 4.17$. The values determined by FFM as well as by experiment (Exp) are taken from Catalanotti and Camanho (2013).

	TCD-CLB	TCD-Taylor	FFM	Exp
$\sigma_{d,F}$ in MPa	569.1	641.5	549.5	526.7
ϵ	8.1 %	21.8 %	4.3 %	-

5.3 Discussion of the results: Filled hole

In the same way as for open holes, the nonlocal failure concepts TCD and FFM are employed and their results are validated against experimental data. Then, the finite-width effect on the failure load reduction in the context of the size effect is discussed.

5.3.1 Validation to experiment

To the author's knowledge, experiments investigating the hole size effect occurring in the filled-hole problem so far are not available in the literature. This would involve capturing the failure stress decrease for increasing hole and bolt diameter based on test data. However, Catalanotti and Camanho (2013) achieved accurate FFM results for quasi-isotropic composite bolted joints with the only hole diameter $d = 6$ mm and the geometry properties $w/d = \{1.5, 1.75, 2\}$ as well as $e/d = \{5.83, 5.83, 4.17\}$, respectively. The setting at failure is depicted in Fig. 5.9. For these test sets, a relative error magnitude of $|\epsilon| \leq 6.7$ % in comparison to experimental test data has been obtained. Hence, FFM can be regarded as reliable assessment means for filled holes. The corresponding failure stresses $\sigma_{d,F}$ are listed in Table 5.2. Note that $\sigma_{d,F} = P_{\text{Bea},F}/d$, where $P_{\text{Bea},F}$ denotes the applied bearing (or bolt) load per plate thickness when tension failure occurs. Moreover, Nguyen-Hoang and Becker (2020a) have revealed that the TCD-CLB approach yields an acceptable prediction with $\epsilon = 8.1$ %. In that study, the tension failure stresses of a quasi-isotropic bolted joint with the relative dimensions $w/d = 2$, $e/d = 4.17$ have been predicted. The test results of the configuration with $w/d = 1.75$, $e/d = 5.83$ and a failure stress of $\sigma_{d,F} = 466.2$ MPa (Catalanotti and Camanho, 2013) have been taken to calibrate the characteristic distance. The TCD-T approach, by contrast, has shown a poor prediction with $\epsilon = 21.8$ %.

5.3 Discussion of the results: Filled hole

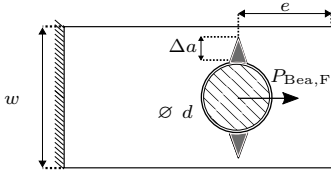


Fig. 5.9 Pin-loaded hole at failure.

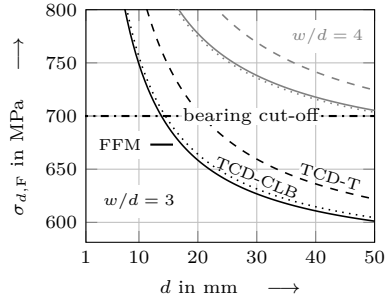


Fig. 5.10 Bearing stresses at failure.

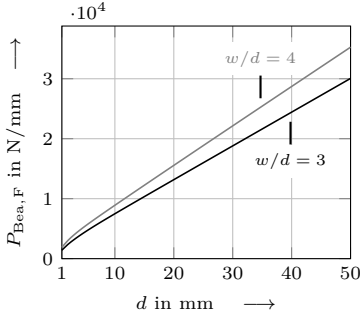


Fig. 5.11 Bolt load at failure derived using FFM.

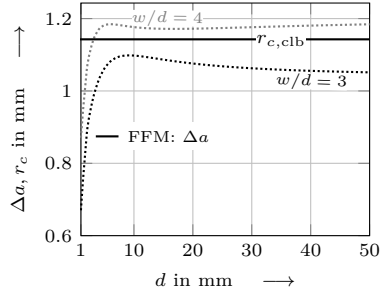


Fig. 5.12 Crack length Δa at failure.

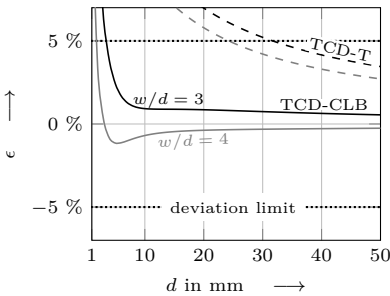


Fig. 5.13 TCD failure stresses: deviations normalised to FFM.

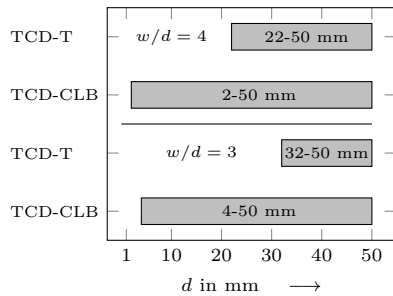


Fig. 5.14 TCD failure stresses: diameter range which yields an error $|\epsilon| \leq 5\%$.

5.3.2 Hole size effect

Let us investigate the hole size effect using the failure stresses derived by FFM. Regarding the plate geometry, the relative dimensions $w/d = \{3, 4\}$ and $e/d = 4.17$ are selected. Connections wider than $w/d = 4$ shall not be treated since net-tension failure is then unlikely to be triggered (Hart-Smith, 1980). The end distance ratio e/d is not varied since it plays a rather insignificant role. This has been identified in the corresponding stress analysis part in Sect. 4.5. Therein, the stress curves and concentrations of connections with a small w/d -ratio are hardly changed when varying e/d (Fig. 4.6-4.9). The failure stresses with respect to the hole and bolt diameter are shown in Fig. 5.10, where a decrease is observable. The analytical expression for the reduction of the failure stresses with respect to d is of the same general form expressed by Eq. (5.20) as derived when analysing open hole (Subsect. 5.2.2). The bearing cut-off is set at $\sigma_d \approx 700$ MPa similar to Catalanotti and Camanho (2013). Beyond this limit, bearing failure is likely to be triggered, for which the employed crack prediction models cannot be used. Note that defining the bearing cut-off involves a certain arbitrariness since there are various definition criteria such as a specific elastic or plastic hole deformation or a particular degradation level of the laminate stiffness noticeable by a nonlinearity in the load-strain curve. From these criteria, the engineer needs to make a selection. However, the bearing limit is commonly defined using a permanent deformation of the laminate, which is chosen to amount 4 % of the hole diameter (ASTM D5961/D5961M-17; Kabeel et al., 2014). Further analysing the finite-width effect on the failure stress reduction using the factors η_d and $\eta_{w/d}$ as performed for the open-hole problem will be covered in Subsect. 5.4.1. This is dedicated to the bolted joint under combined bearing-bypass load, which also includes the special case of filled holes ($\beta = 1$).

Of practical interest might be the critical bolt forces $P_{\text{Bea},F} = \sigma_{d,F} \cdot d$ that lead to failure. The corresponding values derived by FFM are shown in Fig. 5.11. The larger d the higher the sustainable bolt forces, which implies that the designing engineer should avoid small hole and bolt diameters. Moreover, the relationship is weakly nonlinear and may be approximated by a linear curve for most of the investigated hole diameter range. For $d \rightarrow \infty$, nonlocal concepts coincide with local criteria and the stresses are evaluated directly at the hole edge. Hence, the failure stress $\sigma_{d,F}$ converges to a constant value with increasing d . This is already slightly observable for the diameter range of Fig. 5.10. Then, the curve of the bolt force at failure $P_{\text{Bea},F}$ becomes linear with respect to d . Furthermore, the effect of finite width leads to higher sustained forces for wider plates. This is more pronounced for larger d . For small diameter, the diminishing effect due to the significant

load concentration along half of the hole edge becomes dominant and the finite-width impact is hardly observable.

5.3.3 Performance of TCD concepts

The failure load predictions by the TCD approaches are compared to those of FFM. As for the open hole, the FFM calculated crack length Δa depends on the defect size d shown in Fig. 5.12. Therein, a plateau is reached for $d \approx 5$ mm, in which Δa may be approximated by a constant value. Again, the TCD should yield similar predictions if the corresponding characteristic distance lies nearby or within the plateau, which is true for the used calibrated characteristic distance $r_{c,clb} = 1.143$ mm. Be reminded that this distance has been derived based on the test data of the joint with the geometric ratios $w/d = 1.75$, $e/d = 5.83$. Due to the limited data available this value shall be taken to model the size effect for all joints investigated. Be reminded that these have the dimensions $w/d = \{3, 4\}$ and $e/d = 4.17$. Moreover, the impact of a different width-to-diameter ratio w/d on the crack length Δa is rather slight. All in all, the TCD-CLB approach leads to fairly accurate predictions (Fig. 5.13). In particular, for $w/d = 3$ a relative error $|\epsilon| \leq 3\%$ with $d \geq 5$ mm and for $w/d = 4$ an error $|\epsilon| \leq 1\%$ with $d \geq 3$ mm is obtained. This is also illustrated in Fig. 5.14. As for open holes, the calibrated characteristic distance can be regarded as experimentally determined crack length and its proximity to Δa may be seen as further confirmation of the FFM crack initiation model.

For all TCD concepts, the deviation to FFM decreases with increasing hole diameter as observed for open holes (Fig. 5.7). However, the TCD-T approach yields nonprecise results. The characteristic distance by Taylor $r_{c,T} = 1.632$ mm does not lie nearby the FFM calculated crack length Δa and hence is not shown in Fig. 5.12. Further, $r_{c,T} > \Delta a$ means that the evaluation occurs along a wider distance, in which the net-section stresses have decayed more. Therefore, the predicted failure stresses by the TCD-T approach are higher than those of FFM and thus can be regarded as nonconservative. A tolerable relative error magnitude of $\epsilon \leq 10\%$ is obtained for $d \geq 11$ mm and $w/d = 3$ as well as for $d \geq 8$ mm regarding $w/d = 4$. With the goal to create a lightweight optimal design, an error magnitude $|\epsilon| \leq 5\%$ may be considered as acceptable and the diameter range in which this requirement is fulfilled can be taken from Fig. 5.14. Therein, it can be observed that the TCD-T approach involves a very limited diameter range with sufficiently accurate failure stress predictions.

5.4 Discussion of the results: Bearing-bypass interaction

In this Section, the failure stresses of the bolted joint under combined bearing-bypass load are discussed. In doing so, means of FFM and TCD are employed again. The size effect is captured and the impact of finite-width and the load factor $\beta = P_{\text{Bea}}/P$ on the failure load reduction with increasing hole diameter is analysed. The investigations are dedicated to quasi-isotropic laminates. As experiments have been available only for the special cases of open and filled holes, a validation for the combined load case cannot be performed in the present thesis. However, with validation of the extreme cases the employed brittle failure prediction concepts can be regarded as promising assessment means and the methodology is assumed to be also applicable for a superposition of the special cases.

5.4.1 Hole size effect

In the following, the hole size effect is extensively discussed based on the FFM failure stresses $\sigma_{0,\text{F}}$. These are shown in Fig. 5.15 and 5.16 for $w/d = \{3, 4\}$, respectively. Therein, the quantity $\sigma_{0,\text{F}}$ represents the far-field stress at failure, which is normalised to the plain strength of the laminate X_{T}^{L} . In general, the failure stress of the bolted joint under combined bearing-bypass load lies in between the special cases $\beta \rightarrow \{0, 1\}$. The former load factor represents the open hole and the latter the filled hole. As assumed in the stress analysis (Sect. 4.6) revealing that higher load factors β involve more critical stress concentration factors, the filled hole yields the lowest and the open hole the highest failure stresses. Generally, the failure stresses behave asymptotically with increasing hole diameter. In order to quantify their reduction, these shall be normalised to the corresponding value for the unit hole diameter $d = 1$ mm. This is done by using the reduction factor η_d as defined in Eq. (5.23). In Fig. 5.17 and 5.18, it is revealed that the size effect and the corresponding failure stress reduction with increasing hole diameter are the more significant the higher β and the wider w/d .

As done for open holes in Sect. 5.2, let us investigate the error of the employed local concepts by deriving the normalised deviation $\chi_{\sigma_{0,\text{F}}}$ as defined in Eq. (5.15). The results are shown in Fig. 5.19 and 5.20 revealing that the failure stresses are significantly underestimated even for finite-sized diameters. Furthermore, the deviation measure is hardly affected by the finite width w/d and the load factor β . Thus, the quantitative loss of lightweight potential is about the same for all problem settings treated in this thesis, which further

5.4 Discussion of the results: Bearing-bypass interaction

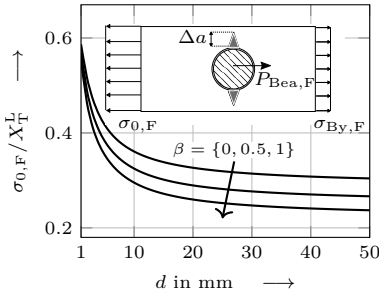


Fig. 5.15 Predicted failure stresses for $w/d = 3$

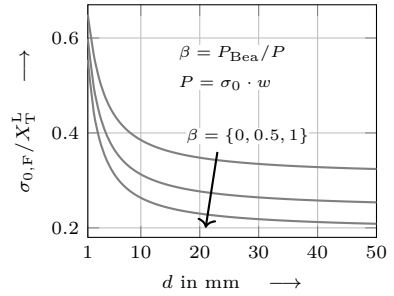


Fig. 5.16 Predicted failure stresses for $w/d = 4$

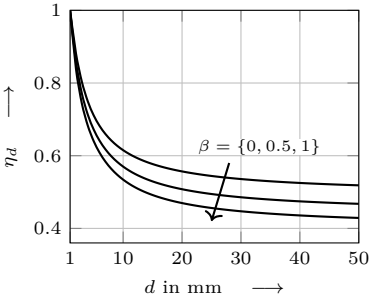


Fig. 5.17 Reduction factor describing size effect for $w/d = 3$.

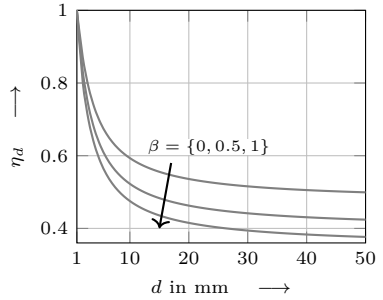


Fig. 5.18 Reduction factor describing size effect for $w/d = 4$.

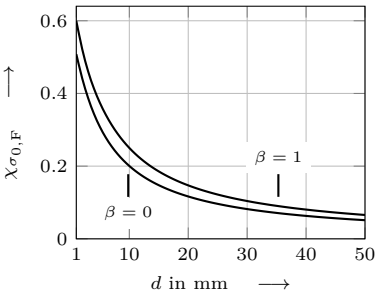


Fig. 5.19 Deviations of failure loads by local concepts for $w/d = 3$.

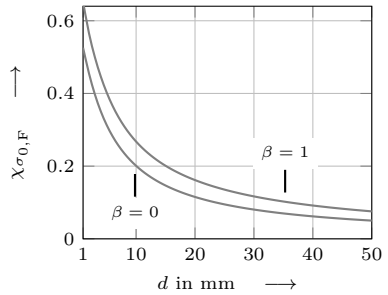


Fig. 5.20 Deviations of failure loads by local concepts for $w/d = 3$.

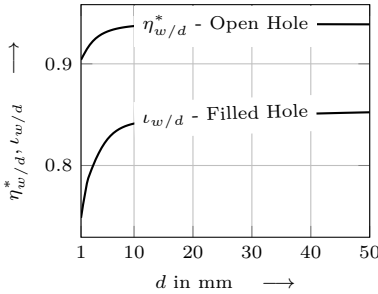


Fig. 5.21 Reduction factor investigating finite-width influence on size effect.

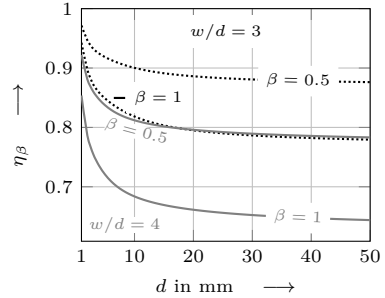


Fig. 5.22 Reduction factor investigating load factor influence on size effect.

emphasises that nonlocal concepts as FFM should be used instead local criteria.

To study finite-width effects, let us assess the failure stresses of $w/d = 3$ and normalise them to those values of $w/d = 4$. Regarding the open hole, the failure load reduction factor $\eta_{w/d}^*$ and concerning the filled hole, the measure $\nu_{w/d}$ is taken¹². These quantities read

$$\text{Open hole: } \eta_{w/d}^* = \frac{\sigma_{0,F}(w/d = 3, d)}{\sigma_{0,F}(w/d = 4, d)}, \quad (5.24)$$

$$\text{Filled hole: } \nu_{w/d} = \frac{\sigma_{d,F}(w/d = 3, d)}{\sigma_{d,F}(w/d = 4, d)}, \quad \sigma_{d,F} = w/d \cdot \sigma_{0,F}. \quad (5.25)$$

Be reminded that configurations $w/d > 4$ shall not be investigated and inserted in the denominator since net-tension failure, then, is unlikely to be triggered. The factor $\eta_{w/d}^*$ is rather unsuitable for the filled hole since the same sustained far-field stress $\sigma_{0,F}$ for connections of different width would indicate no effect, although in fact the wider configuration can bear a higher bolt load ($P_{\text{Bea},F} = \sigma_{0,F} \cdot w$ for $\beta = 1$). Vice versa, the quantity $\nu_{w/d}$ shall not be used for the open hole. In fact, no finite-width effect is indicated when the far-field stresses for open-hole problems of different width are the same. However, their corresponding stresses $\sigma_{d,F}$, which may be interpreted as sustained force, are different and would do so. Therefore, these stresses are not suitable to measure finite-width effects. Fig. 5.21 reveals a converging

¹²For disambiguation: The factor $\eta_{w/d}$ involves a reference value of $\sigma_{0,F}(w/d = 10, d)$ and is employed in Subsect. 5.2.2. By contrast, $\eta_{w/d}^*$ involves a reference value of $\sigma_{0,F}(w/d = 4, d)$ in the current Section.

5.4 Discussion of the results: Bearing-bypass interaction

behaviour for $\eta_{w/d}^*$ and $\iota_{w/d}$ with increasing hole diameter. Assuming that these factors can be compared, the finite-width effect on the failure stress reduction of the open hole is less significant involving a convergence to $\eta_{w/d}^* \rightarrow 93.9\%$, whereas regarding the filled hole $\iota_{w/d} \rightarrow 85.2\%$. In general, the finite-width effects are rather moderate since the relative width is only reduced by 25% as the values $w/d = \{3, 4\}$ are considered. This is done since connections bounded by these relative dimensions or smaller are prone for net-section failure. The finite-width effect is more pronounced for filled holes in comparison to open holes. For the special case of $d \rightarrow \infty$, the FFM prediction coincides with local criteria and the stresses are evaluated directly at the hole edge. Then, the reduction factors $\eta_{w/d}^*, \iota_{w/d}$ should yield the inverse value of the corresponding ratio of the stress concentration factors (SCFs) as follows.

Open Hole:

$$\lim_{d \rightarrow \infty} \eta_{w/d}^* = \lim_{d \rightarrow \infty} \frac{\sigma_{0,F}(w/d = 3, d)}{\sigma_{0,F}(w/d = 4, d)} = \frac{K_{t0}(w/d = 4)}{K_{t0}(w/d = 3)} = \frac{3.25}{3.45} \approx 94.2\%, \quad (5.26)$$

Filled Hole:

$$\lim_{d \rightarrow \infty} \iota_{w/d} = \lim_{d \rightarrow \infty} \frac{\sigma_{d,F}(w/d = 3, d)}{\sigma_{d,F}(w/d = 4, d)} = \frac{K_{td}(w/d = 4)}{K_{td}(w/d = 3)} = \frac{1.29}{1.50} \approx 86.0\%. \quad (5.27)$$

Although considering finite-sized hole diameters $d \leq 50$ mm, the quantities $\eta_{w/d}^*, \iota_{w/d}$ are already quite near the convergence value.

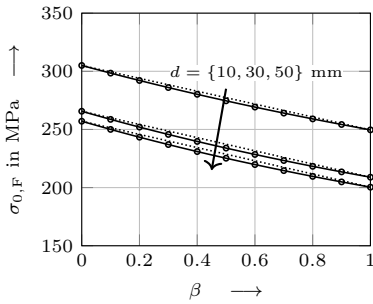
To investigate the effect of an increased bearing load on the failure stress reduction, let us introduce the reduction factor

$$\eta_\beta = \frac{\sigma_{0,F}(0 < \beta \leq 1)}{\sigma_{0,F}(\beta = 0)} = \frac{\sigma_{d,F}(0 < \beta \leq 1)}{\sigma_{d,F}(\beta = 0)}, \quad (5.28)$$

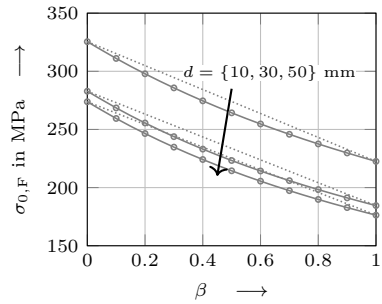
which normalises the failure stress of the bolted joint under combined bearing-bypass load to that of the open hole. The reduction factor η_β is shown in Fig. 5.22 revealing a converging behaviour. Furthermore, the wider w/d the more significant is an increasing load ratio β regarding the failure stress reduction. E.g. for $w/d = 3$, the filled hole's failure stress converges to 77.9% and for $w/d = 4$ to 64.4% of the value of the open hole.

Of practical interest might be the sustained far-field stress $\sigma_{0,F}$ with respect to the load factor β as well as failure envelopes, which enable the graphical determination of the bearing and bypass stresses at predicted net-tension failure. In Fig. 5.23, the far-field stress $\sigma_{0,F}$ with respect to β is

Chapter 5 Failure analysis



a) $w/d = 3$.



b) $w/d = 4$.

Fig. 5.23 Far-field stress $\sigma_{0,F}$ at failure with respect to load factor β showing a nonlinear behaviour. The dotted lines denote linear estimations.

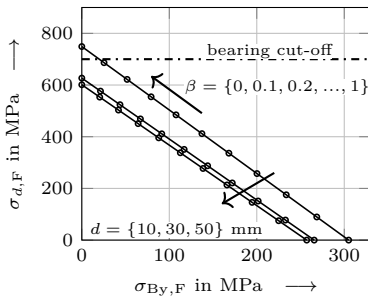


Fig. 5.24 Failure envelope for $w/d = 3$.

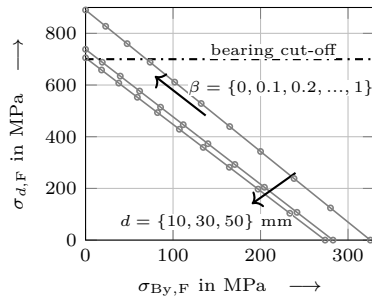


Fig. 5.25 Failure envelope for $w/d = 4$.

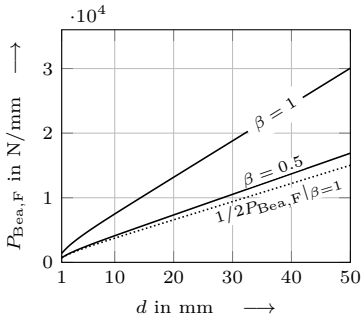


Fig. 5.26 Bolt load at failure for $w/d = 3$.

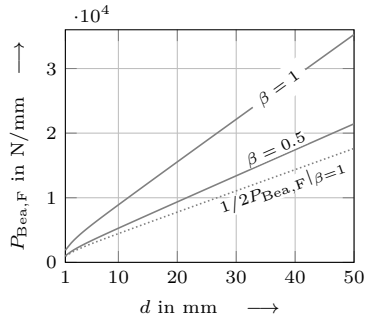


Fig. 5.27 Bolt load at failure for $w/d = 4$.

5.4 Discussion of the results: Bearing-bypass interaction

Table 5.3

Maximum relative deviations $\epsilon_{\sigma_{0,F}}$ of linear curves for $\sigma_{0,F}$ occurring at $\beta = 0.5$.

	$d = 10 \text{ mm}$	$d = 30 \text{ mm}$	$d = 50 \text{ mm}$
$w/d = 3$	1.0 %	1.4 %	1.5 %
$w/d = 4$	3.7 %	4.7 %	5.0 %

shown for $w/d = \{3, 4\}$ and $d = \{10 \text{ mm}, 30 \text{ mm}, 50 \text{ mm}\}$. Therein, the size effect and the corresponding failure stress reduction can be observed. The gap between the curves of $d = \{10 \text{ mm}, 30 \text{ mm}\}$ is larger than that of $d = \{30 \text{ mm}, 50 \text{ mm}\}$. This is due to the fact that for the first values, the hole diameter triples. Regarding the second pair, there is only a relative increase of 66.7 %. Furthermore, there exists a nonlinear relationship between $\sigma_{0,F}$ and β . The wider w/d and the larger d the more significant is the nonlinearity. However, for $w/d = 3$ the nonlinearity is rather weak. For quantitative assessment, let us assume a linear behaviour of $\sigma_{0,F}(\beta)$ and let us calculate its maximum deviation to the actual nonlinear curve, which occurs at $\beta = 0.5$. The corresponding relative deviations read

$$\epsilon_{\sigma_{0,F}} = \frac{\sigma_{0,F}^{\text{lin}} - \sigma_{0,F}^{\text{FFM}}}{\sigma_{0,F}^{\text{FFM}}} \quad (5.29)$$

and are listed in Table 5.3. Therein, the highest value of 5.0 % occurs for the connection with the largest plate width $w/d = 4$ and the largest hole diameter $d = 50 \text{ mm}$. This error can be regarded as acceptable. The engineer in practice may encounter a situation in which only the failure stresses of the special cases of open and filled holes are known. For instance, there might be test data only available for these settings. Circumventing this knowledge gap by assuming a linear relationship $\sigma_{0,F}(\beta)$ has led to acceptable errors for the investigated quasi-isotropic layup of the material system Hexcel IM7-8552. Note that the linear estimations yield higher values than FFM and therefore are nonconservative. For other problem settings with different material systems involving material orthotropy or another plain strength and fracture toughness, the discrepancy between linear approximation and actual nonlinear curve of $\sigma_{0,F}(\beta)$ is not quantified yet. Hence, a general recommendation to use this linear estimation even in early design stages is not given. Furthermore, each percentage accuracy matters in lightweight optimal design. Hence, it is recommended to model the nonlinear curve, which can be done with ease by using FFM.

The failure envelopes that illustrate the bearing and bypass stresses when a crack initiates are shown in Fig. 5.24, 5.25 for $w/d = \{3, 4\}$, respectively. The corresponding failure stresses can be calculated by

$$\sigma_{\text{By,F}} = (1 - \beta) \sigma_{0,\text{F}}, \quad \sigma_{d,\text{F}} = \beta w/d \sigma_{0,\text{F}}, \quad (5.30)$$

where the total far-field stress at failure $\sigma_{0,\text{F}}$ is directly determined by solving the coupled criterion in Eq. (5.7). The asymptotic behaviour of the size effect can be observed by the reduced gap between the curves for $d = \{30, 50\}$ mm in comparison to those of $d = \{10, 30\}$ mm. The bearing cut-off is set at $\sigma_d \approx 700$ MPa as in Sect. 5.3. Beyond this limit bearing failure occurs.

The sustainable bolt loads shown in Fig. 5.26 and 5.27 might be of interest for the engineer in practice. Therein, the bolt load at failure $P_{\text{Bea,F}}$ for the setting with a load factor $\beta = 0.5$ is more than half of the value of the pin-loaded hole's value ($\beta = 1$). This again shows the nonlinear interaction of the bearing-bypass loads, which is more significant for wider relative plate widths w/d and larger hole diameters d . Regarding $\beta = 0.5$, the total force that can be introduced into the connection is

$$P = \frac{P_{\text{Bea,F}}}{\beta} \Big|_{\beta=0.5} = 2 P_{\text{Bea,F}}(\beta = 0.5), \quad (5.31)$$

which is larger than the total sustainable force of the filled-hole problem with $P = P_{\text{Bea,F}}(\beta = 1)$. This implies that a high load factor reduces the total load which can be sustained by the connection. Thus, it is suggested to create designs that involve a low load factor β yielding a higher bearable total force. This can be achieved by placing more fasteners.

5.4.2 Performance of TCD concepts

The FFM derived crack length Δa for $\beta = \{0, 0.5, 1\}$ and $w/d = \{3, 4\}$ is shown in Fig. 5.28. Therein, the higher β the longer Δa . This is more pronounced the larger the defect size d . However, the spread is generally rather small and for approximately $d \geq 5$ mm, there exists a plateau area in which the crack length may be estimated by a single constant for all values of w/d and β considered. If the characteristic distance used in the TCD lies near the plateau similar predictions as FFM will be determined.

In the following, the TCD failure stresses are compared against FFM for the combined load case with $\beta = 0.5$. Regarding the TCD-CLB approach, the calibrated characteristic distance $r_{c,\text{clb}}$ used for the filled hole (Subsect. 5.3.1) is taken. This is done since there exist no experimentally determined failure stresses for the combined bearing-bypass load case. Further, the characteristic

5.4 Discussion of the results: Bearing-by-pass interaction

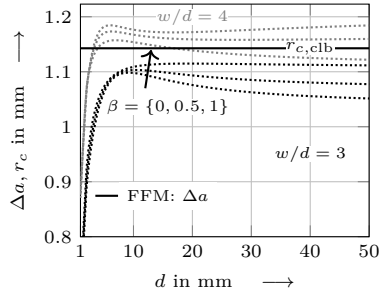


Fig. 5.28 Crack length Δa at failure.

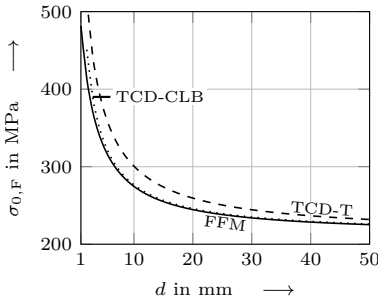


Fig. 5.29 Bearing stresses at failure for $\beta = 0.5$ and $w/d = 3$.

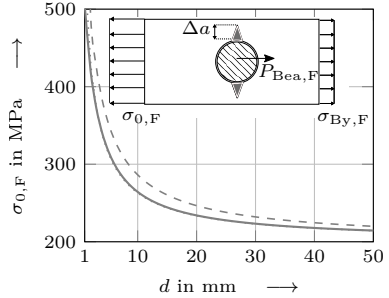


Fig. 5.30 Bearing stresses at failure for $\beta = 0.5$ and $w/d = 4$. The predictions by the TCD-CLB concept yield good correlation to FFM and hence overlap with the reference values.

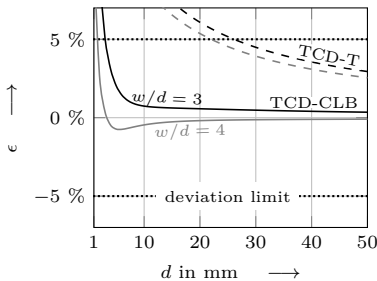


Fig. 5.31 TCD failure stresses: deviations normalised to FFM for $\beta = 0.5$.

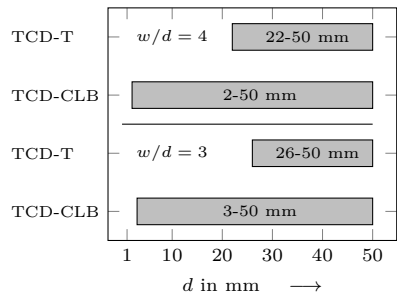


Fig. 5.32 TCD failure stresses: diameter range yielding an error $|\epsilon| \leq 5\%$.

distance of the filled hole belongs to a test set with $w/d = 1.75$ involving significant finite-width effects. Contrary, the test data of the open holes is based on a rather large plate with $w/d = 6$ involving slight finite-geometry effects. Hence, these data are not taken to derive failure stresses of a joint that is bounded by the relative plate width of $w/d = \{3, 4\}$. The calibrated characteristic distance $r_{c, \text{clb}} = 1.1143$ mm of the filled hole lies within the plateau of Δa . Due to this proximity the TCD-CLB approach yields rather accurate predictions involving relative errors $|\varepsilon| \leq 5\%$ for $w/d = 3$ with $d \geq 3$ mm and for $w/d = 4$ with $d \geq 2$ mm (Fig. 5.31, 5.32). Furthermore, $|\varepsilon| \leq 1\%$ is obtained for $w/d = 3$ with $d \geq 8$ mm and for $w/d = 4$ with $d \geq 3$ mm. Hence, the application of the TCD-CLB concept can be recommended for most configurations of the present bolted-joint problem. However, the engineer should be aware that this is based on the condition that experiments are available for the determination of the characteristic distance. From a scientific perspective, another general drawback of the TCD concept is the fact that the relative location of the stress evaluation ξ_{r_c} defined in Eq. (5.11) may lie outside the plate for $d \rightarrow 0$. Furthermore, a failure stress which is higher than the plain strength might be derived. This can occur if the net-section stresses are smaller than the far-field stress σ_0 , e.g. in finite plates where an undisturbed stress state is not reached for large hole distances. For example, this occurs for open and filled holes in a finite isotropic plate of the relative width $w/d = 3$ as shown in Fig. 4.5a, 4.6 and 4.10a. The quantity ξ_{r_c} increases with decreasing d and the normalised net-section stresses $\sigma_y(\xi, 0)/\sigma_0$ may become smaller than one for a wide hole distance. When employing a TCD approach based on the point method, failure stresses that are higher than the material strength may be derived, which is unphysical.

In the context of the TCD-T approach, results with errors $|\varepsilon| \leq 5\%$ for $d \geq 26$ mm regarding $w/d = 3$ and for $d \geq 22$ mm concerning $w/d = 4$ are obtained. The diameter range fulfilling this precision limit is rather small and the overall performance is a lot worse than that of the TCD-CLB approach. This is due to the corresponding characteristic distance $r_{c, \text{T}} = 1.632$ mm, which deviates from the FFM crack length Δa and is hence not shown in Fig. 5.28. The length parameter $r_{c, \text{T}}$ as defined in Eq. (5.10) stays the same no matter what problem setting is treated. Regarding open holes, the TCD-T concept has revealed good agreement (Sect. 5.2). By contrast, rather poor results are obtained for filled holes (Sect. 5.3). Then, the achieved accuracy regarding the bearing-bypass load case in comparison to FFM depends on the load ratio β . In particular, the higher β the more inaccurate are the predictions. For the special case $\beta = 1$ representing the filled-hole problem, the TCD-T approach performs worst as shown in Fig. 5.10, 5.13, 5.14 in comparison to FFM but also to experiments (Table 5.2). For open holes,

5.4 Discussion of the results: Bearing-bypass interaction

contrary, the TCD-T approach has turned out as a precise assessment means in comparison to FFM (Fig. 5.6, 5.7) as well as to experiment (Table 5.1). It might be concluded from these observations that the way how the external load is introduced (sinusoidal radial stresses along half of the hole boundary for the filled hole versus uniform tension at infinity for the open hole) and then transferred as well as the underlying symmetry properties have a significant impact on the applicability of the TCD-T approach. The mode I through crack, to which the characteristic distance by Taylor $r_{c,T}$ is related, as well as the open hole are doubly symmetric. Furthermore, the load transfer mechanism of both is dominated by uniform tensile stresses. The only difference lies in the load transfers' perturbation by defects which are of different shapes (circular hole or crack). By contrast, the filled-hole problem is single symmetric and the load transfer occurs mainly by radial tractions (Sect. 4.2). Other problems with different load transfer and symmetry properties might be investigated in future studies for further confirmation of this hypothesis.

As observed for the special cases of the open and filled hole, the deviations of the TCD concepts are smaller with increasing hole diameter. However, it is not recommended to generalise this observation to other problem settings, which shall be now further illustrated. Using nonlocal concepts, the stress evaluation is performed along the normalised hole distance

$$\text{FFM: } \Delta\xi = \frac{\Delta a(d)}{d/2(w/d-1)}, \quad \text{TCD: } \xi_{r_c} = \frac{r_c}{d/2(w/d-1)}. \quad (5.32)$$

For the quantity r_c , the characteristic distance $r_{c,elb}$ or $r_{c,T}$ by Taylor is inserted. With increasing diameter d the crack length Δa can be assumed as constant (see Fig. 5.2, 5.12, 5.28) and the difference

$$\Delta\xi_{\text{TCD,FFM}} = \xi_{r_c} - \Delta\xi = \frac{\overbrace{r_c - \Delta a}^{\approx \text{const.}}}{d/2(w/d-1)} \quad (5.33)$$

decreases with $1/d$. This means that the mismatch of the relative location of the TCD concepts to FFM is the smaller the larger d . However, it generally cannot be deduced that the prediction by the TCD then deviate less. For illustration, let us investigate the net-section stresses at $\xi_{r_c}(d), \Delta\xi(d)$. The net-section stress deviation of the TCD then is

$$\Delta\sigma_y(\Delta\xi_{\text{TCD,FFM}}(d), y=0) = \sigma_y(\xi_{r_c}(d), y=0) - \sigma_y(\Delta\xi(d), y=0). \quad (5.34)$$

For a larger hole diameter $d + \Delta d$, the amount of the stress deviation might be smaller, equal or larger depending on the shape of the net-section stress curve. Hence, it cannot be generalised that a smaller mismatch of the relative

location of the stress evaluation necessarily yields smaller errors in the failure load prediction.

To conclude, in the context of the TCD-CLB approach a single characteristic distance is sufficient to capture the hole size effect with almost the same accuracy as FFM. This is true for a wide diameter range and the small width-to-diameter ratio of $\{w/d = 3, 4\}$, for which net-section failure is likely to be triggered. However, reliable predictions are only obtained if the characteristic distance lies near the plateau of the crack length Δa derived by FFM. Conducting experiments is essential for its accurate determination. The TCD by Taylor, however, cannot be recommended to be applied for the present structural problem since serious errors have been shown. Another general drawback of the TCD concepts is the unknown extent in which the characteristic distances might be used for other configurations. This may be considered when conducting further experiments is not feasible. However, assessing if this step yields acceptable predictions requires reference values e.g. by experiment or by more sophisticated concepts such as FFM. Then, once obtained, there is no need from a practical point of view to have derived TCD predictions since the reference values can also be taken. In the context of lightweight optimal design, each percentage accuracy matters and especially for small defect sizes (approximately $d \leq 5$ mm) FFM should be preferred. Further, this failure prediction concept is physically motivated and requires only standard material parameters. Moreover, the overall effort to implement and solve the coupled criterion is rather small since formulae in handy form exist for the quasi-isotropic case. Other material systems can be included by inserting the corresponding plain material parameters. These advantages emphasise the capabilities and universality of FFM and the author recommends its application in industry contexts. Currently, when bolted joints with anisotropic plate material shall be assessed the quantities involved in the coupled criterion need then to be derived by numerical means. However, the effort should be moderate since 2D analyses need to be conducted only.

The employed nonlocal failure criteria emphasise that capturing the hole size effect is essential for a lightweight optimal design. The extreme cases of defect sizes are $d \rightarrow 0$ for which the failure stress specialises to that of the plain material strength for the open hole and to those of the plain plate reacting to a single force regarding the filled hole. For the special case of $d \rightarrow \infty$, the predictions coincide with local criteria. The failure stress of a finite-sized hole diameter is in between and for a sufficient material exploitation, nonlocal criteria requiring accurate net-section stresses and not only stress concentration factors are vital.

Chapter 6

Conclusion and outlook

The present thesis provides an efficient and comprehensive framework for the assessment of the tension-failure mode of composite bolted joints. This is based on analytical methods, which are beneficial in terms of computational cost and can be documented in technical design guidelines in the ideal case.

In typical design contexts, bolts are placed in rows. Then, the total load is split into two parts: one part is transferred into a bolt (bearing load) while the remaining load stays in the plate (bypass load). This problem setting is also referred to as bolted joint under bearing-bypass load. Aiming to employ analytical methods, linear 2D problem idealisations are preferable. In this context, the bolted joint under bearing-bypass load is modelled as plane problem, in particular as superposition of the open- and filled (or pin-loaded) hole. Regarding the latter setting, the bolt contact is idealised by radial hole tractions of sinusoidal shape as commonly done in literature.

One main goal of the present thesis is to develop an analytical means for the stress field determination of this bolted joints' mechanical idealisation. In doing so, use is made of the complex potential method in the Lekhnitskii formalism for the stress-state representation of the composite laminates that are connected by fasteners. Special consideration is given to finite plate dimensions. This is done because narrow connections are likely to trigger tension (or net-section) failure in the laminate. As the present bolted joint under combined bearing-bypass load is modelled as a superposition of the open and filled hole, the stress field of these partial problems is derived first. In doing so, the corresponding infinite-domain solution is determined and iteratively supplemented with three types of auxiliary (or correction) functions, which enable to take into account finite plate dimensions. Core of this concept thereby is a novel periodic arrangement technique that enables to efficiently implement stress-free edges of symmetric finite-domain problems. Hence, the present methodology is limited to symmetrical problem settings and only composite laminates with orthotropic material behaviour can be treated.

A validation against results from Finite Element analyses reveals excellent agreement for typical dimensions and layouts of connected composite

laminates. In particular, settings involving quasi-isotropic and symmetric $[0^\circ/\pm 45^\circ/90^\circ]_s(50\%/40\%/10\%)$ -laminates bounded by a small relative width-to-diameter ratio $w/d = 3$ and a narrow end-distance to hole-diameter ratio $e/d = 3$ yield normalised errors $|e| \leq 2\%$ along the net-section stresses in the vicinity of the hole. This region is relevant for crack initiation assessment of technical structures with bolt and hole diameters which are not smaller than a few millimetres. However, the calculus shows larger errors for plate geometries involving effects regarding finite dimensions that are mostly or exclusively due to a small end distance. This is caused by nonzero shear tractions therein, which are not covered by the present method. Note that such configurations are very unlikely to be designed since undesirable shear-out failure would then be triggered.

The present stress results are also compared against heuristic approaches that take into account finite width as follows. The infinite-domain solution of a particular problem is taken and scaled such that its integrated net-section stresses equilibrate the external load along the width of the actual finite-domain setting. This has been done in the context of the well known Tan solution treating anisotropic plates weakened by a hole. However, the good agreement for many layups is more or less by chance and not physically justified. Relative errors up to 39% arise for the balanced layup $[\pm 45^\circ]_s$ when assessing the entire net-section plane. Furthermore, adapting the heuristic concept to filled (or pin-loaded) holes generally reveals poor results. Hence, application to other problem settings without knowing the solution of the actual finite-domain boundary value problem is not recommended. The present stress calculus, however, provides a robust and efficient means to treat symmetric finite-domain problems. External loadings different from the bolted joint may be also treated. This can be achieved by adapting the Fourier series representation employed in the complex potential method to model the bolt contact idealisation.

Extensive stress analysis shows that raising effects due to finite width are more significant for laminates with relatively high effective shear stiffness such as $[0^\circ/\pm 45^\circ/90^\circ]_s(50\%/40\%/10\%)$ and quasi-isotropic layups. Laminates such as $[0^\circ]$ or $[0^\circ/90^\circ]_s$ yield very high stress concentrations due to a high orthotropy degree or a low shear stiffness. Additional increasing effects due to finite dimensions then are less significant. These observations are also made for the special cases of open and filled holes. In the context of combined bearing-bypass loads, the stress concentrations are generally more pronounced for higher bearing (or bolt) loads. The effects of finite plate dimensions are generally more pronounced for higher bearing loads. The raising effect by a bearing load is more significant with higher orthotropy degree and lower shear stiffness. Moreover, wider plates react more sensitively to bearing

loads implying that the corresponding increase in the stress concentrations is generally more pronounced.

Based on the present stress results, a failure analysis is conducted with the goal of accurately predicting the critical and minimal loads that lead to fatal net-section failure. This is the most critical of all failure modes in bolted joints and must be avoided in safety-relevant structures. The following nonlocal concepts capable of capturing the hole size effect are employed as means of assessment. First, the Theory of Critical Distances (TCD), which is commonly used in current industry contexts. A drawback of this criterion is that experiments are required to determine the characteristic distance. Along this length, the net-section stresses are evaluated to predict brittle crack initiation. Second, the state-of-the-art concept of Finite Fracture Mechanics (FFM) is used. This criterion only requires standard material parameters and can serve as a reference to assess the capabilities and limits of the TCD. Some settings of the special cases of open and filled holes are validated against experimental data. This considers quasi-isotropic laminates and the failure analysis is dedicated to those only. First, the special cases of open and filled holes are discussed. Then, the combined load case is treated. These steps involve rendering the size effect and, in this context, the corresponding failure load reduction with increasing hole and bolt diameter. In addition, finite-width effects are analysed. The drawbacks of local concepts that underestimate the failure loads are quantified by comparing their predictions to those of FFM. The smaller the hole and bolt diameter, the larger the relative error. For technical structures with finite-sized diameter, the relative error can exceed 55 %, implying that designs according to local criteria may overlook significant potentials for weight reduction. The reduction in failure stress with increasing diameter is more significant for wider plates and higher ratios between bearing and bypass load. Moreover, the nonlinear relationship of the failure stress with respect to the load factor is modelled. The nonlinearity is more pronounced with larger d and wider connections. Of practical interest might be the bearable bolt loads that can be introduced into the connection. From this perspective, it is quantitatively revealed that the design should involve wider plates and larger bolt and hole diameter. Furthermore, the load factor should be low, which can be achieved by placing more fasteners. Finally, failure envelopes that enable the graphical determination of the sustained bypass and bearing stresses are provided.

The following topics may be treated in future work. In this thesis, the stress calculus is limited to symmetric settings. This is mainly due to the periodic arrangement technique used to implement longitudinal stress-free edges. The methodology may be extended to antisymmetric problem settings, which refer to anisotropic laminates but also to load cases with external

forces that contain a lateral component. Finding a concept that is capable of rendering antisymmetric settings will eventually enable the treatment of any problem since each problem can be decomposed into one symmetric and one antisymmetric part. Regarding the bypass load case, uniform tension is assumed. In fact, this is valid for longitudinal joint distances larger than about ten times the hole and bolt diameter. However, in industry contexts joints may be placed with a smaller distance and the errors by the assumption of uniform bypass loads should be quantified. The stress calculus might also be extended by columns of bolts placed in the lateral direction. The developed periodic arrangement technique already provides a solid basis for such an extension and the correction functions would simply need to be applied to the virtual auxiliary plates. The employed mechanical idealisation is dedicated to tension load cases. Under compression, however, dual contact occurs beyond a certain threshold of the bearing-bypass load ratio. In this case, the linear idealisation as a superposition of the open- and pin-loaded hole problem cannot be used. Then, contact elasticity should be taken into account, which may lead to a more suitable mechanical idealisation. The employed 2D plate model also enables the derivation of the corresponding effective stiffness and compliance values. These play an important role in the load transfer calculation prior to a detailed 2D stress analysis. With the present method, the influence on the effective stiffness by parameters such as finite plate dimensions and plate material can be efficiently investigated. The stress calculus has been extensively documented in LTH Design Criteria, a technical handbook used by many European aerospace firms and is ready for immediate use in industry contexts. However, providing an efficient code in an accessible format, e.g. Python or a Excel spreadsheet, would further facilitate the implementation of the method in practical applications.

Future work regarding failure analysis might involve the investigation of orthotropic laminates. Currently, this can only be done using numerical methods when employing FFM. In particular, this refers to the corresponding stress intensity factors which cannot yet be derived by analytical means. However, the calculus developed to determine the stress field of finite-dimensioned bolted joint connections with orthotropic laminates may be adapted to stress intensity factors. The methodology would remain unchanged and would only need to be applied to a setting that involves a finite-sized crack emanating from the hole edge. For quasi-isotropic layups, the change of the material system and its impact on the effective failure loads could be analysed. This is of interest since the fracture toughness involved in the coupled criterion of FFM reacts very sensitively to temperature changes. Lastly, tests should be conducted for the combined load case. In doing so, FFM might be further validated and more confidence in this concept could be gained.

References

- T. L. Anderson. *Fracture mechanics: Fundamentals and Applications*. CRC Press, Boca Raton FL, 2005.
- ASTM D5961/D5961M-17. Standard test method for bearing response of polymer matrix composite laminates. Testing standard, ASTM International, West Conshohocken, PA, 2017.
- J. Awerbuch and M. S. Madhukar. Notched strength of composite laminates: Predictions and experiments - A review. *Journal of Reinforced Plastics and Composites*, 4(1):3–159, 1985.
- G. Bao, S. Ho, Z. Suo, and B. Fan. The role of material orthotropy in fracture specimens for composites. *International Journal of Solids and Structures*, 29(9): 1105 – 1116, 1992.
- Z. P. Bažant. Size effect in blunt fracture: concrete, rock, metal. *Journal of Engineering Mechanics*, 110(4):518–535, 1984.
- Z. P. Bažant. Size effect. *International Journal of Solids and Structures*, 37(1):69 – 80, 2000.
- Z. P. Bažant, I. M. Daniel, and Z. Li. Size Effect and Fracture Characteristics of Composite Laminates. *Journal of Engineering Materials and Technology*, 118(3): 317–324, 1996.
- Z. P. Bažant, Y. Zhou, D. Novák, and I. Daniel. Size effect on flexural strength of fiber-composite laminate. *Journal of Engineering Materials and Technology*, 126(1):29–37, 2004.
- Z. Bažant, R. Gettu, and M. Kazemi. Identification of nonlinear fracture properties from size effect tests and structural analysis based on geometry-dependent R-curves. *International Journal of Rock Mechanics and Mining Sciences & Geomechanics Abstracts*, 28(1):43–51, 1991.
- W. Becker. Complex method for the elliptical hole in an unsymmetric laminate. *Archive of Applied Mechanics*, 63:159–169, 1993.
- W. Becker and D. Gross. *Mechanik elastischer Körper und Strukturen*. Springer-Verlag Berlin Heidelberg, 2002.
- P. Berbinau and C. Soutis. A new approach for solving mixed boundary value problems along holes in orthotropic plates. *International Journal of Solids and Structures*, 38(1):143 – 159, 2001.

References

- W. G. Bickley. The Distribution of Stress Round a Circular Hole in a Plate. *Philosophical Transactions of the Royal Society of London*, 227:383–415, 1928.
- O. Bowie and D. Neal. A modified mapping-collocation technique for accurate calculation of stress intensity factors. *International Journal of Fracture Mechanics*, 6:199–206, 1970.
- K. Broberg. *Cracks and Fracture*. Academic Press, San Diego, London, 1999.
- P. Camanho and M. Lambert. A design methodology for mechanically fastened joints in laminated composite materials. *Composites Science and Technology*, 66: 3004–3020, 2006.
- P. Camanho and F. Matthews. Stress analysis and strength prediction of mechanically fastened joints in FRP: a review. *Composites Part A: Applied Science and Manufacturing*, 28(6):529 – 547, 1997.
- P. Camanho, G. Erçin, G. Catalanotti, S. Mahdi, and P. Linde. A finite fracture mechanics model for the prediction of the open-hole strength of composite laminates. *Composites Part A: Applied Science and Manufacturing*, 43(8):1219 – 1225, 2012.
- A. Carpinteri, P. Cornetti, N. Pugno, A. Sapora, and D. Taylor. A finite fracture mechanics approach to structures with sharp V-notches. *Engineering Fracture Mechanics*, 75(7):1736–1752, 2008.
- A. Carpinteri, P. Cornetti, and A. Sapora. A finite fracture mechanics approach to the asymptotic behaviour of U-notched structures. *Fatigue & Fracture of Engineering Materials & Structures*, 35:451–457, 2012.
- N. Carrere, E. Martin, and D. Leguillon. Comparison between models based on a coupled criterion for the prediction of the failure of adhesively bonded joints. *Engineering Fracture Mechanics*, 138:185–201, 2015.
- G. Catalanotti and P. Camanho. A semi-analytical method to predict net-tension failure of mechanically fastened joints in composite laminates. *Composites Science and Technology*, 76:69–76, 2013.
- G. Cherepanov. *Mechanics of Brittle Fracture*. McGraw-Hill, New York, 1979.
- C.-H. Chue, C.-H. Tseng, and C.-I. Liu. On stress singularities in an anisotropic wedge for various boundary conditions. *Composite Structures*, 54(1):87–102, 2001.
- M. Ciavarella, A. Baldini, J. Barber, and A. Strozzi. Reduced dependence on loading parameters in almost conforming contacts. *International Journal of Mechanical Sciences*, 48(9):917–925, 2006.
- T. Collings. The strength of bolted joints in multi-directional CFRP laminates. *Composites*, 8(1):43 – 55, 1977.
- T. Collings. On the bearing strengths of CFRP laminates. *Composites*, 13(3):241 – 252, 1982.

- P. Cornetti, N. Pugno, A. Carpinteri, and D. Taylor. Finite fracture mechanics: A coupled stress and energy failure criterion. *Engineering Fracture Mechanics*, 73(14):2021 – 2033, 2006.
- P. Cornetti, A. Sapora, and A. Carpinteri. Mode mixity and size effect in V-notched structures. *International Journal of Solids and Structures*, 50:1562–1582, 2013.
- Crews, C. Hong, and I. Raju. Stress Concentration Factors for Finite Orthotropic Laminates With a Pin-Loaded Hole. *NASA Technical Paper*, 1981.
- A. Curtis and P. Grant. The strength of carbon fibre composite plates with loaded and unloaded holes. *Composite Structures*, 2(3):201–221, 1984.
- T. de Jong. Spanningen rond een gat in een elastisch orthotrope of isotrope plaat, belast door een pen die zich daarin wrijvingsloos kan bewegen. *Technische Hogeschool Delft, Afdeling der Luchtvaart-en Ruimtevaarttechniek, Rapport LR-223*, 1976.
- T. de Jong. Stresses around pin-loaded holes in elastically orthotropic or isotropic plates. *Journal of Composite Materials*, 11:313–331, 1977.
- T. de Jong and H. A. Vuil. Stresses around pin-loaded holes in elastically orthotropic plates with arbitrary load direction. *Delft University of Technology, Department of Aerospace Engineering, Report LR-333*, 1981.
- J. Dundurs and M. Stippes. Role of elastic constants in certain contact problems. *Journal of Applied Mechanics*, 37:965–970, 1970.
- G. Dvorak and A. Suvorov. Size effect in fracture of unidirectional composite plates. *International Journal of Fracture*, 95(1-4):89–101, 1999.
- S. Dölling, J. Hahn, J. Felger, S. Bremm, and W. Becker. A scaled boundary finite element method model for interlaminar failure in composite laminates. *Composite Structures*, 241:111865, 2020.
- S. Dölling, S. Bremm, A. Kohlstetter, J. Felger, and W. Becker. Predicting thermally induced edge-crack initiation using finite fracture mechanics. *Engineering Fracture Mechanics*, 252:107808, 2021.
- C. Echavarría, P. Haller, and A. Salenikovich. Analytical study of a pin-loaded hole in elastic orthotropic plates. *Composite Structures*, 79(1):107 – 112, 2007.
- J. Ekh and J. Schön. Load transfer in multirow, single shear, composite-to-aluminium lap joints. *Composites Science and Technology*, 66(7):875–885, 2006.
- I. Eriksson, J. Bäcklund, and P. Möller. Design of multiple-row bolted composite joints under general in-plane loading. *Composites Engineering*, 5(8):1051–1068, 1995.
- J. Felger, N. Stein, and W. Becker. Mixed-mode fracture in open-hole composite plates of finite-width: An asymptotic coupled stress and energy approach. *International Journal of Solids and Structures*, 122-123:14 – 24, 2017a.

References

- J. Felger, N. Stein, and W. Becker. Asymptotic finite fracture mechanics solution for crack onset at elliptical holes in composite plates of finite-width. *Engineering Fracture Mechanics*, 182:621–634, 2017b.
- J. Felger, N. Stein, C. Frey, and W. Becker. Scaling laws for the adhesive composite butt joint strength derived by finite fracture mechanics. *Composite Structures*, 208, 2018.
- C. Frey, S. Dölling, and W. Becker. Closed-form analysis of interlaminar crack initiation in angle-ply laminates. *Composite Structures*, 257:113060, 2021a.
- C. Frey, S. Dölling, M. Leštáková, and W. Becker. Free-edge crack onset induced by thermal loading. *International Journal of Solids and Structures*, 230-231:111160, 2021b.
- G. M. Gladwell. *Contact Problems in the Classical Theory of Elasticity*. Springer Netherlands, 1980.
- E. Godwin and F. Matthews. A review of the strength of joints in fibre-reinforced plastics: Part 1. Mechanically fastened joints. *Composites*, 11(3):155 – 160, 1980.
- P. Gray and C. McCarthy. A global bolted joint model for finite element analysis of load distributions in multi-bolt composite joints. *Composites Part B: Engineering*, 41(4):317–325, 2010.
- B. Green, M. Wisnom, and S. Hallett. An experimental investigation into the tensile strength scaling of notched composites. *Composites Part A: Applied Science and Manufacturing*, 38(3):867 – 878, 2007.
- D. Gross and T. Seelig. *Bruchmechanik*. Springer Vieweg, Berlin, Heidelberg, 2016.
- B. Grüber, W. Hufenbach, L. Kroll, M. Lepper, and B. Zhou. Stress concentration analysis of fibre-reinforced multilayered composites with pin-loaded holes. *Composites Science and Technology*, 67(7):1439–1450, 2007.
- B. Grüber, M. Gude, T. Hoyer, R. Gottwald, M. Lepper, and B. Zhou. Calculation method for the determination of stress concentrations in fibre-reinforced multilayered composites due to metallic interference-fit bolt. *Journal of Composite Materials*, 52(18):2415–2429, 2018.
- J. C. Halpin. *Primer on Composite Materials Analysis (Second Edition, Revised)*. CRC Press, Boca Raton, FL, 1992.
- L. J. Hart-Smith. Mechanically-Fastened Joints for Advanced Composites — Phenomenological Considerations and Simple Analyses. In E. M. Lenoe, D. W. Oplinger, and J. J. Burke, editors, *Fibrous Composites in Structural Design*, pages 543–574. Springer US, Boston, MA, 1980.
- Z. Hashin. Finite thermoelastic fracture criterion with application to laminate cracking analysis. *Journal of the Mechanics and Physics of Solids*, 44(7):1129–1145, 1996.

- J. Hebel and W. Becker. Numerical analysis of brittle crack initiation at stress concentrations in composites. *Mechanics of Advanced Materials and Structures*, 15(6-7):410–420, 2008.
- J. Hebel, R. Dieringer, and W. Becker. Modelling brittle crack formation at geometrical and material discontinuities using a finite fracture mechanics approach. *Engineering Fracture Mechanics*, 77(18):3558–3572, 2010.
- S. Hell, P. Weißgraeber, J. Felger, and W. Becker. A coupled stress and energy criterion for the assessment of crack initiation in single lap joints: A numerical approach. *Engineering Fracture Mechanics*, 117, 2014.
- R. B. Heywood. *Designing by Photoelasticity*. Chapman & Hall, London, 1952.
- H. Hill. Stress-Concentration Factors Around a Central Circular Hole in a Plate Loaded Through Pin in the Hole. In M. Leven and M. Frocht, editors, *Photoelasticity*, pages 159–170. Pergamon, 1969.
- K. Ho and K. Chau. An infinite plane loaded by a rivet of a different material. *International Journal of Solids and Structures*, 34(19):2477–2496, 1997.
- J. P. Hou and D. A. Hills. Contact between a pin and a plate with a hole under interference-fit and clearance-fit conditions. *Proceedings of the Institution of Mechanical Engineers, Part C: Journal of Mechanical Engineering Science*, 215(6):629–639, 2001.
- H. Huth. Influence of Fastener Flexibility on the Prediction of Load Transfer and Fatigue Life for Multiple-Row Joints. In *Fatigue in Mechanically Fastened Composite and Metallic Joints*, page 221–250. 1986.
- M. Hyer and E. Klang. Contact stresses in pin-loaded orthotropic plates. *International Journal of Solids and Structures*, 21(9):957 – 975, 1985.
- M. Hyer, E. Klang, and D. Cooper. The effects of pin elasticity, clearance, and friction on the stresses in a pin-loaded orthotropic plate. *Journal of Composite Materials*, 21(3):190–206, 1987.
- K. Iyer. Solutions for contact in pinned connections. *International Journal of Solids and Structures*, 38(50):9133–9148, 2001.
- Y. Jenq and S. P. Shah. Two parameter fracture model for concrete. *Journal of Engineering Mechanics*, 111(10):1227–1241, 1985.
- K. L. Johnson. *Contact Mechanics*. Cambridge University Press, 1987.
- A. Kabeel, P. Maimí, N. Gascons, and E. González. Net-tension strength of double lap joints taking into account the material cohesive law. *Composite Structures*, 112:207–213, 2014.
- A. Kabeel, P. Maimí, E. González, and N. Gascons. Net-tension strength of double-lap joints under bearing-bypass loading conditions using the cohesive zone model. *Composite Structures*, 119:443–451, 2015.

References

- M. F. Kanninen and C. H. Popelar. *Mechanics of Brittle Fracture*. Oxford University Press, 1985.
- G. Kirsch. Die Theorie der Elastizität und die Bedürfnisse der Festigkeitslehre. *Zeitschrift des Vereins deutscher Ingenieure*, 42:797–807, 1898.
- R. Knight. The action of a rivet in a plate of finite breadth. *Philosophy Magazine*, 19(7):517–540, 1935.
- J. Koord, J.-L. Stüven, E. Petersen, O. Völkerink, and C. Hühne. Investigation of exact analytical solutions for circular notched composite laminates under tensile loading. *Composite Structures*, 243:112180, 2020.
- J. Kratochvil and W. Becker. Structural analysis of composite bolted joints using the complex potential method. *Composite Structures*, 92(10):2512–2516, 2010.
- G. Kretsis and F. Matthews. The strength of bolted joints in glass fibre/epoxy laminates. *Composites*, 16(2):92–102, 1985.
- J. Lecomte, C. Bois, H. Wargnier, and J.-C. Wahl. An analytical model for the prediction of load distribution in multi-bolt composite joints including hole-location errors. *Composite Structures*, 117:354–361, 2014.
- D. Leguillon. Strength or toughness? A criterion for crack onset at a notch. *European Journal of Mechanics - A/Solids*, 21(1):61–72, 2002.
- S. Lekhnitskii. On the problem of the elastic equilibrium of an anisotropic strip. *Journal of Applied Mathematics and Mechanics*, 27(1):197–209, 1963.
- S. Lekhnitskii. *Anisotropic Plates*. Gordon and Breach Science Publishers, New York, 1968.
- J. Li and X. Zhang. A criterion study for non-singular stress concentrations in brittle or quasi-brittle materials. *Engineering Fracture Mechanics*, 73:505–523, 2006.
- E. Madenci, L. Ileri, and J. Starnes. Analysis of pin-loaded holes in composite laminates under combined bearing-bypass and shear loading. *International Journal of Solids and Structures*, 32(14):2053–2062, 1995.
- E. Madenci, S. Shkarayev, B. Sergeev, D. Oplinger, and P. Shyprykevich. Analysis of composite laminates with multiple fasteners. *International Journal of Solids and Structures*, 35(15):1793–1811, 1998.
- E. Martin, D. Leguillon, and N. Carrere. A twofold strength and toughness criterion for the onset of free-edge shear delamination in angle-ply laminates. *International Journal of Solids and Structures*, 47:1297–1305, 2010.
- E. Martin, D. Leguillon, and N. Carrère. A coupled strength and toughness criterion for the prediction of the open hole tensile strength of a composite plate. *International Journal of Solids and Structures*, 49(26):3915–3922, 2012.

- F. Matthews. Theoretical Stress Analysis of Mechanically Fastened Joints. In F. Matthews, editor, *Joining Fibre-Reinforced Plastics*, pages 65–103. Elsevier Applied Science Publishers Ltd, Springer Netherlands, 1987.
- C. McCarthy and P. Gray. An analytical model for the prediction of load distribution in highly torqued multi-bolt composite joints. *Composite Structures*, 93(2):287 – 298, 2011.
- M. McCarthy, C. McCarthy, and G. Padhi. A simple method for determining the effects of bolt–hole clearance on load distribution in single-column multi-bolt composite joints. *Composite Structures*, 73(1):78–87, 2006.
- J. H. Michell. On the direct determination of stress in an elastic solid with application to the theory of plates. *Proceedings of the London Mathematical Society*, 31: 100–124, 1899.
- C. Mittelstedt and W. Becker. *Strukturmechanik ebener Laminate*. Studienbereich Mechanik, Technische Universität Darmstadt, 2016.
- N. Muskhelishvili. *Some Basic Problems of the Mathematical Theory of Elasticity*. Springer, Dordrecht, 1977.
- H. Neuber. Elastisch-strenge Lösungen zur Kerbwirkung bei Scheiben und Um-drehungskörpern. *ZAMM*, 13:439–442, 1933.
- H. Neuber. Zur Theorie der Kerbwirkung bei Biegung und Schub. *Ingenieur-Archiv*, 5(3):238–244, 1934.
- H. Neuber. *Kerbspannungslehre: Theorie der Spannungskonzentration. Genaue Berechnung der Festigkeit*. Springer-Verlag, Berlin, Heidelberg, 2013.
- J. Newman. An improved method of collocation for the stress analysis of cracked plates with various shaped boundaries. *NASA Technical Note*, NASA TN D-6376, 1971.
- M. Nguyen-Hoang and W. Becker. Tension failure analysis for bolted joints using a closed-form stress solution. *Composite Structures*, 238:111931, 2020a.
- M. Nguyen-Hoang and W. Becker. Open Circular Hole in a Finite Plate Under Tension Treated by Airy Stress Function Method. In H. Altenbach, N. Chinchaladze, R. Kienzler, and W. H. Müller, editors, *Analysis of Shells, Plates, and Beams: A State of the Art Report*, pages 311–330. Springer International Publishing, Cham, 2020b.
- M. Nguyen-Hoang and W. Becker. Stress analysis of finite dimensions bolted joints using the Airy stress function. *International Journal of Solids and Structures*, 224:111023, 2021a.
- M. Nguyen-Hoang and W. Becker. Stress analysis of finite orthotropic plates loaded by a bolted joint. *Composite Structures*, 276:114454, 2021b.

References

- M. Nguyen-Hoang and W. Becker. Stress analysis of orthotropic composite bolted joints using complex potentials FL 33 100-37. Technical handbook, LTH Composite Design Criteria (FL), 2021c.
- M. Nguyen-Hoang and W. Becker. Closed-form stress solution for finite dimensions orthotropic composite laminate open holes FL 33 100-36. Technical handbook, LTH Composite Design Criteria (FL), 2021d.
- M. Nguyen-Hoang and W. Becker. Stress analysis of a bolted finite dimensions plate under bearing-bypass load interaction using the Airy stress function. *Engineering Structures*, 256:113943, 2022a.
- M. Nguyen-Hoang and W. Becker. Stress analysis of orthotropic composite bolted joints under bearing-bypass load using complex potentials FL 33 100-38. Technical handbook, LTH Composite Design Criteria (FL), 2022b.
- M. Nguyen-Hoang and W. Becker. Stress concentration and distribution in a finite pin-loaded plate HSB 34112-10 - in B status. Technical handbook, Handbuch Strukturberechnung (IASB working group), 2022c.
- M. Nguyen-Hoang and W. Becker. Open holes in composite laminates with finite dimensions: structural assessment by analytical methods. *Archive of Applied Mechanics*, 2022d.
- J. Ogonowski. Effect of Variances and Manufacturing Tolerances on the Design Strength and Life of Mechanically Fastened Composite Joints AFWAL-TR-81-3041, 3. Technical report, McDonnell Aircraft Company, 1981.
- X. Peng, X. Li, G. Liu, and J. Zhao. Prediction of net-tension failure of multi-bolt composite joints: A fast approach for laminates with arbitrary layup. *European Journal of Mechanics - A/Solids*, 87:104213, 2021.
- A. Persson. *On the stress distribution of cylindrical elastic bodies in contact*. PhD thesis, Chalmers University of Technology, 1964.
- R. Peterson and A. Wahl. Two and Three dimensional Cases of Stress Concentration, and Comparison With Fatigue Tests. *Journal of Applied Mechanics*, 3(1):A15–A22, 1936.
- W. D. Pilkey and D. F. Pilkey. *Peterson's Stress Concentration Factors*. John Wiley & Sons, Hoboken, NJ, 2008.
- R. B. Pipes, R. C. Wetherhold, and J. John W. Gillespie. Notched strength of composite materials. *Journal of Composite Materials*, 13(2):148–160, 1979.
- J. N. Reddy. *Mechanics of Laminated Composite Plates and Shells: Theory and Analysis*. CRC Press, Boca Raton FL, 2004.
- P. Rosendahl, P. Weißgraeber, N. Stein, and W. Becker. Asymmetric crack onset at open-holes under tensile and in-plane bending loading. *International Journal of Solids and Structures*, 113-114:10–23, 2017.

- A. Sackfield, D. Hills, and D. Nowell. *Mechanics of Elastic Contacts*. Elsevier, 2013.
- M. H. Sadd. *Elasticity: Theory, Applications, and Numerics - Second Edition*. Elsevier Butterworth-Heinemann, Burlington MA and Oxford UK, 2005.
- A. Sapora and P. Cornetti. Crack onset and propagation stability from a circular hole under biaxial loading. *International Journal of Fracture*, 214:97–104, 2018.
- A. Sapora, P. Cornetti, A. Carpinteri, and D. Firrao. Blunt V-Notch Brittle Fracture: An Improved Finite Fracture Mechanics Approach. *Advanced Materials Research*, 1105:237–244, 2015.
- G. Savin. *Stress Concentration Around Holes*. Pergamon Press, London, 1961.
- H. Schürmann. *Konstruieren mit Faser-Kunststoff-Verbunden*. Springer-Verlag, Berlin, 2007.
- R. Sevenois and S. Koussios. Analytic methods for stress analysis of two-dimensional flat anisotropic plates with notches: An overview. *Applied Mechanics Reviews*, 66:060802, 2014.
- V. Shivakumar and R. Forman. Green’s function for a crack emanating from a circular hole in an infinite sheet. *International Journal of Fracture*, 16(4):305–316, 1980.
- D. Song, K. Zhang, Y. Li, P. Liu, X. Yan, and W. Su. Effect of interference percentage on damage mechanism of carbon fiber reinforced plastics laminate during interference-fit bolt installation. *Journal of Composite Materials*, 51(8):1031–1043, 2017.
- V. Srivastava and D. Kumar. Prediction of notched strength of laminated fibre composites under tensile loading conditions. *Journal of Composite Materials*, 36(9):1121–1133, 2002.
- N. Stein, P. Weißgräber, and W. Becker. A model for brittle failure in adhesive lap joints of arbitrary joint configuration. *Composite Structures*, 133:707–718, 2015.
- N. Sundaram and T. Farris. Mechanics of advancing pin-loaded contacts with friction. *Journal of the Mechanics and Physics of Solids*, 58(11):1819–1833, 2010a.
- N. Sundaram and T. Farris. The generalized advancing conformal contact problem with friction, pin loads and remote loading – case of rigid pin. *International Journal of Solids and Structures*, 47(6):801–815, 2010b.
- T. Swift. Development of the Fail-safe Design Features of the DC-10. In *Damage Tolerance in Aircraft Structures*, page 164–214. ASTM International, West Conshohocken, PA, 1971.
- H. Tada, P. Paris, and G. Irwin. *The Stress Analysis of Cracks Handbook*. ASME Press, New York, 2000.

References

- A. Talmon, S. Hell, P. Rosendahl, J. Felger, and W. Becker. Nonlinear crack opening integral: Mode mixity for finite cracks. *Engineering Fracture Mechanics*, 186: 283–299, 2017.
- S. Tan. *Stress Concentrations in Laminated Composites*. CRC Press, Boca Raton, FL, 1994.
- S. C. Tan. Fracture strength of composite laminates with an elliptical opening. *Composites Science and Technology*, 29(2):133 – 152, 1987.
- S. C. Tan. Finite-width correction factors for anisotropic plate containing a central opening. *Journal of Composite Materials*, 22(11):1080–1097, 1988.
- S. C. Tan and R. Y. Kim. Strain and stress concentrations in composite laminates containing a hole. *Experimental Mechanics*, 30(4):345–351, 1990.
- M. B. Tate and S. J. Rosenfeld. Preliminary Investigation of the Loads Carried by Individual Bolts in Bolted Joints. Technical report, National Advisory Committee for Aeronautics, 1946.
- D. Taylor. Predicting the fracture strength of ceramic materials using the theory of critical distances. *Engineering Fracture Mechanics*, 71(16):2407–2416, 2004.
- D. Taylor. *The Theory of Critical Distances*. Elsevier Oxford, UK, 2007.
- D. Taylor. The theory of critical distances. *Engineering Fracture Mechanics*, 75(7): 1696–1705, 2008.
- D. Taylor. Applications of the theory of critical distances in failure analysis. *Engineering Failure Analysis*, 18(2):543–549, 2011.
- P. S. Theocaris. The Stress Distribution in a Strip Loaded in Tension by Means of a Central Pin. *Journal of Applied Mechanics*, 23(1):85–90, 1956.
- S. Timoshenko and J. N. Goodier. *Theory of Elasticity*. McGraw-Hill Book Company, Inc., New York, Toronto, London, 1951.
- Q. To, Q.-C. He, M. Cossavella, K. Morcant, and A. Panait. Closed-form solution for the contact problem of reinforced pin-loaded joints used in glass structures. *International Journal of Solids and Structures*, 44(11):3887–3903, 2007.
- S. W. Tsai. *Strength & Life of Composites*. Stanford University, Stanford, CA, 2008.
- T. Tung. On computation of stresses around holes in anisotropic plates. *Journal of Composite Materials*, 21(2):100–104, 1987.
- V. Ukadgaonker and D. Rao. A general solution for stresses around holes in symmetric laminates under inplane loading. *Composite Structures*, 49(3):339–354, 2000a.

- V. Ukadgaonker and D. Rao. A general solution for stress resultants and moments around holes in unsymmetric laminates. *Composite Structures*, 49(1):27–39, 2000b.
- J. P. Waszczak and T. A. Cruse. Failure mode and strength prediction of anisotropic bolt bearing specimens. *Journal of Composite Materials*, 5:421–425, 1971.
- F. Wei-Xun and Q. Chun-Tu. Load distribution of multi-fastener laminated composite joints. *International Journal of Solids and Structures*, 30(21):3013–3023, 1993.
- P. Weißgraeber and W. Becker. Finite Fracture Mechanics model for mixed mode fracture in adhesive joints. *International Journal of Solids and Structures*, 50: 2383–2394, 2013.
- P. Weißgraeber, J. Felger, D. Geipel, and W. Becker. Cracks at elliptical holes: Stress intensity factor and Finite Fracture Mechanics solution. *European Journal of Mechanics - A/Solids*, 55:192–198, 2015a.
- P. Weißgraeber, J. Felger, A. Talmon, and W. Becker. Crack initiation in single lap joints: effects of geometrical and material properties. *International Journal of Fracture*, 192:155–166, 2015b.
- P. Weißgraeber, D. Leguillon, and W. Becker. A review of Finite Fracture Mechanics: Crack initiation at singular and non-singular stress-raisers. *Archive of Applied Mechanics*, 86:375–401, 2015c.
- J. M. Whitney and R. J. Nuismer. Stress fracture criteria for laminated composites containing stress concentrations. *Journal of Composite Materials*, 8:253–265, 1974.
- M. Wisnom. Size effects in the testing of fibre-composite materials. *Composites Science and Technology*, 59(13):1937–1957, 1999.
- T. Wu and M. Tian. An analytical stress model for composite multi-pinned plates considering the combination effects of pin load and bypass load in different positions. *Advances in Mechanical Engineering*, 13(4):1–12, 2021.
- Y. Xiao and T. Ishikawa. Bearing strength and failure behavior of bolted composite joints (part I: Experimental investigation). *Composites Science and Technology*, 65(7):1022 – 1031, 2005.
- Y. Xiong. An analytical method for failure prediction of multi-fastener composite joints. *International Journal of Solids and Structures*, 33(29):4395–4409, 1996.
- J. York, D. Wilson, and R. Pipes. Analysis of the net tension failure mode in composite bolted joints. *Journal of Reinforced Plastics and Composites*, 1(2): 141–152, 1982.
- Z. Yosibash, E. Priel, and D. Leguillon. A failure criterion for brittle elastic materials under mixed-mode loading. *International Journal of Fracture*, 141:291–312, 2006.

References

- K.-D. Zhang and C. E. Ueng. Stresses around a pin-loaded hole in orthotropic plates. *Journal of Composite Materials*, 18(5):432–446, 1984.
- K. D. Zhang and C. E. Ueng. Stresses around a pin-loaded hole in orthotropic plates with arbitrary loading direction. *Composite Structures*, 3(2):119–143, 1985.
- L. Zhao, Z. Fang, F. Liu, M. Shan, and J. Zhang. A modified stiffness method considering effects of hole tensile deformation on bolt load distribution in multi-bolt composite joints. *Composites Part B: Engineering*, 171:264–271, 2019.

This document has 168 references.